
Cyclobutane Pyrimidine Dimers via Photosensitization – Combined Stationary and Time-resolved Studies

Lizhe Liu



München 2016

**Cyclobutane Pyrimidine Dimers via
Photosensitization – Combined Stationary and
Time-resolved Studies**

Lizhe Liu

Dissertation

an der Fakultät für Physik
der Ludwig-Maximilians-Universität
München

vorgelegt von
Lizhe Liu
aus Nanjing

München, den 18. Mai 2016

Erstgutachter: Prof. Dr. Wolfgang Zinth

Zweitgutachter: Prof. Dr. Regina de Vivie-Riedle

Tag der mündlichen Prüfung: 06. Juli 2016

Contents

Kurzfassung	ix
Abstract	xi
1 Introduction	1
2 Theoretical Background	5
2.1 The Structure of DNA and RNA	5
2.2 DNA Photophysics and Photochemistry	7
2.2.1 The Basic Concepts of Photophysics and Photochemistry	8
2.2.2 Photophysics of Thymine Derivatives	11
2.3 UV-induced DNA Damages and Mutations	13
2.3.1 Cyclobutane Pyrimidine Dimer	13
2.3.2 (6-4) Photoproduct and Dewar Lesion	15
2.3.3 Oxidative Damages	17
2.4 Photosensitization	18
2.4.1 Different Types of Photosensitization	18
2.4.2 Acetophenone	19
3 Experimental Methods	23
3.1 Pump-probe Spectroscopy	23
3.1.1 Principle of the UV-pump MIR-probe Spectroscopy	23
3.1.2 Generation of Probe Pulses in the MIR Range	24
3.1.3 Generation of Femtosecond Pump Pulses by NOPA	26
3.1.4 Pump Pulses in the Nanosecond Range	27
3.1.5 Data Acquisition and Processing	28
3.1.6 Data Fitting	29
3.2 The Sample Circulation Setup	30
3.3 Stationary Characterization of the Sample	31
4 Selection and Characterization of an Appropriate Photosensitizer	33
4.1 Test of Different Acetophenone Compounds	33
4.1.1 Prerequisites for the Sensitizer	34
4.1.2 Selection of the Sensitizer in the UV-A Range	35
4.1.3 Selection of a Sensitizer by MIR Spectroscopy	37

4.2	Characterization of Acetophenone	39
4.2.1	Stationary Spectra of Acetophenone and Deuterated Acetophenone	39
4.2.2	Time-resolved Absorption Measurement on Deuterated Acetophenone	40
4.3	Spectroscopic Characterization of 2-Methoxyacetophenone	44
4.4	Time-resolved Measurements on 2-Methoxyacetophenone	47
4.4.1	Fluorescence Measurement in the Picosecond to Nanosecond Range	47
4.4.2	Absorption Measurement in the Picosecond to Nanosecond Range	49
4.4.3	Absorption Measurement in the Nanosecond to Microsecond Range	51
4.5	Summary of the Important Properties of 2-Methoxyacetophenone	53
5	Formation of CPD Lesions in Thymine Dinucleotide via Triplet Sensitization	55
5.1	Reaction Model	55
5.2	Quantum Yield Determined by Stationary Illumination	57
5.3	Oxygen Dependent Measurement	61
5.4	Time-resolved Measurement on TpT	63
5.4.1	Experimental Results	65
5.4.2	Modeling and Interpretation of the Data	65
5.5	Time-resolved Measurement on 2-M and TpT Mixtures	67
5.5.1	Low Concentration of TpT (9.16 mM)	67
5.5.2	High Concentration of TpT (18.32 mM)	69
5.6	Discussion	75
6	Formation and Deamination of CPD Lesions in Cytosine Containing Dinucleotides	77
6.1	Spectroscopic Characterization of the Dinucleotides	77
6.2	Formation of Cytosine Containing CPD Lesions	79
6.3	Deamination of Cytosine Containing CPD Lesions	80
7	Summary and Outlook	85
	List of Figures	89
	List of Tables	91
	Bibliography	93
	List of Abbreviations	105

Publications	107
Acknowledgment	109

Kurzfassung

UV-Strahlung ist eine der größten Bedrohungen für den Erhalt der genetischen Information. Der häufigste UV-induzierte Photoschaden ist das Cyclobutan Pyrimidin Dimer (CPD), welches für viele Mutationen und sogar Hautkrebs verantwortlich ist. Neueste Forschungen zeigen, dass der CPD-Schaden bei Belichtung mit UV-C und UV-B überwiegend über den angeregten Singulett Zustand eines Pyrimidins innerhalb von 1 ps gebildet wird. Der Mechanismus der CPD-Bildung über den Triplett-Kanal eines Pyrimidins ist hingegen noch nicht ausreichend verstanden, da die Interkombinationsrate zu gering ist. Um die Quantenausbeute der CPD-Bildung über den Triplett-Kanal zu quantifizieren, benutzt diese Arbeit einen neuen Photosensibilisator, der im UV-A Bereich eine sehr hohe Absorption besitzt ($\epsilon_{320} = 2560 \text{ M}^{-1}\text{cm}^{-1}$). Da der UV-A Bereich der dominante Anteil der UV-Sonnenstrahlung ist, spielt auch die CPD-Bildung über die Sensibilisierung eine wichtige Rolle.

Die Auswahl und die Charakterisierung des passenden Sensibilisators: Die üblichen Sensibilisatoren absorbieren nur schwach im UV-A Bereich ($\epsilon_{320} < 50 \text{ M}^{-1}\text{cm}^{-1}$), was eine genaue Bestimmung der Quantenausbeute erschwert und eine zeitaufgelöste Messung im MIR Bereich verhindert. In dieser Arbeit werden einige Acetophenon-Substituenten getestet. Diese substituierten Acetophenone werden mit dem Thymin-Dinukleotid TpT gemischt und bei 320 nm belichtet. Dabei kann 2'-Methoxyacetophenon (2-M) TpT über Photosensibilisierung mit hoher Effizienz in einen CPD-Schaden umwandeln. Deshalb wird 2-M als Photosensibilisator in dieser Arbeit gewählt. Seine kleine Emissionsausbeute (2.6%) aus der Fluoreszenzmessung weist auf einen effizienten nichtstrahlenden Zerfall hin. Da keine Erholung des Ausbleichens in der zeitaufgelösten Pikosekunden-Absorptionsmessung beobachtet wird, kann der nichtstrahlende Zerfall als eine Interkombination identifiziert werden.

Untersuchung der Bildung der CPD-Schäden über Sensibilisierung mit 2-M: Im Rahmen eines Reaktionsmodells wird die wichtigste Größe, die Quantenausbeute der CPD-Bildung über den Triplett-Kanal des TpT ϕ_{CPD3} , durch zwei unabhängige Methoden zu circa 4% bestimmt. Die zwei Methoden sind: 1. Eine Reihe von stationären Belichtungsexperimenten bei verschiedenen Konzentrationen. 2. Kombinierte zeitaufgelöste und stationäre Experimente bei gleichen Konzentrationen. Die relativ kleine Quantenausbeute von $\phi_{CPD3} \approx 4\%$ wird über die Energie der beteiligten Zustände erklärt. 2-M kann auch TpC und CpT über Sensibilisierung in CPD-Schäden umwandeln. Die cytosin-beihaltenden CPD-Schäden sind thermisch instabil und können durch Desaminierung mit einer Halbwertszeit von 12 Stunden in die hoch mutagenen uracil-enthaltenden CPD-Schäden übergehen.

Abstract

Ultraviolet radiation is one of the most important threats to the integrity of genetic information. The most frequent photolesion, the cyclobutane pyrimidine dimer (CPD), is considered to be responsible for many mutations and even skin cancer. Recent studies clearly show that illuminated by UV-C and UV-B light the CPD lesions are predominantly formed via the singlet excited state of the pyrimidine within 1 ps. In contrast, the mechanism of CPD formation via the triplet channel of a pyrimidine remains not well understood due to the low intersystem crossing (ISC) rate of the pyrimidines. In order to quantify the efficiency of CPD formation via the triplet channel this work uses a new photosensitizer, which has strong absorption in the UV-A range ($\epsilon_{320} = 2560 \text{ M}^{-1}\text{cm}^{-1}$). Considering that UV-A is the predominant part of the solar UV light, CPD formation through the indirect photosensitization also plays a very important role for the integrity of the genome.

The selection and characterization of a suitable sensitizer: The usually used sensitizers have very weak absorption in the UV-A range ($\epsilon_{320} < 50 \text{ M}^{-1}\text{cm}^{-1}$), which makes an exact quantum yield measurement difficult and prevents time-resolved experiments in the MIR range. In this thesis, some acetophenone substitutions with strong absorption in the UV-A range are tested. In a series of experiments different substitutions of acetophenone mixed with the thymine dinucleotide TpT are illuminated at 320 nm. Of special interest is 2'-methoxyacetophenone (2-M) which can sensitize TpT to form the CPD lesions with high efficiency. Thus, it is selected for the further investigations of this thesis. A relative low emission yield (2.6%) obtained from the fluorescence measurement indicates an efficient non-radiative decay. No recovery of the original bleach is observed in the time-resolved picosecond absorption measurement, which identifies this decay exclusively as intersystem crossing.

Using 2-M to investigate the CPD lesions formed via sensitization: A reaction model describing the CPD formation via sensitization allows to determine the most interesting quantity, the quantum yield ϕ_{CPD3} of the CPD formation via the triplet channel of TpT. It is estimated with two independent sets of experiments to be $\phi_{CPD3} \approx 4\%$. The two approaches are: 1. A set of steady state illumination measurements at various concentrations of TpT. 2. Combined time-resolved and steady state illumination measurements at same concentrations. The relative low quantum yield is explained by the energies of the triplet state and the product CPD. 2-M is also able to sensitize TpC and CpT to form the CPD lesions. The cytosine containing CPDs are thermal unstable and can undergo a deamination with a half-life of 12 hours to the highly mutagenic uracil containing CPDs.

1 Introduction

Deoxyribonucleic acid (DNA) is the most important macromolecule, which stores genetic information. Its famous structure was discovered by Franklin and Wilkins with X-ray diffraction experiments [FG53, WSW53] and interpreted by Watson and Crick as a double helix [WC53]. Nucleotides are the basic units of DNA and are composed of a sugar deoxyribose, a phosphate group and one of four nucleobases: cytosine, guanine, adenine and thymine. The two helical strands are bound with hydrogen bridges between either cytosine and guanine or thymine and adenine according to the complementary base pairing rule. A gene is a segment of DNA with 10^3 to 10^6 base pairs that encodes proteins. Gene expression is the most fundamental level at which the microscopic genotype leads to the macroscopic phenotype. It requires mainly two steps: the transcription from DNA to messenger RNA and the translation from messenger RNA to a protein. The sequence of the nucleotides along the DNA strands determines the type of the amino acids, where a set of three nucleotides (codons) correspond to a certain amino acid. The amino acid chain then folds into a protein and performs its function in the organism. Although these processes are executed with high precision, mistakes by DNA replication and transcription are still inevitable. Any alteration in the chemical structure of DNA, i.e. DNA damage, can lead to severe consequences like synthesis of nonfunctional or even toxic proteins. Those cells which accumulate too many damages end up with either cell senescence, apoptosis or unregulated cell division. The latter one is extremely hazardous, because it can lead to cancer. DNA damages can be induced by chemical attacks, UV radiations and even normal cell metabolism.

Among the different DNA damages caused by UV illumination the cyclobutane pyrimidine dimer (CPD) is the most frequent photolesion. Since the 1960s the mechanisms for the CPD formation were widely investigated [BB60]. Recently Schreier et al. showed that illuminated by UV-C and UV-B light, the formation of the CPD lesions is an ultrafast process (within 1 ps) [Sch07] and proceeds predominantly via the singlet excited state of the pyrimidine [Sch09]. This applies not only to simple model system of thymine oligonucleotide but also to isolated and cellular DNA. On the other hand, the mechanism of CPD formation under UV-A irradiation is subjected to discussions. While Douki et al. believe that in DNA the CPD lesions are mainly formed indirectly via photosensitization [Dou03], there are also strong evidences that the CPD lesions can be produced directly in DNA [Jia09, Mou10]. Comparing to the CPD lesions formed between two adjacent thymine bases, the cytosine containing CPD lesions occur much less frequently in DNA. However, cytosine containing CPDs

can easily undergo deamination and thus become uracil containing CPDs. The normal deamination under physiological conditions from a cytosine base to a uracil base happens with a halftime of 30000 years in double stranded DNA. Since the C5-C6 bond of cytosine in a CPD is saturated, the deamination is significantly accelerated to a few hours for cytosine containing CPDs [BCL95].

Fortunately, although DNA damages occur tens of thousands times per cell per day in humans [Hoe09], most lesions are immediately repaired by different mechanisms. The Nobel Prize in Chemistry 2015 was awarded jointly to Tomas Lindahl, Paul Modrich and Aziz Sancar for their pioneering contributions on mechanistic studies of DNA repair. Base excision repair (BER) repairs DNA when a base of a nucleotide is damaged, for example the deamination from cytosine to uracil. In 1974, Tomas Lindahl identified the uracil-DNA glycosylase (UNG) as the first repair enzyme responsible for the detection and excision of uracil base [Lin74]. When an incorrect nucleotide is introduced during DNA replication, it is repaired by mismatch repair, which can reduce the error frequency by about a thousandfold. Paul Modrich reconstituted DNA mismatch correction for a defined in vitro system in 1989 [LAM89] and later for human cells in 2004 [Dza04]. DNA damages induced by UV irradiation including CPD are repaired by nucleotide excision repair (NER). In 1983, Aziz Sancar reconstituted the human NER pathway with purified proteins [SR83]. In addition Aziz Sancar also found photoreactivation [SR78], which is the first discovered DNA repair mechanism. A series of DNA damages induced by UV irradiation can be reactivated in the presence of photolyase by visible light [San87a, Jor87, San87b].

Aim and outline of the thesis: This thesis focuses on the investigation of the CPD formation in the model system pyrimidine dinucleotides via photosensitization, since the complicated environment and the extremely low quantum yield prevent time-resolved measurements in the MIR range for natural DNA. The probe in the MIR range outperforms the UV-VIS range, because the molecular vibrations in the MIR contain structural information and have their own marker bands, which allow the characterization of different species and states. The primary goal is to quantify the quantum yield ϕ_{CPD3} of the CPD formation via the triplet channel of the thymine dinucleotide TpT, which was not exactly determined before. Considering the very inefficient intersystem crossing rate of TpT upon the direct excitation in the UV-C and the UV-B range, the triplet states can hardly be occupied. As a consequence, the CPD formation yield from the triplet channel cannot compete with the yield from the singlet channel. We circumvent this problem by exciting the sensitizer molecules in the UV-A range, where the absorption of DNA bases can be neglected. The sensitizer molecules undergo efficient intersystem crossing and then transfer their triplet energy to thymine upon diffusional collision. With this method, the triplet state of TpT can be effectively occupied and at the same time there is no disturbance from the singlet channel of thymine. 2'-methoxyacetophenone (2-M), which has extremely strong absorption in the UV-A range, is used as the photosensitizer in the

measurements. The quantum yield of the CPD formation via the triplet channel is determined by means of two independent approaches using both steady state and time-resolved spectroscopy in the MIR range. The CPD formation and especially the deamination of cytosine containing dinucleotides are also investigated by using 2-M. This thesis is structured as follows:

Chapter 2 explains the basic knowledge about the UV-induced damages and the photophysics of DNA bases and the photosensitizer. At first, a short overview of the DNA and RNA bases is presented. Then the photophysics and photochemistry of the DNA bases, especially the thymine base, are discussed. Different UV-induced DNA damages and their potential mutations are described as well. This chapter ends with the introduction of different types of photosensitization. The photophysics of the sensitizer acetophenone is discussed in detail.

Chapter 3 presents the principle of the time-resolved experimental setup. A Ti-sapphire laser-amplifier system provides tunable femtosecond pulses in the UV range as pump pulses and in the MIR range as probe pulses. For the measurements in the nanosecond to microsecond range, an external OPO laser system is used as pump source. Afterwards, the flow cells used for the quantum yield measurements and the data analysis procedures are introduced.

Chapter 4 describes at first the selection of an appropriate sensitizer molecule. Thereby, 2-M turns out to be a promising sensitizer due to its strong absorption in the UV-A range and its high photo-stability. Thereafter, the absorption and the emission properties of 2-M are characterized with steady state and time-resolved spectroscopy. Time-resolved absorption measurements are also performed on deuterated acetophenone for comparison.

Chapter 5 proposes a diffusion-controlled reaction model for the sensitization process. The quantum yield of the CPD formation via the triplet channel of the thymine dinucleotide TpT, ϕ_{CPD3} , is determined with two independent approaches. There are: 1. A set of steady state illumination experiments at various concentrations. 2. Combined time-resolved and steady state illumination experiments at one concentration. The time-resolved measurements in the MIR range provide additional information about the transient dynamics of 2-M and support the validity of the reaction model.

Chapter 6 extends the use of 2-M to cytosine containing dinucleotides. The formation of the CPD lesions is also observed for them. More interestingly, the de-amination process from TC-CPD to TU-CPD is quantified by measuring the time-dependent absorbance changes in the MIR range.

Chapter 7 gives the summary of this thesis and the important results and a brief outlook on further investigations.

2 Theoretical Background

This chapter deals with the fundamental theoretical knowledge for this thesis. It begins with an introduction to the nomenclature and the structure of the genetic information carrier DNA. Although upon UV excitation the major part of DNA decays through internal conversion and other deactivation channels back to the ground state, the UV-induced DNA damages cannot be underestimated. They are responsible for a series of diseases including skin cancer. The most common UV-induced DNA damages together with their formation mechanisms and potential mutation effects will be presented. In the last part, photosensitizers are discussed in detail. They can absorb the abundant UV-A irradiation and then transfer their excited triplet energy to the DNA bases and potentially lead to indirect UV damages.

2.1 The Structure of DNA and RNA

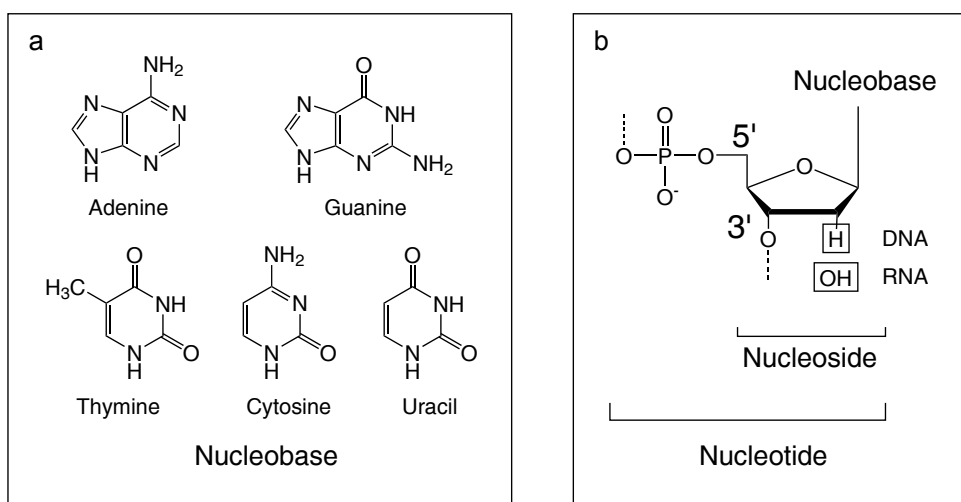


Figure 2.1: (a) The five nucleobases. Cytosine, thymine, guanine and adenine are fundamental DNA bases, in RNA thymine is replaced by uracil. (b) Schemes of nucleotide and nucleoside. A nucleoside consists of a nucleobase and a five-carbon sugar 2'-deoxyribose. A nucleotide is composed of a nucleoside and a phosphate group.

The most important macromolecule DNA is assembled as a chain of nucleotides. A nucleotide is composed of a nucleobase, a five-carbon sugar 2'-deoxyribose and a

phosphate group. A nucleobase linked via a N-glycosidic bond to the 2'-deoxyribose is called nucleoside. For a better understanding, a schematic description of the above mentioned DNA building blocks is displayed in [Figure 2.1b](#). There are two different classes of nucleobases: the single-ringed pyrimidines thymine (T), cytosine (C), uracil (U) and the double-ringed purines adenine (A), guanine (G) (see [Figure 2.1a](#)). While cytosine, adenine and guanine exist both in DNA and ribonucleic acid (RNA), thymine can only be found in DNA. Uracil which appears in RNA is similar to thymine just without the methyl group.

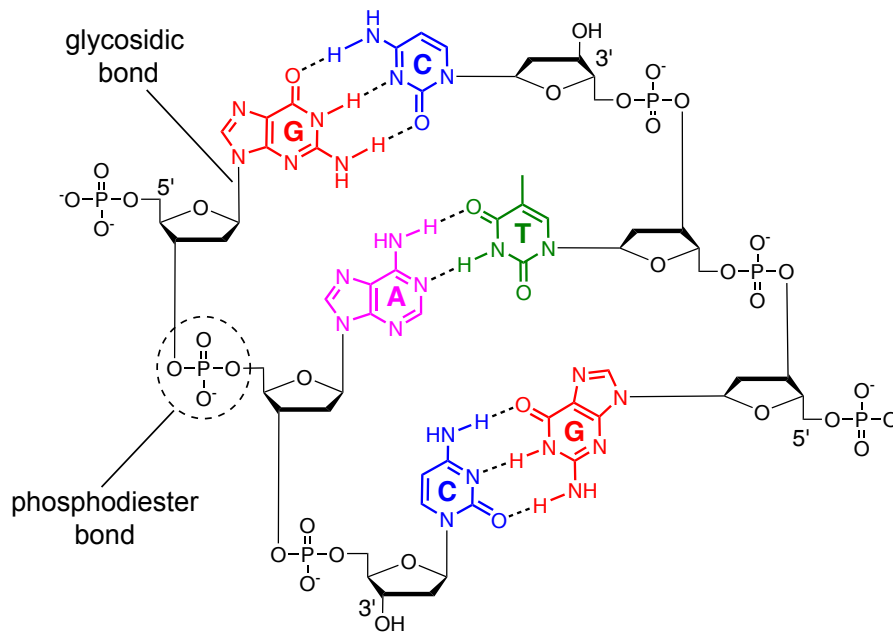


Figure 2.2: The backbone of the DNA strand is composed of alternating phosphate and sugar groups. The two strands are anti-parallel to each other. There are two hydrogen bonds between the adenine base and the thymine base, three hydrogen bonds between the guanine base and the cytosine base, which stabilize the double helix structure.

The structure of DNA was interpreted by Watson and Crick as a double helix [[WC53](#)], based on the X-ray diffraction experiments performed by Franklin and Wilkins [[FG53](#), [WSW53](#)]. Franklin, Watson and Crick shared the Nobel Prize in Physiology or Medicine 1962 for their groundbreaking contributions to the discovery of DNA structure. In organisms DNA exists usually as double strands. The backbone of the DNA strand consists of alternating phosphate and sugar groups. The 3rd carbon atom of a sugar is linked by a phosphodiester bond to the 5th carbon atom of its adjacent sugar. The asymmetric nature of the phosphodiester bond gives the DNA strand a definite direction, where the 5' end has a phosphate group as terminal and the 3' end has a hydroxyl group as terminal. The two strands coil around the

same axis in opposite directions to each other and hence are anti-parallel.

A schematic description of DNA backbones is shown in [Figure 2.2](#). The double helix structure of DNA is stabilized by two factors: the horizontal interstrand hydrogen bonding and the vertical intrastrand base stacking. According to the complementary pairing rule, adenine pairs thymine with two hydrogen bonds and guanine pairs cytosine with three hydrogen bonds (see the central part of [Figure 2.2](#)). A-T and C-G are called Watson-Crick base pairs, whose complementary nature supplies a copy of the genetic information stored in the double stranded DNA. In comparison with the weak hydrogen bond, the base stacking contributes much more to the stability of DNA structure [[YPF06](#)]. The π - π stacking between the adjacent planar aromatic bases provides attractive and noncovalent interactions.

In contrast to DNA, RNA is often found as a single strand in organisms. In RNA the complementary base for adenine is uracil instead of thymine. Another difference between RNA and DNA is the five-carbon sugar, where the 2'-deoxyribose for DNA is replaced by a ribose for RNA. The hydroxyl group at the 2' position makes RNA less stable than DNA, because it tends to hydrolysis.

2.2 DNA Photophysics and Photochemistry

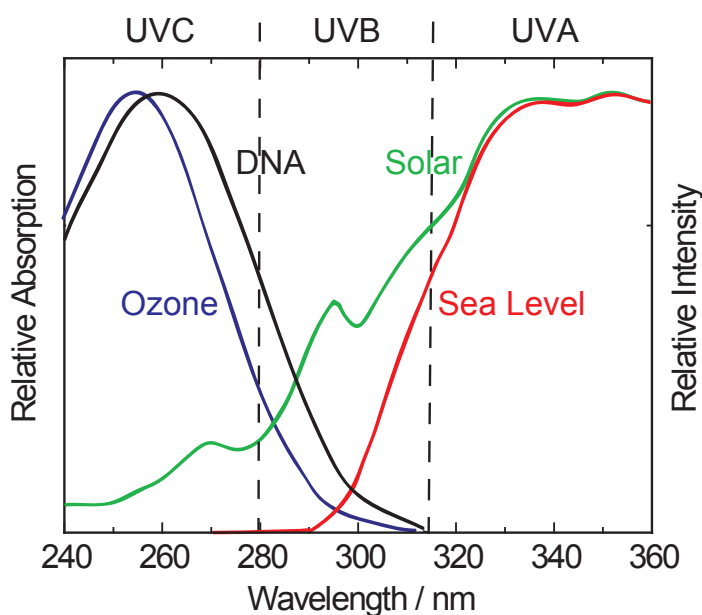


Figure 2.3: The absorption spectra of ozone (blue curve) and DNA (black curve) together with the solar irradiation spectra above the atmosphere (green curve) and at the sea level (red curve) in the UV range. The ozone layer can absorb the solar irradiation very efficiently in UV-C, partly in UV-B, but is almost transparent in UV-A. Figure adapted from W. Schreier [[Sch08](#)].

UV light can be divided into three ranges: UV-C (100 nm - 280 nm), UV-B (280 nm - 315 nm) and UV-A (315 nm - 400 nm). As can be seen from [Figure 2.3](#), DNA has very strong absorption in the UV-C and the UV-B range, but not in the UV-A. The high energetic UV-C light is extremely hazardous to DNA. It can even ionize the DNA molecules. The UV-C and the UV-B light can be strongly and partly absorbed by the ozone layer, respectively. In contrast, the ozone layer is almost transparent to the long wavelength UV-A light. The ozone layer itself is a product from the interaction between the UV irradiation and ordinary oxygen molecules. At the early period of the earth, DNA suffered crucially from UV irradiation which was much stronger without the protection by the ozone layer. As a consequence, DNA has to be inherently a photo-stable molecule. This means that natural selection has chosen those molecules as the genetic information carrier which can survive under the harsh UV exposure. The question why DNA is so photo-stable can be answered by its photophysical and photochemical properties.

2.2.1 The Basic Concepts of Photophysics and Photochemistry

In a photophysical process optical excitation leads to the same molecules as originally illuminated. A photochemical process leads to the formation of new molecules. The ground state of most molecules is usually a singlet state. This means that they have even numbered electrons oriented pairwise anti-parallel in the molecular orbitals (total spin number $S = 0$, multiplicity $2S + 1 = 1$)¹. Absorption of light can lead to the occupation of electronic excited states. There are two different kinds of transitions: the spin-allowed transitions and the spin-forbidden transitions. While after a spin-allowed transition the total spin number remains unchanged, there is a spin flip after a spin-forbidden transitions. Principally, the transition from the singlet state to the triplet state is forbidden by the selection rule. However, strong spin-orbital interactions can also induce efficient spin-forbidden transitions.

The molecules in the singlet ground state (S_0, μ'') can be optically excited to the higher electronic singlet states (S_1 or S_n, μ')². Considering the poor coupling between the same vibrational levels in different electronic states, the higher vibrational levels (μ') are often occupied which is followed by a fast vibrational relaxation to the lower vibrational levels. The vibrational energy can be dissipated through an intramolecular vibrational energy redistribution within molecules and through an intermolecular heat transfer to the surrounding solvent molecules. This process is called cooling of the vibrational hot molecules. According to Kasha's rule [[Kas50](#)], the higher singlet states (S_n) deactivate ultrafast and radiationless via vibrational

¹There are also exceptions. For example the ground state of molecular oxygen is a triplet state (total spin number $S = 1$, multiplicity $2S + 1 = 3$).

²The molecule is initially in the ground electronic state (S_0) and usually also in a low lying vibrational state μ'' .

relaxation to the first excited state (S_1). The S_1 state then either decays through a fluorescence emission to the ground state S_0 or is depopulated via a radiationless process. There are two sorts of the radiationless processes: the spin-allowed internal conversion (IC) and the spin-forbidden intersystem crossing (ISC). While internal conversion refers to the transitions between states with same multiplicity, intersystem crossing describes a spin-forbidden transition between the singlet state and the triplet state. The triplet state, which can usually not be directly excited from the ground state, either emits the long-lived phosphorescence or decays with a radiationless process back to the ground state. Figure 2.4 shows a Jablonski diagram for the above mentioned transitions and the corresponding states. The different deactivation processes contribute to the high photostability of DNA molecules.

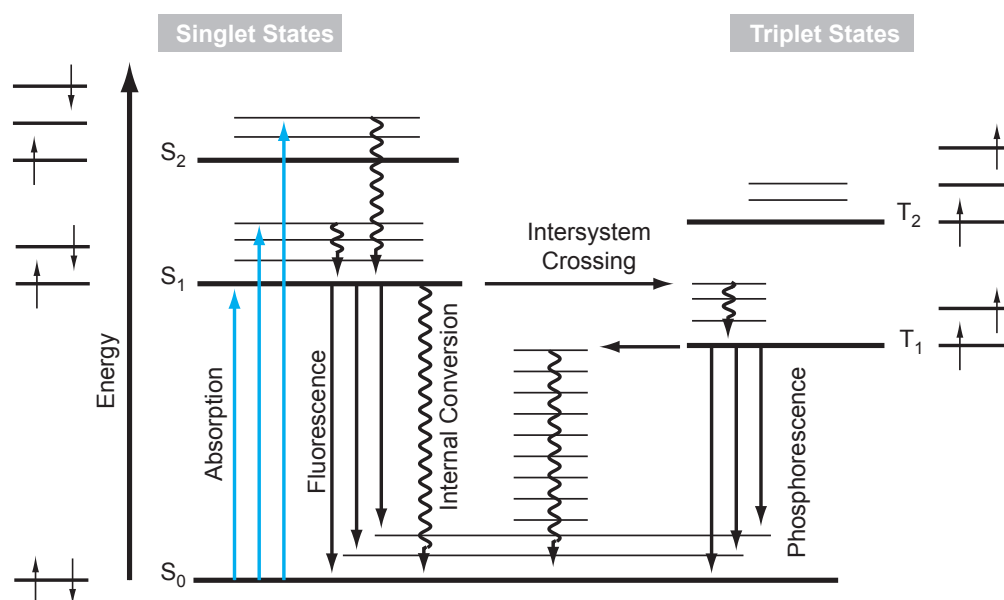


Figure 2.4: The Jablonski diagram for different transitions and states. The corresponding spin configurations are shown beside the energy levels. The solid lines and the wave-like lines represent the radiation process and the radiationless process, respectively. Figure reprinted from W. Schreier [Sch08].

Since only the nucleobases are responsible for the UV absorption of DNA, this section mainly deals with the photophysical and photochemical properties of simple bases instead of the DNA double strand³. In addition, restricted by the ability of quantum chemical calculations and the complex environment of DNA backbones, theoretical investigations focus primarily on nucleobases. The strong absorption of

³The 2'-deoxyribose and the phosphate group do not absorb in the near UV. Although they can influence the photophysical properties such as the lifetime of the singlet state, the basic processes are similar for all DNA derivatives.

nucleobases between 240 nm and 280 nm is attributed to a ${}^1\pi\pi^*$ transition, where an electron initially in the bonding π orbital is excited to the anti-bonding π^* orbital. Another common transition is the ${}^1n\pi^*$ transition, where an electron is moved from a non-bonding electron pair to a π^* anti-bonding orbital. The non-bonding electron is usually located on a heteroatom, for example on the oxygen atom of a carbonyl group. The ${}^1n\pi^*$ transition has a relatively weak oscillator strength and can be rarely excited directly.

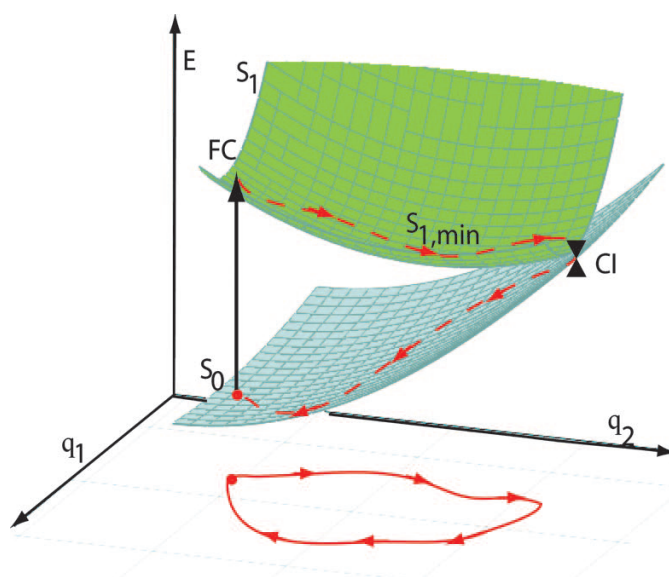


Figure 2.5: A schematic description of a radiationless decay path. S_0 and S_1 represent the ground state and the lowest singlet excited state, respectively. Upon optical absorption the molecule is excited to the Franck-Condon region of its excited state. It can undergo an ultrafast and efficient decay to the ground state through a conical intersection (CI) (reprinted with permission from Hare et al. [HCK07] Copyright (2007) National Academy of Sciences, U.S.A.).

Upon the ${}^1\pi\pi^*$ transition most bases undergo an ultrafast and efficient internal conversion back to the ground state. This is associated with a conical intersection (CI). A conical intersection is a region where two potential energy surfaces intersect. In the proximity of this region Born-Oppenheimer approximation breaks down and non-adiabatic processes take place. A schematic description of CI is shown in Figure 2.5. At first, an electron is excited vertically from the ground state (S_0 , blue surface) to the excited state (S_1 , green surface) according to the Franck-Condon principle. Along the reaction coordinates q_1 and q_2 , this electron reaches a conical intersection and then undergoes an ultrafast and efficient internal conversion back to the ground state. It is worth noting that the CI region is not necessarily a local energy minimum. The short lifetime of the excited state of DNA bases (several hundreds fs) results from the fact

that there is no energetic barrier between the CI region and the Franck-Condon region.

2.2.2 Photophysics of Thymine Derivatives

In this section we focus on the photophysics of thymine derivatives, because the cyclobutane pyrimidine dimer (CPD) lesions occur most probably between two thymine bases in DNA. Thymine nucleotide (TMP), thymine dinucleotide (TpT) and thymine oligonucleotide ((dT)₁₈) are widely used as model molecules for the investigation of direct and photosensitized CPD formation.

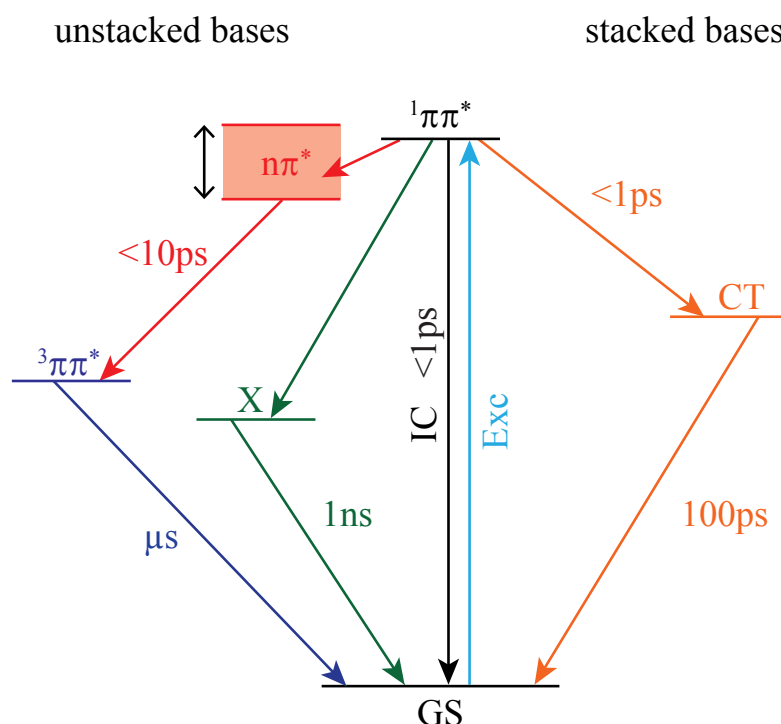


Figure 2.6: The different excited states of thymine. Upon the UV absorption the singlet excited state $^1\pi\pi^*$ is occupied. The major part of the excited molecules decays ultrafast to the ground state. The unstacked bases in TpT and (dT)₁₈ behave like the monomer TMP. For the unstacked bases, population and decay of an unknown state 'X' and the triplet state $^3\pi\pi^*$ are observed (the left part). For the stacked bases in TpT or (dT)₁₈, there exists an additional channel leading to the charge transfer state (the right part).

A schematic description of the reaction model for the monomer TMP dissolved in a deuterated water solution is shown in the left part of Figure 2.6. Upon excitation at 266 nm the singlet excited state $^1\pi\pi^*$ is occupied. Thereafter, most excited molecules return to the ground state through an ultrafast (within the first 1 ps) internal con-

version. Beside that, the population of the $^3\pi\pi^*$ state through a fast intersystem crossing (within the first 20 ps) and an unknown state 'X' (decay with circa 1 ns to the ground state) are observed as well [Pil16]. Kohler et al. also suggest a fast intersystem crossing leading to the $^3\pi\pi^*$ within the first 10 ps in deuterated acetonitrile solution [Har08]. Considering the poor spin-orbital coupling between electronic states with the same geometric configuration, $n\pi^*$ states functioning as intermediates are expected according to El-Sayed's rule [Say63]. While the ISC efficiency varies for solvents with different polarity⁴, the quantum yield of the state 'X' (circa 10%) remains almost unaffected by the solvents. The population of the $n\pi^*$ states and the ISC efficiency depend also strongly on the polarity of the solvent. Therefore, the $n\pi^*$ states are considered as the precursors for the $^3\pi\pi^*$. Their energetic accessibility in solvents with different polarity is responsible for the solvent dependence of ϕ_{ISC} (see the red box in Figure 2.6). The nature of the state 'X' is still a matter of discussion. The oligomer (dT)₁₈ is composed of two distinct classes depending on the relative orientation between the adjacent bases. On the one hand, the unstacked bases behave just like the monomer TMP as described above. On the other hand, the stacked bases are inclined to form a delocalized charge transfer state from the $^1\pi\pi^*$ state with a quantum yield of 7% [Pil14a]. A scheme describing the charge transfer state is demonstrated in the right part of Figure 2.6. The charge transfer states between hetero bases in DNA strands are well characterized by D. Bucher et al. [Buc14]. Their occurrence is explained by the different redox potentials of the DNA bases. The guanine base has the lowest oxidation potential among the DNA bases. As a consequence, guanine radical cation (G^+) can be formed in DNA strands with highest probability. Recent studies by B. Pilles et al. also suggest the formation of the charge transfer state between two identical DNA bases (here two thymine bases in (dT)₁₈) [Pil14a]. The charge transfer state is formed within the first 1 ps probably directly from the $^1\pi\pi^*$ state and decays with a time constant of circa 100 ps to the ground state.

It is also worth noting that the possibility for TpT or (dT)₁₈ to form the CPD lesions is substantially higher than that for TMP, because the excited thymine base has directly one (for TpT) or two (for (dT)₁₈) thymine bases in their neighborhood. In contrast, the excited TMP molecule has to undergo a long diffusion process to find another TMP molecule. The lifetime of the singlet excited state $^1\pi\pi^*$ is much shorter than the time of diffusion. Thus, CPD formation via the excited singlet state of TMP is negligible.

⁴Upon the excitation at 266 nm, ϕ_{ISC} for TMP in deuterated water and in deuterated methanol is 1.4% and 10%, respectively.

2.3 UV-induced DNA Damages and Mutations

DNA possesses different deactivation mechanisms for the UV excitation. However, the UV irradiation is still a major threat to the integrity of DNA. From the last section we know that the absorption spectra of the DNA bases partly overlap with the solar irradiation spectra in the UV-B range. As a consequence, the most frequent damages occurring after the direct UV-B illumination include the Cyclobutane Pyrimidine Dimer (CPD) and the (6-4) photoproduct, which contribute to 75% and 25% of all photolesions, respectively [SH02]. The DNA bases absorb very weakly in the UV-A range. However, protection against the UV-A irradiation is also necessary. Since the (6-4) photoproduct absorbs efficiently in this range and becomes a Dewar Lesion via a secondary photoreaction. In addition, there are also various DNA damages induced indirectly by absorption via photosensitization. For example, CPD lesions and 8-Oxo-2'-deoxyguanosine are found in DNA upon UV-A irradiation [Dou03]. If the UV induced DNA damages are not detected and repaired, they can cause mutations. The above mentioned DNA damages, their formation and mutation mechanisms will be discussed in detail.

2.3.1 Cyclobutane Pyrimidine Dimer

The cyclobutane pyrimidine dimer (CPD) is the most frequent photolesion in DNA induced by UV irradiation [Dou00, Yoo00]. It occurs through a $[2\pi+2\pi]$ cycloaddition of the C5=C6 double bonds between two adjacent pyrimidine bases. Figure 2.7a displays a schematic description of this reaction. Four different stereoisomers can be formed, namely cis-syn, trans-syn, cis-anti and trans-anti [Cad85] (see Figure 2.7b). Both anti conformations can not be found in DNA due to steric constraints imposed by the backbone. While the occurrence of the trans-syn isomer is very low in single stranded DNA, there is almost exclusively the cis-syn isomer in double stranded DNA [RDC01]. Under UV-B irradiation the distribution for all different CPD lesions in natural DNA follow the order 5'-TT-3' > 5'-TC-3' > 5'-CT-3' > 5'-CC-3'. The ratio is 8 : 5 : 2 : 1 for cellular DNA (keratinocytes) [Mou06] and 11 : 7.5 : 3 : 1 for isolated DNA (calf thymus) [DC01], respectively. The situation becomes different in the UV-A range, where TT-CPD is generated with large predominance for both direct UVA-irradiated human keratinocytes [Mou10] and sensitized ⁵ UVA-illuminated calf thymus [Dou03].

The CPD lesions were already discovered in the 1960s [BB60]. However, the mechanism underlying their formation remained controversial for a long time. For direct UV-C and UV-B excitation, Kwok et al. suggested that the triplet state is a precursor for the CPD lesions [KMP08]. Schreier et al. unambiguously showed that the formation of CPD lesion occurs predominantly via the excited singlet state within

⁵Acetophenone and benzophenone were used as photosensitizer.

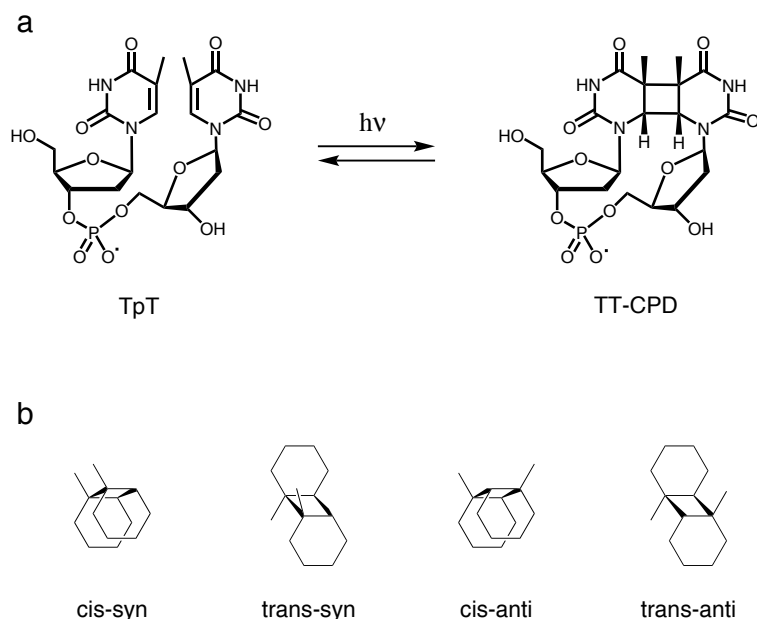


Figure 2.7: (a) The formation of the CPD lesion via a $[2\pi+2\pi]$ cycloaddition of the C5=C6 double bonds between two adjacent thymine bases. (b) Four possible stereoisomers of CPD lesions.

1 ps [Sch07, Sch09]. Although upon UV excitation the intersystem crossing efficiency of TMP is relative low (1.4% at 266 nm), the triplet state was often considered as a precursor for the formation of the CPD lesions. Thymine has the lowest triplet energy among all DNA bases [GWR96]. Due to the base stacking effect, the triplet energy of thymine base in the dimer TpT or the oligomer (dT)₁₈ is even lower than in the monomer TMP [Bos06]. As a consequence, thymine bases serve as the main target of photosensitization via triplet-triplet energy transfer (TTET) in DNA strands and can form the CPD lesions [LY67, GJ68]. The triplet channel becomes particularly important in the UV-A range, where the direct absorption of DNA bases can be neglected but a number of photosensitizers exist in natural systems. This will be discussed in detail later in section 2.4.

The TT-CPD lesion is principally not strongly mutagenic. However, it can block the DNA polymerase, which is responsible for the transcription and replication of DNA [TK93]. If it is not repaired, it can lead to cell death. The cytosine containing CPD lesions are more mutagenic than the thymine derivatives despite of their low occurring frequency. They can often lead to a C→T or a CC→TT mutation. Figure 2.8 demonstrates two possible mutation pathways using a CC-CPD lesion as example. One alternative is explained by the deamination from cytosine bases to uracil bases.

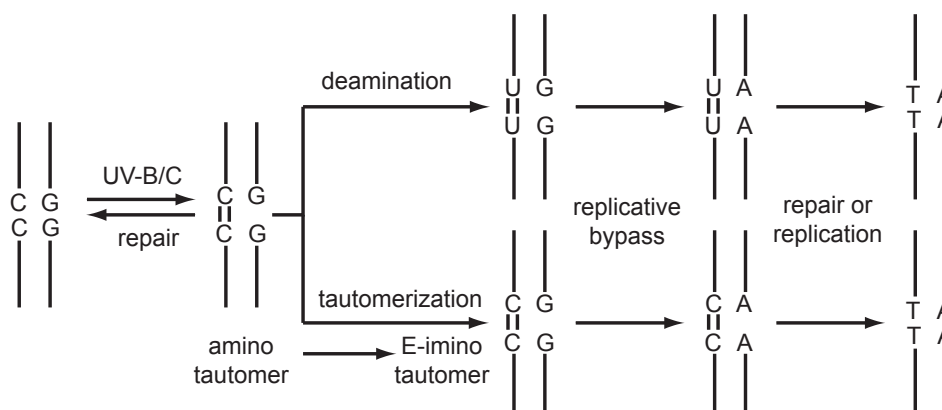


Figure 2.8: Two possible pathways can lead to the CC→TT mutation for a CC-CPD lesion. It arises either due to the deamination of cytosine or due to the tautomerization from amino form to E-imino form. For both situations the CPD lesions are bypassed in the replication. Figure adapted from W. Schreier [Sch08].

When the C5=C6 double bond of cytosine is saturated, the deamination process is greatly accelerated compared to a normal cytosine base [BCL95]. In DNA under physiological conditions the deamination for a normal cytosine base is a very slow process. At 37 °C and pH 7.4 it occurs with a half-life of about 200 and 30000 years in single stranded and double stranded DNA, respectively [FKS90]. In comparison the deamination for a cytosine containing CPD lesion happens with a half-life of several hours at the same conditions [GC57]. After the deamination the CPD lesion can be detected and bypassed by DNA polymerase η in the DNA replication process [JPP99, Mas99]. However, two adenine bases instead of two guanine bases are incorporated by the replicative bypass. In the subsequent replication or repair the original CC-CPD is replaced by two thymine bases. Thereby a CC→TT mutation is induced upon deamination and the subsequent replicative bypass. Another explanation is based on the tautomerization of the cytosine base in a CPD lesion, where the normal amino form is converted to the E-imino form [JT93]. The E-imino tautomer can also be bypassed in replication leading to pair with two adenine bases. Thus, the same CC→TT mutation occurs.

2.3.2 (6-4) Photoproduct and Dewar Lesion

Besides the most frequent CPD lesions, the (6-4) photoproduct is another common DNA damage induced by UV-C and UV-B irradiation, which contributes to circa 25% of all photolesions [SH02]. Figure 2.9 demonstrates a schematic description of the reactions for TpT. The (6-4) photoproduct is formed upon UV excitation via a Paterno-Büchi reaction between the C5=C6 double bond of one pyrimidine and the C4=O carbonyl group of the adjacent pyrimidine [BIL54]. For TpT it is formed

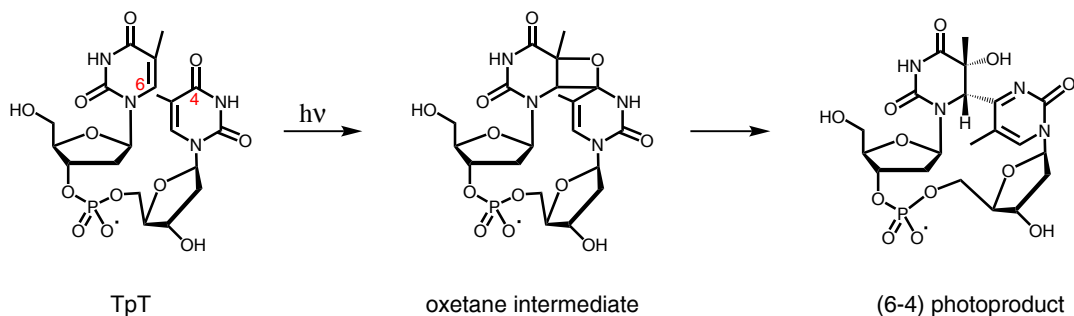


Figure 2.9: The mechanism of (6-4) photoproduct formation for a TpT molecule. Upon excitation an oxetane intermediate is formed between the C5=C6 double bond of one thymine and the C4=O carbonyl group of another thymine. The unstable intermediate undergoes rearrangement and becomes a (6-4) photoproduct.

via a four-membered oxetane ring [VW68]. For TpC it is formed from the (E)-imino tautomer of cytosine via a four-membered azetidine ring [WV67]. The intermediated oxetane or azetidine ring is not stable. They rearrange through ring opening to the final (6-4) product [Tay94, RDC01]. The yields of all different (6-4) products induced by UV-B irradiation follow the order 5'-TC-3' > 5'-TT-3' > 5'-CC-3' > 5'-CT-3' with a ratio of 150 : 25 : 10 : 1 for isolated DNA (calf thymus) [DC01]. Under UV-A illumination, no detectable (6-4) products are observed for all four derivatives [Dou03, Mou06, Mou10].

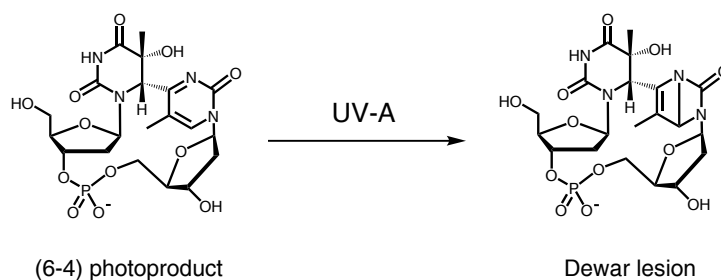


Figure 2.10: Scheme depicting the formation of Dewar lesion from a (6-4) photoproduct.

The (6-4) product has a unique absorption band around 320 nm. Upon irradiation of UV light over 300 nm the (6-4) lesion undergoes a secondary photoreaction and becomes a Dewar lesion. The Dewar lesion is formed by a 4π -electrocyclic ring closure reaction of the (6-4) pyrimidone ring (see Figure 2.10) and has a heterocyclic version of the bicyclic structure of benzene proposed by Dewar in 1867 [Dew69].

Time-resolved absorption measurements show that the Dewar lesion is formed directly from the excited state with a time constant of 130 ps and a relative high quantum yield of 8.2% [Hai12b]. The backbone structure of the DNA is necessary for this reaction by preventing the C4 rehybridization and the subsequent internal conversion back to the reactant [Hai12b].

The (6-4) product is very mutagenic, especially for the TT derivative. Figure 2.11 shows a schematic description for a T→C mutation. The 3' thymine of the (6-4) product can be bypassed in the replication and tends to pair with a guanine base [LBL91, LHC99]. Then in the subsequent replication or repair process a cytosine is incorporated as complementary base and thus leads to a T→C mutation. In contrast, the Dewar lesion is less mutagenic. The repair enzyme perceives the Dewar lesion as an abasic site. DNA polymerases tend to built in an adenine base when they read an abasic site [LBC00]. This process is called as A-rule [Tay02] and can potentially cause mutations.

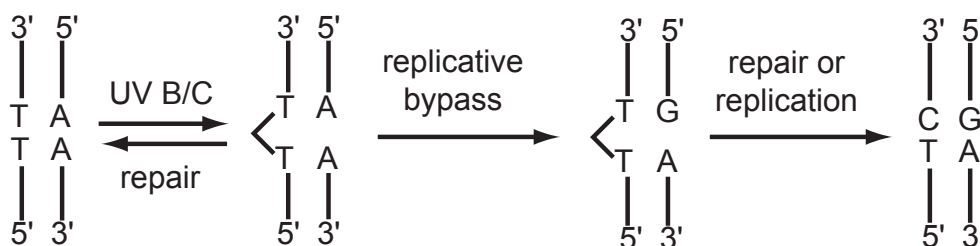


Figure 2.11: A schematic description for a T→C mutation of a TT (6-4) product occurring in the DNA replication process. Figure adapted from W. Schreier [Sch08].

2.3.3 Oxidative Damages

The oxidative damages have a different formation mechanism as the above described dimer lesions. Normal cell metabolism can generate reactive oxygen species (ROS), including peroxide (O_2^{2-}), superoxide (O_2^-), hydroxyl radical (OH^\cdot), and singlet oxygen (1O_2), which can lead to oxidative damages. Normal cellular processes are considered as the background level of oxidative DNA damage in cells [COO03]. The ROS level in cells can also be greatly enhanced upon UV-A irradiation. Guanine is the major target of ROS due to its highest oxidative potential among the four DNA bases. More than 20 oxidative damages are identified so far [COO03]. Among them 8-Oxo-2'-deoxyguanosine (8-oxo-dG) draws the most attention and is intensively investigated. 8-OH-dG refers to the same damage, where the keto form 8-oxo-dG can undergo a tautomerization to the enol form 8-OH-dG (see Figure 2.12). Recent investigations by Yasui et al. show that circa 14% of 8-oxo-dG undergo mutations, where the G:C to T:A transversion with a frequency of 5.9% plays the most important role [Yas14]. In addition, the concentration of 8-oxo-dG is an important measure of

oxidative stress in the human body [YOK02, Hag05]. Oxidative stress is associated with many diseases and cancers.

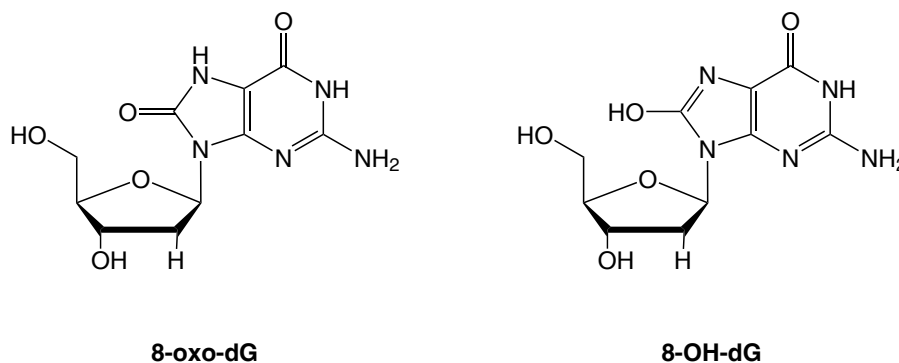


Figure 2.12: The structure of 8-oxo-dG (keto tautomer) and 8-OH-dG (enol tautomer).

2.4 Photosensitization

Acetophenone and benzophenone are widely used as triplet sensitizers for thymine bases [LY67, GWR96, Cuq12]. The energy levels and the configuration of the triplet states of acetophenone [HSF13] and benzophenone [Ser14] and their interaction with DNA [Hui15, DM13, Dum15] have been intensively investigated in recent years.

2.4.1 Different Types of Photosensitization

Photosensitization is a process in which a molecule called sensitizer absorbs the photon energy and activates the reaction of another molecule called substrate. Depending on the mechanism of this activation, there are basically three kinds of photosensitization: type I is based on electron transfer, type II is based on the generation of singlet oxygen which can oxidize other molecules (in DNA mostly guanine) [Foo91]. A third mechanism involves a triplet-triplet energy transfer (TTET) from the sensitizer to the substrate molecules (type III). In all photosensitization processes, the sensitizer (S) is excited by absorption of a photon.



The molecule oxygen is often involved in photosensitization. Below, molecule oxygen will serve as an example to explain the difference between type I and type II reactions. For a type I reaction, the excited sensitizer molecule (S^*) reacts with the substrate molecule (R) via an electron transfer to form radicals. Although the electron transfer can take place in both directions, usually a sensitizer anion radical ($S^{\cdot-}$) and a

substrate cation radical (R^+) are generated (see equation 2.2). $S^{\cdot-}$ can further react with molecule oxygen and produce the extremely reactive superoxide radical anion ($O_2^{\cdot-}$) (see equation 2.3), which is responsible for many DNA oxidative damages.



For a type II reaction, the excited sensitizer molecule (S^*) reacts with O_2 via an energy transfer to generate another extremely reactive oxygen species, the singlet oxygen (1O_2) (see equation 2.4). 1O_2 can further react with substrate molecule (R) and induce oxidative damages (R') (see equation 2.5). Unlike most organic molecules whose ground states are singlet states, O_2 in its ground state has two parallel unpaired electrons and therefore its ground state is a triplet state.



The type III reaction deals with a TTET process. In general, the molecule oxygen has not to be involved in this TTET process. In the presented experiments the high concentration of nucleobases (much higher than the concentration of O_2) makes DNA bases the most important TTET acceptors. According to the research of Douki et al. CPD lesion rather than 8-oxo-dG is the main type of DNA damages upon solar UV-A radiation [Dou03]. The ratio between these two photoproducts is 10:3. Notably, in contrast to the UV-B, the UV-A generates CPD lesions with a predominance of TT-CPD. This strongly suggests a TTET from sensitizer to thymine, because among the four DNA bases thymine has the lowest triplet energy [Lam67].

2.4.2 Acetophenone

In this section we focus on the molecule acetophenone (see Figure 2.13a for its structure) which is known for its ability to sensitize thymine via TTET. Acetophenone also serves as the model molecule for photosensitizers in this thesis. Figure 2.13b shows the absorption spectrum of acetophenone dissolved in deuterated water. It has a main absorption band at 245 nm and a weak absorption shoulder around 280 nm. While the band at 245 nm is assigned to an intramolecular charge transfer [TNK56, Leo81], the shoulder around 280 nm is attributed to a $^1\pi\pi^*$ transition localized at the phenyl ring [TNK56, KN65]. Between 300 nm and 340 nm there is another weak absorption band which arises from $^1n\pi^*$ transitions in the carbonyl group [McM41, TNK56]. Notably, the 300 nm to 340 nm band corresponds to the excitation to the Franck-Condon region, where the excitation from S_0 to S_1 is vertical.

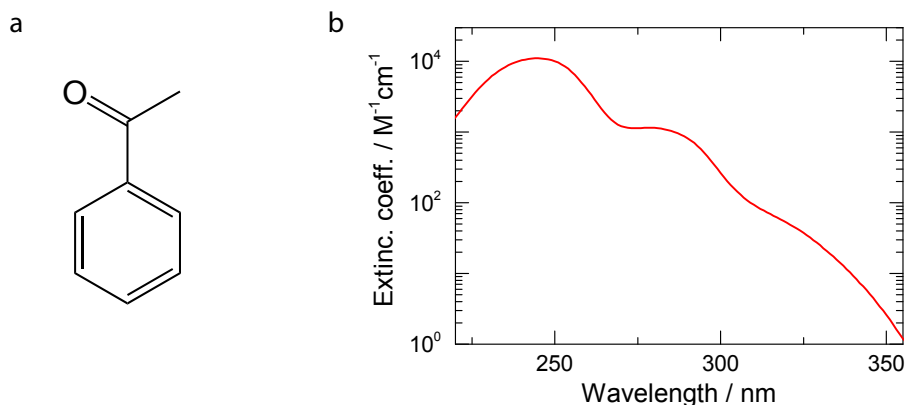


Figure 2.13: (a) The structure of acetophenone. (b) Extinction coefficient of acetophenone. The main absorption band at 245 nm and the weak absorption shoulder around 280 nm are assigned to an intramolecular charge transfer and a $^1\pi\pi^*$ transition localized at the phenyl ring, respectively. The non-vanishing absorption band above 300 nm is due to a $^1n\pi^*$ transition in the carbonyl group.

Exact values of the energy levels are obtained by measurements on isolated jet-cooled acetophenone (see Table 2.1). Its S_1 state lies $27\,279\text{ cm}^{-1}$ [OSI88] and the S_2 lies $35\,402\text{ cm}^{-1}$ above the S_0 state [WB86]. Limited by the inherent weak direct absorption from the singlet ground state to the triplet state, the $S \rightarrow T$ transition cannot be conveniently measured by absorption spectroscopy. The phosphorescent excitation method developed by Kearns et al. provides a reliable technique for the determination of the triplet state energy levels of crystallized acetophenone [KC66, CK70]. A value of $26\,396\text{ cm}^{-1}$ is reported for the T_1 ($^3n\pi^*$) state. A similar value of $25\,791\text{ cm}^{-1}$ is reported by Ohmori et al. on isolated jet-cooled acetophenone [OSI88]. The blue shift of circa 600 cm^{-1} is assigned to the influence of the crystal field. It is also predicted that there is another close lying triplet state T_2 ($^3\pi\pi^*$), which is located circa 300 cm^{-1} below T_1 both in crystallized acetophenone and in isolated acetophenone [CK70, OSI88]. However, the ordering of these two triplet states strongly depends on the external environment. For example, in polar solution the energy level of T_2 ($^3\pi\pi^*$) is higher than T_1 ($^3n\pi^*$) [LBL73]. We can conclude that T_2 and T_1 of acetophenone are quasi degenerate either in isolated form or in solution. The excited state energies of acetophenone are summarized in Table 2.1. Both the S_1 state and the T_1 state of acetophenone have $n\pi^*$ electronic configurations. Therefore, spin-orbital coupling is expected to be small for the direct $S_1 \rightarrow T_1$ transition. The efficient ISC from S_1 to T_1 for acetophenone in solution is explained by the dense vibrational states supplied from phonons of the environment [OSI88]. However, although the phonons are absent in isolated acetophenone, efficient ISC from S_1 to T_1 is still observed. It is assumed that the T_2 contributes with its $^3\pi\pi^*$

State	Transition	E(cm ⁻¹)	λ(nm)
S_1	$^1n\pi^*$	27279	366.6
S_2	$^1\pi\pi^*$	35402	282.5
T_1	$^3n\pi^*$	25791	387.7
T_2	$^3\pi\pi^*$	~	~

Table 2.1: The excited states energies and corresponding wavelengths measured on isolated jet-cooled acetophenone. The values of S_1 and T_1 are taken from [OSI88], the values of S_2 are reported by [WB86]. There are no exact values for the T_2 state, which is believed to lie circa 300 cm⁻¹ below the T_1 state.

configuration to the ISC. Fang et al. suggest that there exists a $S_1/T_1/T_2$ intersection, at which these three levels are degenerated [FP02] (see Figure 2.14). The $S_1/T_1/T_2$ intersection is predicted to be only circa 5 kcal/mol above the minimum of S_1 [Fan08]. Upon the excitation to the Franck-Condon region of the S_1 state, the excited molecules can easily reach the $S_1/T_1/T_2$ intersection. At this intersection an efficient $S_1 \rightarrow T_2$ intersystem crossing is followed by a quick $T_2 \rightarrow T_1$ internal conversion. As a consequence, a $S_1 \rightarrow T_1$ transition takes place via the T_2 state. Besides this $S_1/T_1/T_2$ intersection, Rotllant et al. propose that at the Franck-Condon region of the S_1 state, T_2 and S_1 are quasi degenerate [HSF13]. At this region an efficient intersystem crossing can also occur.

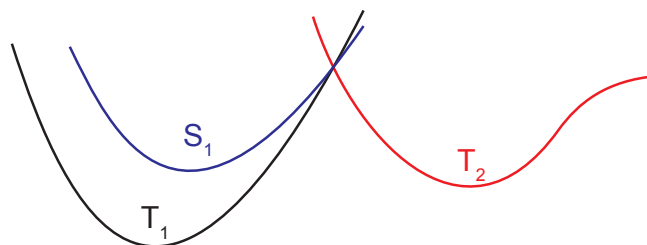


Figure 2.14: The $S_1/T_1/T_2$ intersection is probably responsible for the efficient ISC from S_1 to T_1 in isolated acetophenone.

The triplet population of acetophenone strongly depends on the initial excited singlet state [HSF13]. Excitation to the S_1 state (corresponds to the absorption band between 300 nm and 340 nm) leads to a very efficient (almost unity) intersystem crossing to the triplet states. This is the reason why most of the photosensitization experiments using acetophenone are performed in this wavelength range. In contrast, excitation to the S_2 state (corresponds to the shoulder around 280 nm) results in a

population of the triplet states with significant lower efficiency and the excess energy can lead to photocleavage reactions [WB86, PFZ06].

Theoretical investigations by using molecular dynamics and quantum mechanics/molecular mechanics show that the features of the triplet states for acetophenone in gas phase are also conserved in the macromolecular environment [Hui15]. Therefore, an efficient and fast intersystem crossing from the singlet state to the triplet state is expected to occur in DNA strands as well.

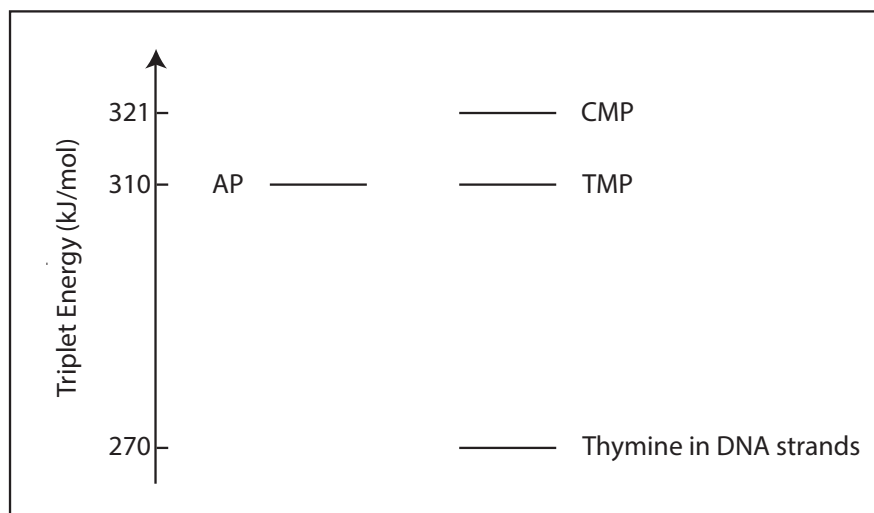


Figure 2.15: Triplet energy of acetophenone, CMP, TMP and thymine in DNA strands [WR96, Bos06].

The triplet energies of acetophenone, CMP and TMP measured in aqueous solution at room temperature are shown in Figure 2.15. Both acetophenone and TMP have a value of circa 310 kJ/mol. The triplet energy of CMP, UMP, GMP and AMP are 321 kJ/mol, 320 kJ/mol, 317 kJ/mol and 314 kJ/mol, respectively [WR96]. Thus, efficient TTET by using acetophenone as sensitizer is only observed for TMP. Notably, the triplet energy for thymine in DNA strands (270 kJ/mol) is significantly lower than in TMP [Bos06]. As a consequence, thymine in DNA strands can be sensitized much easily.

3 Experimental Methods

In this chapter the experimental methods used in the context of this thesis will be discussed. The first part deals with the UV-pump MIR-probe spectroscopy for the time-resolved measurements. Depending on the measuring time range different laser systems are used as pumping sources. The second part presents the sample circulation setup for the quantum yield measurements.

3.1 Pump-probe Spectroscopy

The time-resolved experimental setup has already been described in detail in several theses [Sch08, Hai12a]. In this section a short overview of the UV-pump MIR-probe absorption spectroscopy will be presented.

3.1.1 Principle of the UV-pump MIR-probe Spectroscopy

A schematic description of the pump-probe setup is demonstrated in [Figure 3.1](#). For the time-resolved measurements in different time ranges, either a femtosecond laser system (Spitfire Pro, Spectra Physics) or a nanosecond laser system (NT242, Ekspla) serves as pumping source. The sample molecules are excited by the pump pulses into their excited states. Their absorption properties are different as in the ground state, because the electronic configuration changes. At a certain delay time their excited states are probed by the temporally delayed probe pulses. Depending on the probing wavenumbers and delay times, the probe pulses undergo transmittance changes with different strength. The transmitted probe pulses are then spectrally separated in the spectrometer (Chromex 250 IS, Bruker) and recorded by a 64-channel mercury cadmium telluride (MCT) array detector (IR-0144, Infrared Systems Development). At the end, the signals are amplified and converted to absorbance changes.

The time delay in the ps to ns range is achieved by a mechanical delay stage (length 30 cm). The stage consists of a set of mirrors, two of them are movable. The light pulses propagate four times between the mirrors. Each distance between the movable mirrors and the stationary mirrors corresponds to a certain delay time. The mechanical delay stage is not suitable for the time delay in the ns to μ s range. A time delay of 4 ns corresponds to an optical path of 1.2 m. For a delay stage with a four-time folded light path, a minimal length of 30 cm is required. Since the optical elements in our setup are compactly assembled, there is not enough space for a larger

stage. In addition, the alignment of the optical pathways becomes more difficult with an increasing delay distance. At later delay times, the risk of losing the spatial overlap between the pump pulses and the probe pulses becomes significantly higher. Therefore, the delay in the ns to μ s range is realized by a separate pump laser and electronic control. In the following, the pump pulses at 320 nm for the measurements in different time ranges and the generation of the MIR probe pulses will be described in detail.

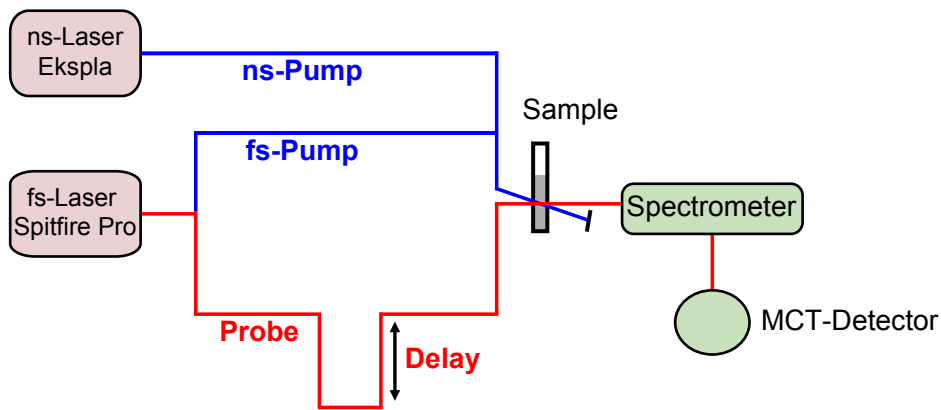


Figure 3.1: The principle of the UV-pump MIR-probe absorption spectroscopy. For measurements in the ps to few ns time range, the fs-pump pulses are generated by a two-stage NOPA from the fs-laser system Spitfire Pro and the time delay is achieved by a mechanical delay stage. For measurements in the ns to μ s time range, the ns-pump pulses are supplied by the ns-laser system NT242 from Ekspla and the time delay is electronically controlled. The transmitted probe pulses are spectrally separated in a spectrometer and recorded by a MCT detector array.

3.1.2 Generation of Probe Pulses in the MIR Range

The generation of the probe pulses in the MIR range is schematically shown in [Figure 3.2](#). It consists of three nonlinear optical processes. The fundamental pulses at the output of Spitfire Pro have a wavelength of 800 nm and a duration of 100 fs. The beam is divided into two optical pathways by a beam splitter. The major part is used for the first part of the nonlinear optical processes, a non-collinear optical parametric amplifier (NOPA) [[Rie00](#)]. At first, the 800 nm pulses propagate through a telescope to reduce their beam diameter. Thereafter, a small part (4%) is reflected and focused on a sapphire crystal (SA) to generate the white-light continuum (WL). An iris diaphragm (ID) and a variable attenuator (VA) are used for the optimization of the WL. The dominant part of the 800 nm pulses is frequency-doubled in a beta barium borate (BBO) crystal (Type I, $\theta = 29^\circ$) to produce second harmonic pulses

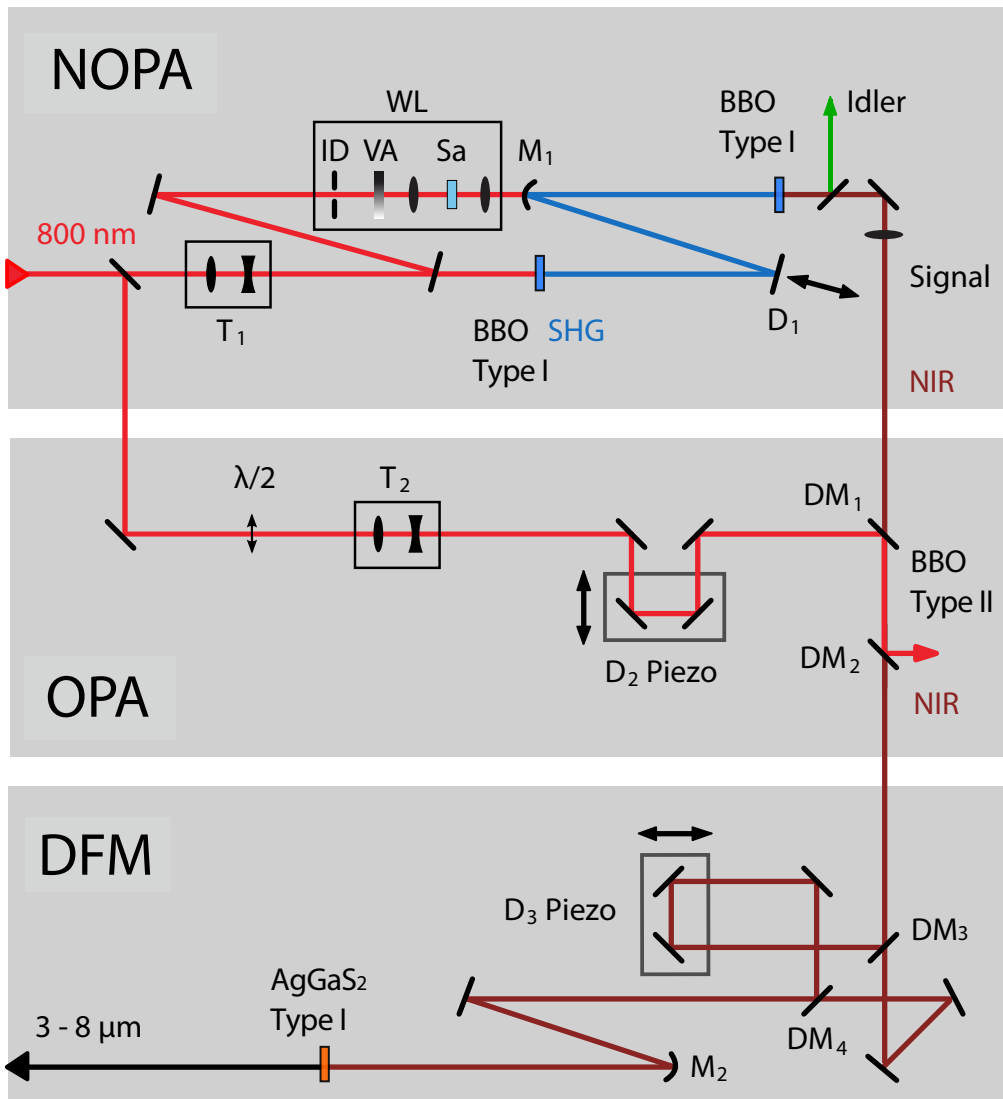


Figure 3.2: The setup for the probe pulse generation in the MIR. In the first step, NIR pulses at 1400 nm are generated by a NOPA from the SHG 400 nm pulses and white light. In the second step, NIR pulses at 1800 nm are generated by an OPA from the original 800 nm pulses and the NIR pulses at 1400 nm. These two NIR pulses are then frequency mixed in a AgGaS₂ crystal to generate the MIR probe pulses ranging from 5-8 μm . Figure adapted from K. Haiser [Hai12a].

(SHG) at 400 nm. At the end of the conversion process the SHG pulses and the WL pulses are temporally and spatially overlapped in a BBO crystal (Type I, $\theta = 32.5^\circ$) to generate the desired NOPA pulses. The temporal overlap is controlled by a delay stage (D_1). It is worth noting that in order to suppress the group velocity dispersion, the SHG pulses and the WL pulses propagate not collinearly in the BBO crystal. The outgoing NOPA wavelength can be tuned by the phase-matching angle. In

the BBO crystal the NIR component (1400 nm) is amplified and another pulses at 560 nm are generated according to energy conservation. These idler pulses are reflected on a spectrometer and a photodiode to monitor the NOPA process.

In the second part, the NIR pulses at 1400 nm are further amplified by an optical parametric amplifier (OPA). This time a portion of the fundamental pulses at 800 nm serves as pumping source and is collinearly overlapped with the pulses at 1400 nm in a BBO crystal (Type II, $\theta = 27^\circ$). The temporal overlap is tuned by a piezoelectric delay line (D_2 Piezo). In the OPA the 1400 nm pulses are amplified and as a consequence of energy conservation NIR pulses at 1800 nm are produced.

In the third part, the NIR pulses at 1400 nm and at 1800 nm are at first separated by a dichroic mirror (DM_3) and delayed independently. Again, a piezoelectric delay line (D_3 Piezo) is used for the temporal overlap between the two pulses. Subsequently, they are overlapped in a silver thiogallate ($AgGaS_2$) crystal (Type I) for a difference frequency mixing (DFM) process. The desired MIR pulses from $3 \mu\text{m}$ to $8 \mu\text{m}$ (1250 cm^{-1} to 3333 cm^{-1}) with a spectral width of 150 cm^{-1} and a pulse duration of circa 120 fs are obtained by tuning the phase-matching angle of the DFM crystal and using an appropriate wavelength from the NOPA process. The MIR pulses are used as probe pulses in the time-resolved measurements.

3.1.3 Generation of Femtosecond Pump Pulses by NOPA

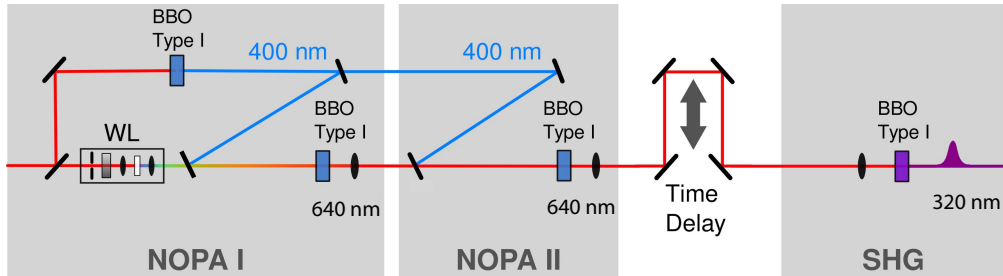


Figure 3.3: The setup for the generation of the femtosecond pump pulses. Visible light at 640 nm is obtained in a two stage NOPA and is subsequently frequency-doubled to generate the pump pulses at 320 nm. Figure adapted from K. Haiser [Hai12a].

For measurements in the ps to few ns time range, the pump pulses are generated by a frequency-doubled two stage NOPA. A schematic description of the setup is shown in Figure 3.3. Similar to the probe pulse generation, in the first NOPA (NOPA I) the fundamental pulses are divided by a beam splitter into two branches. While a small part (4%) of the light is focused on a sapphire crystal to generate the WL, the dominant part is frequency-doubled by a BBO crystal (Type I, $\theta = 29^\circ$) to produce

For measurements in the ns to μ s time range, a tunable diode pumped laser system (NT242, Ekspla) is used. A schematic description is shown in [Figure 3.4](#). A diode pumped Nd:YAG laser emits the fundamental nanosecond pulses at 1064 nm. Its third harmonic (THG) at 355 nm serves as pumping source for an optic parametric oscillator (OPO). Based on two BBO crystals (Type II) the OPO covers a wide spectral range from 400 nm to 2600 nm (orange pattern). For the excitation in the UV range there are two possible pathways: a BBO crystal (Type I) generates the second harmonic (SHG) from the OPO pulses for the wavelengths from 213 nm to 299 nm (violet pattern); another BBO crystal (Type I) produces the sum frequency (SFG) of the fundamental pulses and the OPO pulses for the wavelengths from 300 nm to 399 nm (yellow pattern). The sensitizing measurements are performed with an excitation at 320 nm to fulfill the requirement of selective excitation. For the characterization of the triplet channels of TpT, an excitation at 250 nm is selected, because TpT has a relatively high triplet yield at this wavelength. In order to achieve the temporal overlap and delay in the ns to μ s range, the Ekspla laser system (pump) is externally triggered by the Spitfire Pro laser system (probe). A detailed description of the synchronization can be found in [\[Küb13\]](#).

3.1.5 Data Acquisition and Processing

In the time-resolved measurements the absorbance changes (ΔA) are recorded as a function of the probing wavelength (λ) and the delay time (t_D). In order to obtain ΔA , the relative transmission ($T_{sample}(\lambda, t_D)$) is required, which can be obtained by dividing the signal from probe pulses with pump excitation ($I_{sample,i}^{ex}$) by the signal of probe pulses without pump excitation ($I_{sample,i}^{nonex}$) (see equation 3.1). For this purpose, a chopper wheel synchronized with the pump pulses is used which blocks every second pump pulses. The recorded signals alternate between $I_{sample,i}^{ex}$ and $I_{sample,i}^{nonex}$. The measuring program records $T_{sample}(\lambda, t_D)$ for all wavelengths at a certain delay point for several thousand points i to reduce the signal-to-noise ratio and then moves to the next delay position.

$$T_{sample}(\lambda, t_D) = \frac{\sum_{i=1}^N I_{sample,i}^{ex}}{\sum_{i=1}^N I_{sample,i}^{nonex}} \quad (3.1)$$

If the pulses energies undergo a strong variation between two successive pulses, the obtained signal T_{sample} cannot reflect the real absorption properties of the transient species with high precision, since the measurement with excitation and that without excitation are done with different probe pulses. In order to reduce the influence of this shot-to-shot noise, the probe pulses are divided into two parallel branches

before transversing the sample: the sample path and the reference path. While the sample path overlaps spatially with the pump pulses at the sample position, the reference path is intentionally placed at a position without excitation. The signal of the reference path can be calculated similarly to the sample path.

$$T_{ref}(\lambda, t_D) = \frac{\sum_{i=1}^N I_{ref,i}^{ex}}{\sum_{i=1}^N I_{ref,i}^{nonex}} \quad (3.2)$$

Since the sample path and the reference path originate from the same probe pulse, the inherent shot-to-shot noise of the laser can be circumvented. Dividing $T_{sample}(\lambda, t_D)$ by $T_{ref}(\lambda, t_D)$ can significantly reduce the noise and thus greatly simplify the setup alignment procedure. The commonly used physical quantity absorbance change $\Delta A(\lambda, t_D)$ is defined as:

$$\Delta A(\lambda, t_D) = -\log \frac{T_{sample}(\lambda, t_D)}{T_{ref}(\lambda, t_D)} \quad (3.3)$$

In order to cover the interesting part of the MIR range, the absorbance changes of typically four measuring ranges, each with 150 cm^{-1} spectral width, are combined. The spectra are appropriately scaled by comparing the signal in the overlapping range. As a consequence, a global absorbance spectrum from 1280 cm^{-1} to 1750 cm^{-1} is obtained and can be analyzed. In a typical recorded trace, the data obtained from over 10 000 shots are averaged and the error is reduced to below $10 \mu\text{OD}$.

3.1.6 Data Fitting

For the data analysis the program "Z20" is used, which is developed by our group [Sat04]. It is written in the programming language IDL (Fa.Research System Inc., Ver.5.4). A special feature of this program is that it provides a global fit to a given model function simultaneously for all wavenumbers. In this thesis, a sum of exponential functions convoluted with the cross-correlation function $K(t_D - t)$ between the pump pulse and the probe pulse is used as the model function:

$$\Delta A(\lambda, t_D) = \sum_{i=1}^n \int_0^\infty a_i(\lambda, \tau_i) \cdot \exp(-t/\tau_i) \cdot K(t_D - t) dt \quad (3.4)$$

For a Gaussian shaped pulse with a cross-correlation time of τ_{cc} ¹, the equation can be simplified to [Spö01]:

$$\Delta A(\lambda, t_D) = \sum_{i=1}^n a_i(\lambda, \tau_i) \cdot \exp\left(\frac{\tau_{cc}^2}{4\tau_i^2} - \frac{t}{\tau_i}\right) \cdot \frac{1 + \operatorname{erf}\left(\frac{t}{\tau_{cc}} - \frac{\tau_{cc}}{2\tau_i}\right)}{2} \quad (3.5)$$

$\operatorname{erf}(x) = \frac{2}{\sqrt{\pi}} \int_0^\infty \exp(-t^2) dt$ is the error function. The factor $a_i(\lambda, \tau_i)$ represents the corresponding decay associated difference spectra (DADS) for each time constant τ_i . In the program "Z20", a modified Levenberg-Marquardt algorithm combined with the method of least squares is used for the fitting. Actually, the general description of the occupation of the electronic and vibrational states requires a density matrix. However, if the transition-related vibrational modes in an electronic state are thermally relaxed before the transition in another state occurs, then the transitions can be expressed with rate constants. Thus, equations 3.4 and 3.5 are only suitable for the transitions between thermally relaxed states. If the reaction time is shorter than the relaxation time in the different electronic states (for example the vibrational cooling requires circa 10 ps), the model can result in incorrect time constants and DADS. For our experiments we do not have to concern about vibrational cooling, since the investigated processes are much slower.

3.2 The Sample Circulation Setup

A self-made sample circulation setup is used for the stationary illumination measurements and is schematically shown in Figure 3.5. It consists of a self-made IR-cuvette for stationary measurements, a peristaltic pump (Ismatec, Cole-Parmer) and a fused silica cuvette (4 mm × 10 mm, Hellma Analytics). They are connected with Teflon tubes. In order to reduce the sample volume, the fused silica cuvette serves as the sample reservoir and as the position for the UV-illumination at the same time. The IR-cuvette is composed of two CaF₂ windows (thickness 2 mm, diameter 30 mm) separated by a Teflon spacer with a thickness of 108 μm. It has a large aperture with a diameter of 10 mm, which is specially designed for the stationary characterization of the sample by means of Fourier-Transform Infrared Spectroscopy (FTIR) (IFS 66v/S, Bruker).

For the time-resolved measurements an additional IR-cuvette is connected to the setup, which serves as the position for the UV-illumination and IR-probing. This IR-cuvette also consists of two CaF₂ windows (thickness 2 mm, diameter 30 mm) separated by a Teflon spacer with a thickness of circa 90 μm. Instead of a circular aperture it has a narrow channel with a width of 2 mm, which allows an efficient

¹ $\tau_{cc}^2 = \tau_{pump}^2 + \tau_{probe}^2$. The cross-correlation time for femtosecond pump and probe pulses is circa 300 fs.

exchange of the irradiated sample solution between two successive pump pulses (1 kHz). Notably, upon excitation with the femtosecond UV pulses, the CaF_2 window produces a huge signal in the MIR range within the first nanosecond. The amplitude of this signal depends quadratically on the energy of the pulses and thus originates probably from two-photon absorption. In contrast, the signal of the BaF_2 window decays within 1 ps and does not influence our experiments. Therefore, for the experiments in the ps to few ns time range the CaF_2 windows are replaced by the BaF_2 windows (thickness 3 mm, diameter 30 mm). A detailed characterization of the window materials can be found in [Kub09].

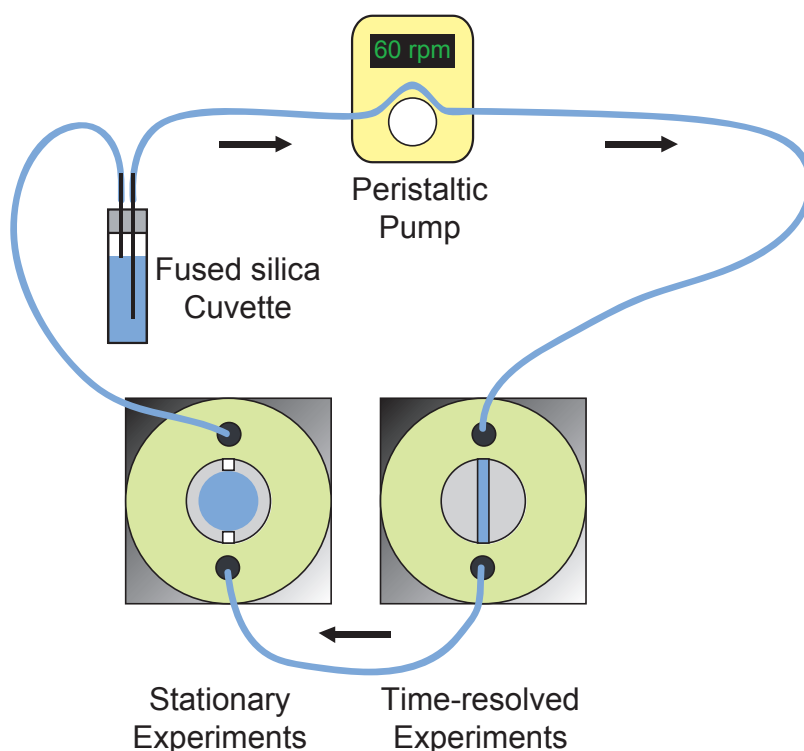


Figure 3.5: A scheme of the sample circulation setup. For stationary illumination measurements it consists of an IR-cuvette, a peristaltic pump and a fused silica cuvette. For time-resolved measurements an additional IR-cuvette is connected. The arrows show the direction of the sample flow.

3.3 Stationary Characterization of the Sample

All samples used in this thesis are prepared in buffered deuterated water solution (50 mM KH_2PO_4 and 50 mM Na_2HPO_4). For the characterization in the UV and

visible range (200 nm - 800 nm), the samples are diluted to a concentration of 0.1 mM - 0.2 mM and stored in a fused silica cuvette (4 mm×10 mm, Hellma Analytics). Their absorption spectra are measured with two spectrometers (UV-1800 or UV-2600, Shimadzu). In case of measuring the UV spectra with the home-made IR-cuvette, another spectrometer (Lambda 750, Perkin Elmer) is used, because its large sample compartment allows the placement of the IR-cuvette. For the characterization in the MIR range (1000 cm^{-1} - 4000 cm^{-1}), the samples do not need to be diluted and are stored in the above-mentioned home-made sample circulation setup. The MIR spectra are recorded with a Fourier-Transform Infrared Spectrometer (FTIR) (IFS 66v/S, Bruker).

4 Selection and Characterization of an Appropriate Photosensitizer

A photosensitizer is a molecule which can absorb photons in a certain wavelength range and then transfer its excited energy to another molecule. As mentioned earlier, this thesis focuses on pyrimidine lesions via photosensitization in the UV-A range. Thus, a suitable sensitizer that absorbs strongly in the UV-A range is necessary. This chapter begins with the search for such a sensitizer. We demonstrate that 2'-methoxyacetophenone (2-M) is a promising sensitizer. Thereafter, the absorption and emission properties of 2-M are characterized with different spectroscopic methods. In the last section, results from a series of time-resolved measurements are presented to describe the transient dynamics of 2-M.

4.1 Test of Different Acetophenone Compounds

Aromatic ketones, such as acetophenone (AP), benzophenone (BP) and xanthone (XAN) have been widely used as photosensitizers on nucleic acids or nucleotides [LY67, GJ68, GWR96]. In this thesis we focus on the investigation of the photolesions formed from the thymine dinucleotide thymidylyl-(3'→5')-thymidine (TpT). The most frequent UV induced photolesion is the cyclobutane pyrimidine dimer (CPD), which occurs most probably between two adjacent thymine bases. Thymine and thymidine monophosphate (TMP) have been intensively used as model molecules in photosensitization [GJ68, GWR96]. To form CPD lesions via photosensitization in solutions with thymine or TMP, an excited sensitizer molecule has to collide with a thymine or TMP upon diffusion and transfer its triplet energy to them. Then these excited thymine or TMP molecules again have to diffuse to meet another thymine or TMP in the solution. Only a small amount of them can form CPD lesions. The two-step diffusion process greatly reduces the quantum yield of the CPD formation and makes the measurements difficult. In contrast, once one thymine base in a TpT molecule is in its triplet state upon a triplet-triplet energy transfer (TTET) from a sensitizer molecule, it has directly the other thymine base of TpT in its neighborhood. Therefore, the dinucleotide TpT has a much higher CPD formation yield than thymine or TMP. This is the reason why we choose TpT instead of thymine or TMP as the simplest model for the investigation of CPD formation.

4.1.1 Prerequisites for the Sensitizer

There are certain prerequisites for a photosensitizer suitable for our investigations of pyrimidine photolesions:

- It should have a high intersystem crossing (ISC) efficiency.
- Its triplet energy should be higher than the triplet energy of TpT.
- It should be well soluble in aqueous solutions.
- It should possess strong absorption in the UV-A range.

The first two requirements are easily fulfilled for all sensitizer molecules mentioned here. Since they have ISC efficiencies almost equal to unity [LH65]. Among all nucleobases, thymine has the lowest triplet energy. Acetone and acetophenone can sensitize TMP in aqueous solution at room temperature [GWR96]. The triplet energy of thymine in TpT or in DNA ($E_T = 270$ kJ/mol [Bos06]) is even lower than that in TMP ($E_T = 310$ kJ/mol [WR96]). As a consequence, benzophenone can sensitize thymine in DNA [Bos06] but hardly in TMP. The third requirement is essential, because in order to achieve more physiological and biological relevance, all experiments are performed in a buffered deuterated water solution. Benzophenone and xanthone have poor solubility in water. Therefore, they are not considered in our experiments.

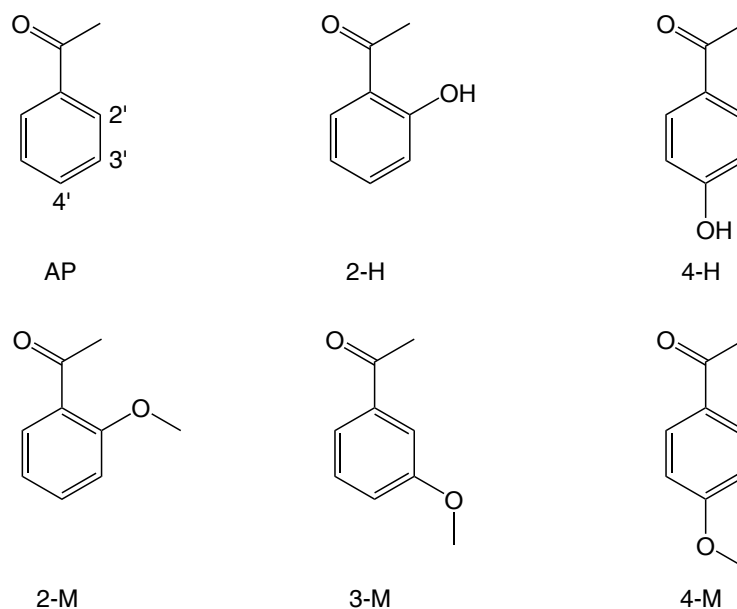


Figure 4.1: The molecular structures of acetophenone (AP) and its different substitutions.

The most challenging task is to find a sensitizer which has a strong absorption in the UV-A range, because we aim to obtain dynamic information from time-resolved measurements. Since in a typical IR time-resolved absorption measurement both sensitizer and dinucleotide have concentrations in the ~ 5 mM range, selective excitation of the sensitizer in the UV-A range is necessary. Direct absorption of the dinucleotide has to be excluded. Thus, the extinction coefficient of the sensitizer should be much larger than that of thymine. Acetone has a very small extinction coefficient ($\epsilon \sim 1 \text{ M}^{-1}\text{cm}^{-1}$ at 320 nm) and is therefore not appropriate. The absorption of acetophenone is larger ($\epsilon \sim 50 \text{ M}^{-1}\text{cm}^{-1}$), but not large enough for a time-resolved measurement. In order to increase the absorption in the UV-A range we tried different acetophenone substitutions, where the 2', 3', or 4' position is substituted by a hydroxy- or methoxy-group. Figure 4.1 shows the molecular structures of acetophenone and its different substitutions.

4.1.2 Selection of the Sensitizer in the UV-A Range

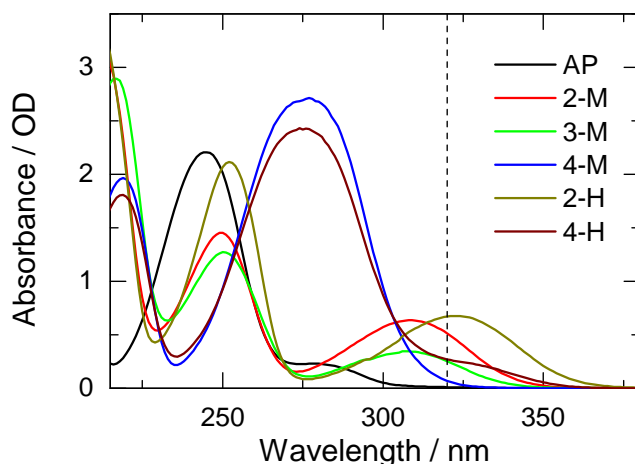


Figure 4.2: The absorption spectra of acetophenone and different acetophenone substitutions in the UV range, recorded from 215 nm to 380 nm, measured at identical concentrations (0.2 mM). The dashed line denotes the excitation wavelength of our sensitizing experiments: 320 nm.

The absorption spectra of acetophenone and some acetophenone substitutions are presented in Figure 4.2 at identical concentrations (0.2 mM). Acetophenone has its absorption maximum at 245 nm and a weak absorption shoulder around 280 nm. The absorption maxima of 4'-methoxyacetophenone (4-M) and 4'-hydroxyacetophenone (4-H) are at 276 nm and are slightly stronger than that of acetophenone. The spectra of 2'-methoxyacetophenone (2-M), 3'-methoxyacetophenone (3-M) and 2'-hydroxyacetophenone (2-H) look similar. However, the maxima are weaker, the

shoulders are red-shifted compared to acetophenone and have larger amplitudes. It is worth noting that besides 4-M all other substitutions show significantly enhanced absorption in the UV-A range.

The next question we need to answer is whether these substituted compounds are still able to transfer their excited triplet energy to TpT. Mixtures of different acetophenone substitutions (0.1 mM) with TpT (0.1 mM) at low concentrations are prepared and illuminated with 320 nm pulses¹. At this wavelength the direct absorption of TpT can be neglected. The pulse energy is about 5 μ J. Their UV absorption spectra are recorded after different illumination times (see Figure 4.3). There are almost no absorption changes for 3-M, 2-H and 4-H upon illumination, which means that they do not react with TpT. On the other hand, a pronounced bleach of the TpT absorption band is observed for 2-M and 4-M. Obviously some TpT molecules undergo photoreaction. From the UV spectra we do not know what kind of photolesions are formed. While the CPD lesions do not have any marker bands in the UV range, the (6-4) product has a marker band at 320 nm, which overlaps with the weak absorption shoulder of the photosensitizers and cannot be analyzed.

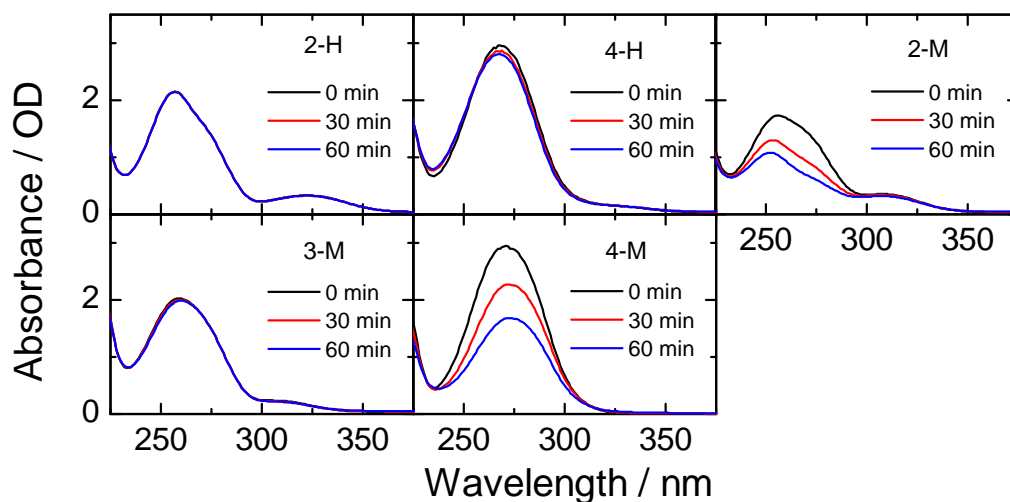


Figure 4.3: UV absorption spectra of mixtures containing TpT (0.1 mM) and different acetophenone substitutions (0.1 mM) recorded after different illumination times: before illumination (black curves), after 30 minutes (red curves), after 60 minutes (blue curves). A significant bleach of the TpT absorption band at 266 nm occurs only in the 2-M and the 4-M mixture.

¹The absorption of 4-M at 320 nm is too weak. In order to have a similar illumination dose, the mixture of TpT and 4-M is excited at 315 nm and the pulse energy is increased by a factor of 5.

4.1.3 Selection of a Sensitizer by MIR Spectroscopy

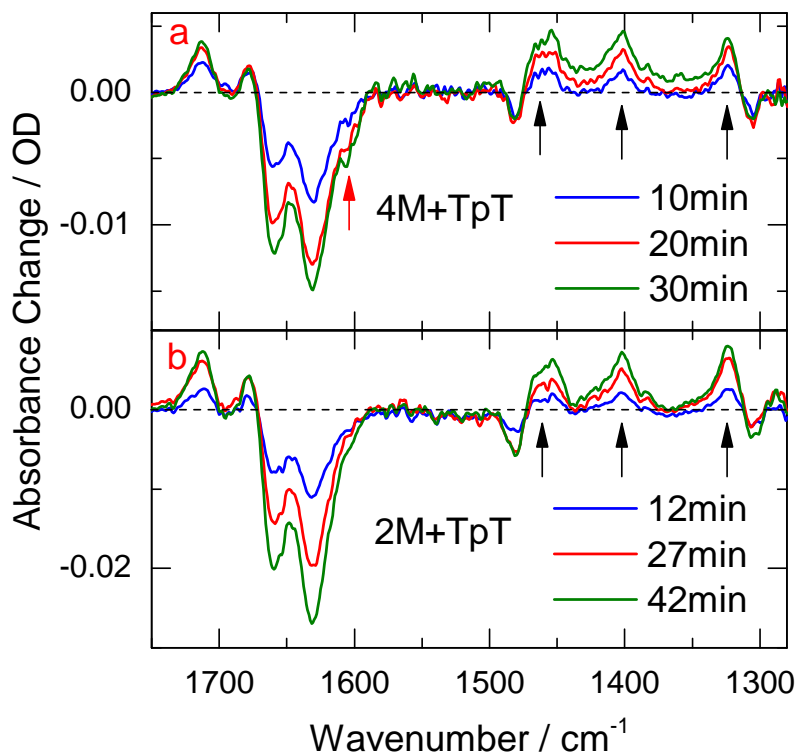


Figure 4.4: The IR absorption difference spectra of the 4-M mixture (a) and the 2-M mixture (b) recorded after different illumination times. For both mixtures, the marker bands of the CPD lesions can be observed, whose positions are marked with black arrows. The red arrow points at the bleach of 4-M at 1600 cm^{-1} after 30 minutes of illumination.

In order to identify the photolesions, we move to the MIR range, where the CPD lesions have marker bands. Considering the thickness of the IR-cuvette ($100\text{ }\mu\text{m}$), solutions with high concentrations ($\sim 5\text{ mM}$) are used in the IR measurements. Figure 4.4 shows the IR absorbance changes recorded after different illumination times. The negative bands at 1663 cm^{-1} and 1631 cm^{-1} are due to the bleach of TpT. In the fingerprint region, three well known marker bands for the CPD lesions [Sch07] at 1465 cm^{-1} , 1402 cm^{-1} and 1324 cm^{-1} are observed. These data indicate that in both solutions CPD lesions are formed by photosensitization. Another feature of interest is that after 30 minutes of illumination, a small negative spike emerges at 1600 cm^{-1} for the mixture of 4-M and TpT (see the red arrow in Figure 4.4a). This band does not belong to TpT but to 4-M. This means that after a long time of

illumination some 4-M molecules undergo photodegradation, which is not observed for the mixture of 2-M and TpT under a similar illumination dose. Thus, 2-M is more photostable than 4-M. Moreover, the extinction coefficient of 2-M ($2560 \text{ M}^{-1}\text{cm}^{-1}$) is much larger than that of 4-M ($350 \text{ M}^{-1}\text{cm}^{-1}$) at 320 nm, which allows a selective excitation of the sensitizer. 2-M can fulfill all the requirements we stated earlier in the chapter. Therefore, it is selected as a suitable photosensitizer in the following experiments.

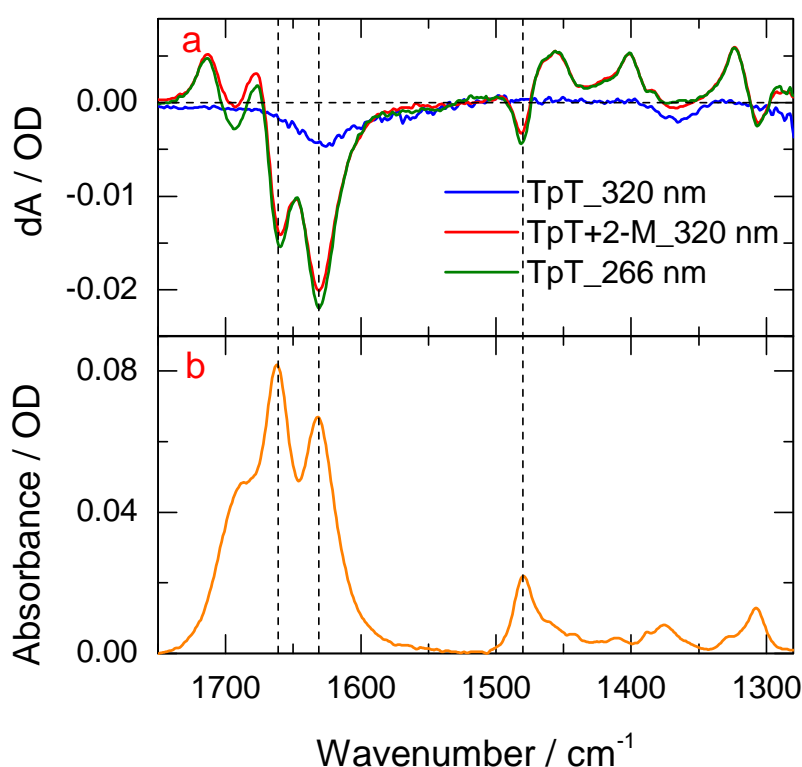


Figure 4.5: (a) The IR absorption difference spectra of a neat TpT solution illuminated at 320 nm (blue curve), a TpT and 2-M mixture illuminated at 320 nm (red curve) and a neat TpT solution illuminated at 266 nm (green curve). (b) IR absorption spectrum of 5 mm TpT. The dashed lines denote the main absorption bands of TpT, which correspond to the negative bands in (a).

A comparison of direct excitation and sensitized excitation is shown in Figure 4.5a. The spectra are scaled in order to show the three marker bands of the CPD lesions at same height. The negative bands in Figure 4.5a at 1661 cm^{-1} , 1631 cm^{-1} and 1480 cm^{-1} are due to the bleach of TpT. The dashed lines in Figure 4.5 mark the main

absorption bands of TpT. The band at 1631 cm^{-1} associated to the C5=C6 double bond undergoes the most significant reduction, which indicates a disappearance of this bond. Notably, more TpT molecules are consumed after the illumination at 266 nm than at 320 nm. The difference is attributed to the exclusive CPD formation in the sensitized photoreaction. After direct excitation at 266 nm, besides the main product, the CPD lesions, the (6-4) photoproduct is also produced [Dou03]. The absorption difference spectrum of a neat TpT solution illuminated at 320 nm is also demonstrated in Figure 4.5a. The small unstructured features of the neat TpT (blue curve) compared to the significant absorption changes of the TpT and 2-M mixture (red curve) confirm the argument that TpT does not absorb in the UV-A range.

4.2 Characterization of Acetophenone

In this section, the most frequently used photosensitizer for DNA bases, acetophenone is investigated. Deuterated acetophenone (APd8) is measured as well, since it has advantages in the MIR range.

4.2.1 Stationary Spectra of Acetophenone and Deuterated Acetophenone

The UV absorption spectrum of acetophenone was already presented before (see figure Figure 4.2). As described earlier in section 2.4.2, acetophenone has a strong absorption band at 245 nm and a weak absorption shoulder around 280 nm, which can be assigned to an intramolecular charge transfer [TNK56, Leo81] and to a $^1\pi\pi^*$ transition located at the phenyl ring [TNK56, KN65], respectively. Between 300 nm and 340 nm its absorption does not exceed the absorption of TpT significantly. This non-vanishing band of acetophenone arises from a $^1n\pi^*$ transition in the carbonyl group [McM41, TNK56]. The UV absorption spectrum of APd8 is almost identical. The absorption spectra of acetophenone and APd8 solutions in the MIR range are shown in Figure 4.6. For acetophenone, the strong absorption band at 1668 cm^{-1} arises from the stretching vibration of the carbonyl group C=O [TNK56]. The band at 1601 cm^{-1} is assigned to the coupling between the carbonyl group and the phenyl ring [Bar53]. The bands at 1583 cm^{-1} and 1451 cm^{-1} are attributed to the C-C ring stretching. The bands at 1428 cm^{-1} and 1367 cm^{-1} originate probably from the asymmetric and symmetric methyl deformations, respectively. The assignment of the absorption bands refers to [Gam80]. For APd8, its main absorption bands show a global redshift relative to the bands of acetophenone. The bands at 1668 cm^{-1} , 1601 cm^{-1} , 1583 cm^{-1} and 1451 cm^{-1} for acetophenone are shifted to 1663 cm^{-1} , 1567 cm^{-1} , 1544 cm^{-1} and 1332 cm^{-1} for APd8, respectively. APd8 does not have an

absorption band near 1600 cm^{-1} , where the well known marker band for thymine in its triplet state is located [Pil14b]. Therefore, APd8 is investigated in time-resolved absorption experiments to obtain further dynamic information.

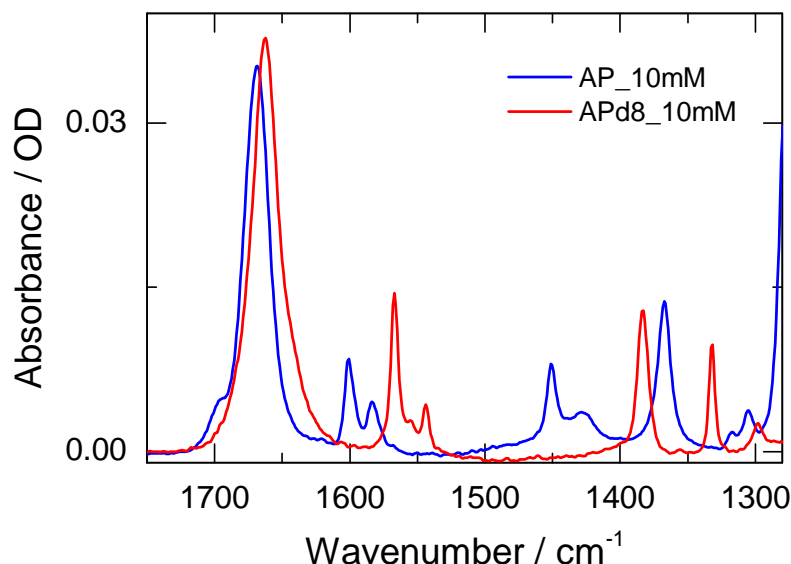


Figure 4.6: (a) The absorption spectra of acetophenone (blue) and deuterated acetophenone (red) in the MIR range.

4.2.2 Time-resolved Absorption Measurement on Deuterated Acetophenone

The very weak absorption of APd8 in the UV-A range corresponds to the excitation to the S_1 state ($^1n\pi^*$). In order to ensure detectable transient signals in the MIR range, the excitation wavelength is set at 300 nm and the concentration is relatively high (30 mM). It is worth noting that the excitation at 300 nm leads presumably to the population of the S_2 state of APd8.

The pump pulses are supplied by a nanosecond OPO laser system (NT242, Ekspla). Pulse energy is $4\text{ }\mu\text{J}$ and pulse duration is 3 ns. The absorbance changes of a neat deuterated acetophenone (APd8) solution recorded as a function of the probing wavenumber (1280 cm^{-1} to 1750 cm^{-1}) and the delay time (1 ns to $50\text{ }\mu\text{s}$) are shown in Figure 4.7a. Transient spectra recorded at 10 ns, 50 ns, 100 ns and a later delay time ($50\text{ }\mu\text{s}$) are displayed in Figure 4.7b - e. Immediately after the excitation (10 ns), negative signals (blue) due to the ground state bleach of APd8 at 1663 cm^{-1} , 1567 cm^{-1} , 1383 cm^{-1} and 1332 cm^{-1} can be observed. At the same

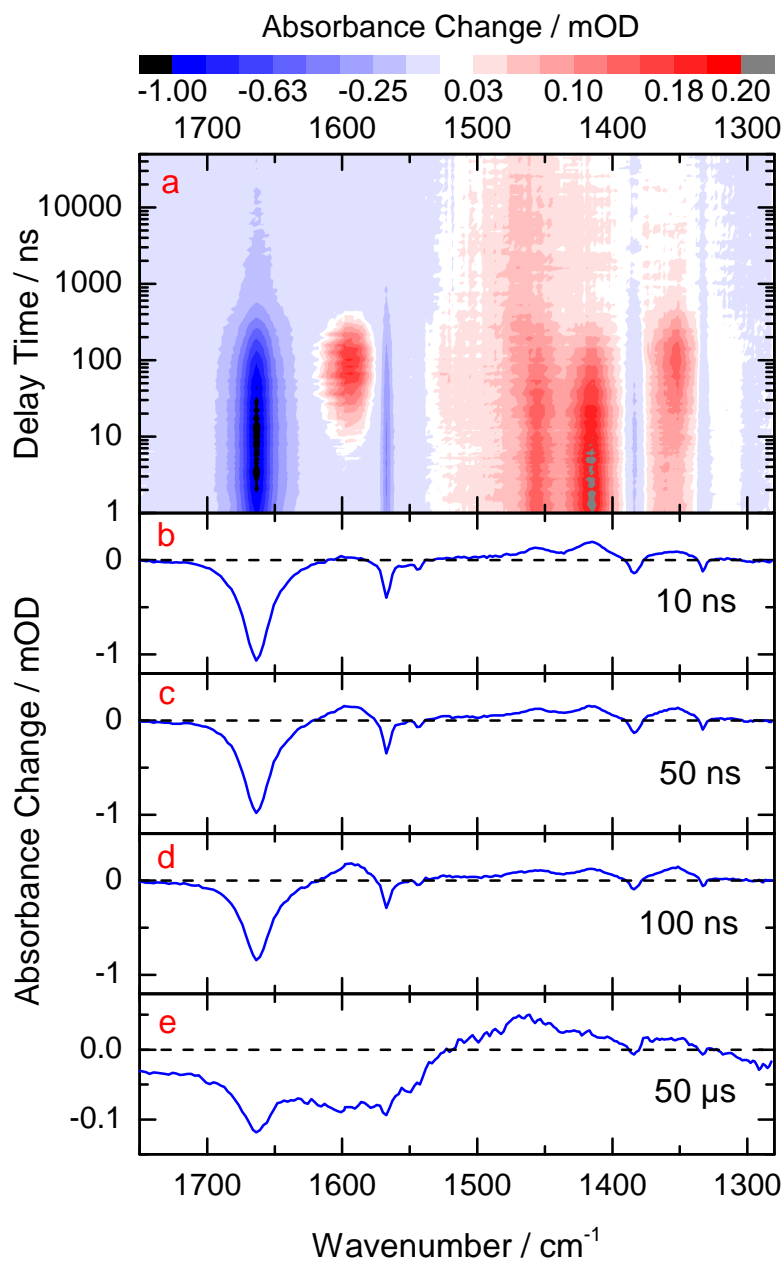


Figure 4.7: Transient absorption data for the nanosecond experiment using excitation pulses at 300 nm. (a) Absorbance changes recorded as a function of the probing wavenumber and the delay time shown in color coding. Transient absorbance difference spectra recorded at delay times of 10 ns (b), 50 ns (c), 100 ns (d) and at the end of the observation range at 50 μ s (e).

time, positive bands can be seen at 1456 cm^{-1} , 1415 cm^{-1} and 1358 cm^{-1} due to the induced absorption of an intermediate state. Between 10 ns and 100 ns, positive bands

at 1593 cm^{-1} and 1353 cm^{-1} emerge and reach their maxima at circa 100 ns. At the same time, the negative signals show only minor recovery which is accompanied by a moderate reduction of the positive bands at 1593 cm^{-1} and 1353 cm^{-1} . At later times only weak absorption changes can be observed, which can be associated to the heating of the solvent (deuterated water) by the disposed excitation energy and to the formation of a photoproduct of APd8 with low efficiency.

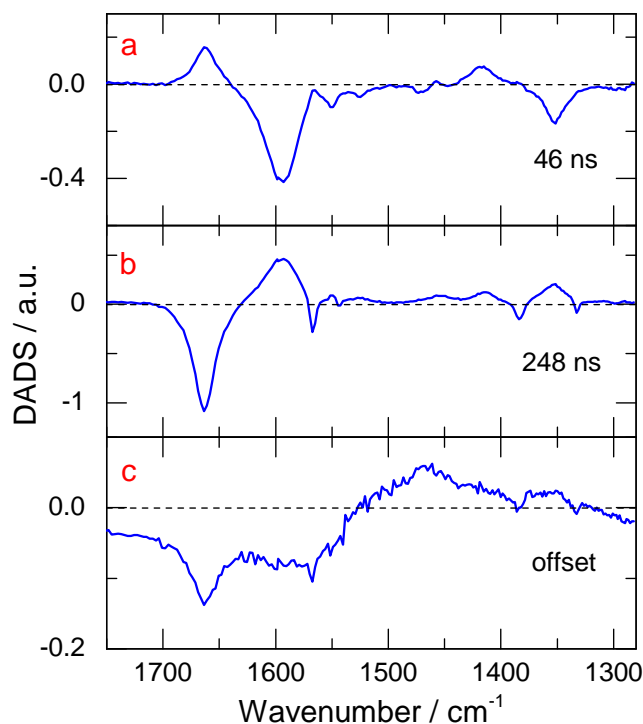


Figure 4.8: Decay associated difference spectra (DADS) for the time constants 46 ns, 248 ns and the offset.

The transient absorption data can be globally fitted with a multi-exponential function with three time constants. The first two time constants obtained from a free iterative fit describe the reaction dynamics. The third constant is set at $10 \cdot 10^8$ ns. Its amplitudes represent the offset spectrum at the end of the time window. Two time constants ($\tau_1 = 46$ ns and $\tau_2 = 248$ ns) are obtained from the fit. The wavenumber-dependent fit amplitudes corresponding to the different time constants are called decay-associated difference spectra (DADS) and are plotted in Figure 4.8. The negative bands at 1593 cm^{-1} and 1353 cm^{-1} of the 46 ns component represent the formation of an intermediate state. The negative bands at 1663 cm^{-1} , 1567 cm^{-1} , 1383 cm^{-1} and 1332 cm^{-1} of the 248 ns component describe the recovery of the ground state bleach. The absorption bands at 1593 cm^{-1} and 1353 cm^{-1} decay with the same time constant.

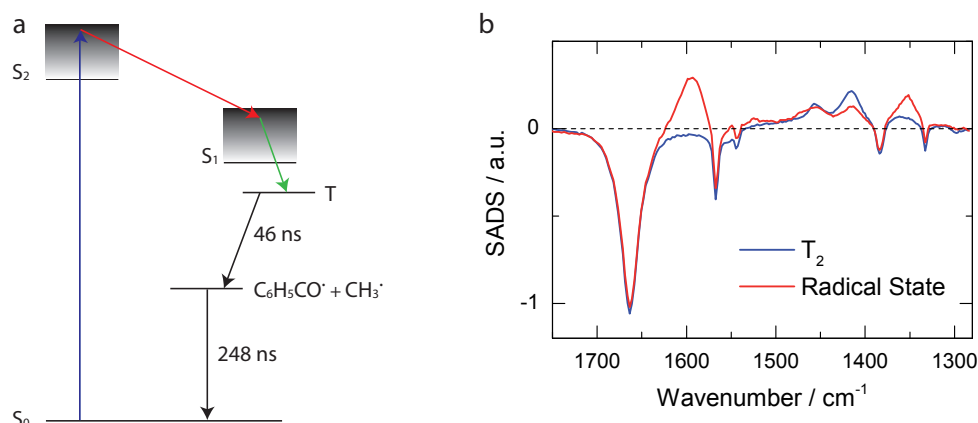


Figure 4.9: (a) Reaction scheme for acetophenone upon excitation to the S_2 state. In our measurement only the transitions drawn with black lines are observed. The ultrafast internal conversion from S_2 to S_1 (red) and the subsequent intersystem crossing from S_1 to T_2 (green) can not be resolved. (b) The species associated absorption difference spectra (SADS) calculated from the absorption difference data for the T_2 state (blue curve) and the radical state (red curve), respectively.

If acetophenone is excited to its S_1 state ($^1n\pi^*$), it will undergo a fast and efficient intersystem crossing to the T_2 state ($^3\pi\pi^*$). Internal conversion subsequently populates the T_1 state ($^3n\pi^*$) [FP02, PFZ06]. From the T_1 state, it can decay either via a radiative or a non-radiative process to the ground state. In the gas phase the phosphorescence quantum yield of acetophenone is almost unity, if it is excited to the S_1 state [BS75, IBT78]. The phosphorescence quantum yield shows a significant drop-off to 10^{-4} , if the S_2 state is initially occupied [WB86].

Upon excitation to the S_2 state, the photophysical and photochemical processes of acetophenone are more complicated. Zewail et al. proposed that for acetophenone in the gas phase, excitation to the S_2 state is followed by an ultrafast internal conversion to the S_1 state. From the S_1 state a bifurcation of pathways should take place between photophysics (intersystem crossing) and photochemistry (radical formation: $C_6H_5CO\cdot + CH_3\cdot$ and molecular dissociation) [PFZ06]. Based on the results from our measurement we propose a reaction model for acetophenone in the condensed phase (see Figure 4.9a). The internal conversion from S_2 to S_1 and the subsequent intersystem crossing from S_1 to T_2 cannot be resolved in our experiments with nanosecond pulses. It seems that the T_2 state is occupied "instantly". The 46 ns process is tentatively assigned to the transition from the triplet state to a radical state. The time constant of 46 ns suggests that this process is a diffusion controlled quenching. The long lived triplet state is probably quenched by the collision with another acetophenone molecule in the ground state and thus is converted to a radical state. The radical state then decays with 248 ns to the ground state. Notably, the S_1

state occupied via internal conversion from S_2 demonstrates different photophysical and photochemical properties as the S_1 state occupied upon direct optical excitation. This may be explained by the assumption that different regions of the S_1 state surface are occupied.

From the kinetic components (DADS) one can calculate the difference spectra related to the intermediate states, i.e. the species associated difference spectra (SADS). The details about how the SADS are obtained from the DADS can be found in the literature [Dom14]. SADS for the T_2 state (blue curve) and the radical state (red curve) are shown in Figure 4.9b, respectively. The negative signals are attributed to the ground state bleach. The positions and the amplitudes of the negative bands indicate that upon formation of the radical state no excited acetophenone decays to the ground state. Besides the band at 1415 cm^{-1} , the triplet state (blue) does not have many marker bands in the MIR range, as reported by Hagamuchi et al. [Yab10]. In contrast, the radical state (red) has two marker bands at 1593 cm^{-1} and 1353 cm^{-1} .

The 46 ns time constant falls into the same time range as the triplet-triplet energy transfer between the sensitizer and TpT molecules. This makes a clear separation of these two processes difficult. Therefore, we use in the sensitizing experiments the molecule 2-M. Its transient spectra decay in the nanosecond to microsecond range mono-exponentially with only one time constant of 400 ns. The details will be shown later in section 4.4.3. In addition, the absorption of 2-M in the UV-A range is also significantly stronger than that of APd8, which allows selective excitation.

4.3 Spectroscopic Characterization of 2-Methoxyacetophenone

In this section, the UV- and IR-absorption spectra of 2-M are discussed in detail. Figure 4.10 shows the extinction coefficient (ϵ) of TpT, 2-M and deuterated acetophenone. TpT has a broad unstructured band with its maximum at 266 nm. This broad band is assigned to the thymine base, which has $^1\pi\pi^*$ transitions with a strong oscillator strength in this range [Cre04]. Its absorption decreases quickly in the UV-B range but presents an extended wing above 310 nm. The absorption spectrum is in good agreement with the literature data [Voe63]. The spectrum of deuterated acetophenone has already been discussed before. Theoretical calculations and experimental measurements for the absorption spectra of 2-M are not found in literature. Therefore, we are unable to give an unambiguous assignment of the absorption bands to the corresponding electronic transitions. The main absorption band of 2-M is red-shifted to 250 nm. At the desired excitation wavelength of 320 nm, the extinction coefficient of 2-M ($2560\text{ M}^{-1}\text{cm}^{-1}$) is two orders of magnitude larger

than the extinction coefficient of TpT ($\sim 10 \text{ M}^{-1}\text{cm}^{-1}$). This makes a selective excitation of 2-M possible.

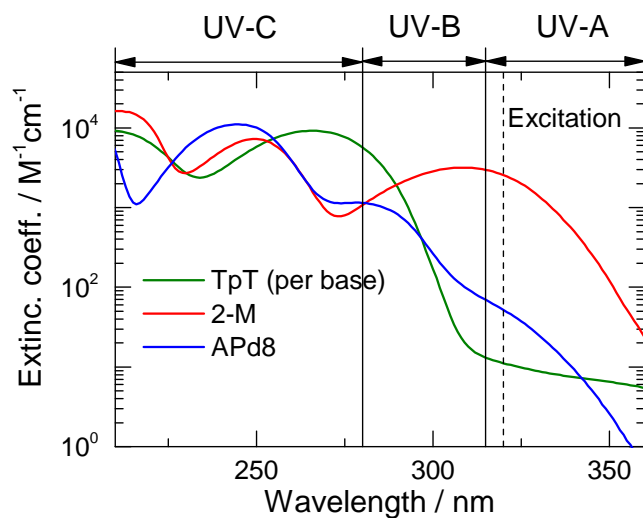


Figure 4.10: Extinction coefficients of TpT (per thymine base, green curve), 2-M (red curve) and deuterated acetophenone (blue curve) plotted on a logarithmic scale. At the excitation wavelength (320 nm, dashed line) the absorption of 2-M is two orders of magnitude larger than that of TpT and APd8.

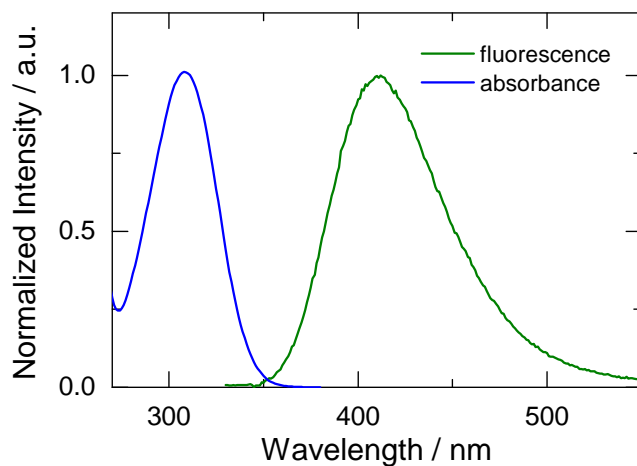


Figure 4.11: Normalized absorption (blue curve) and emission (green curve) spectra of 2-M. The fluorescence has its maximum at 412 nm.

The absorption and emission spectra of 2-M are presented in [Figure 4.11](#). They are

recorded from 270 nm to 550 nm and scaled to have the maxima of absorption and emission at the same height. The fluorescence emission has its maximum around 412 nm which is about 100 nm red-shifted compared to the absorption maximum. From the absorption and the emission spectra one can estimate the radiative lifetime (τ_{rad}) for 2-M to be 33 ns using the Strickler-Berg equation [SB62]. The radiative lifetime (τ_{rad}) is the lifetime of the excited state, if the only process of deactivation is spontaneous emission. For 2-M, a fluorescence quantum yield (η) of 2.6% is measured using 2,5-diphenyloxazole (PPO) as an actinometer. The low fluorescence yield suggests that after UV excitation, the majority of 2-M molecules undergoes a non-radiative decay. Considering the high intersystem crossing (ISC) efficiency of the parent compound, acetophenone, reported in the literature [LH65, OSI88], we may assume that compared to the internal conversion (IC) ISC to the triplet state also dominates in 2-M. An unambiguous confirmation of this assumption requires a time-resolved measurement, which will be shown later in section 4.4.2. Combining the fluorescence lifetime and the fluorescence quantum yield, one can estimate the lifetime of the excited singlet state ($\tau_{S1} = \eta \cdot \tau_{rad}$) to be 860 ps. An exact value for τ_{S1} will be measured directly with the time-resolved experiments.

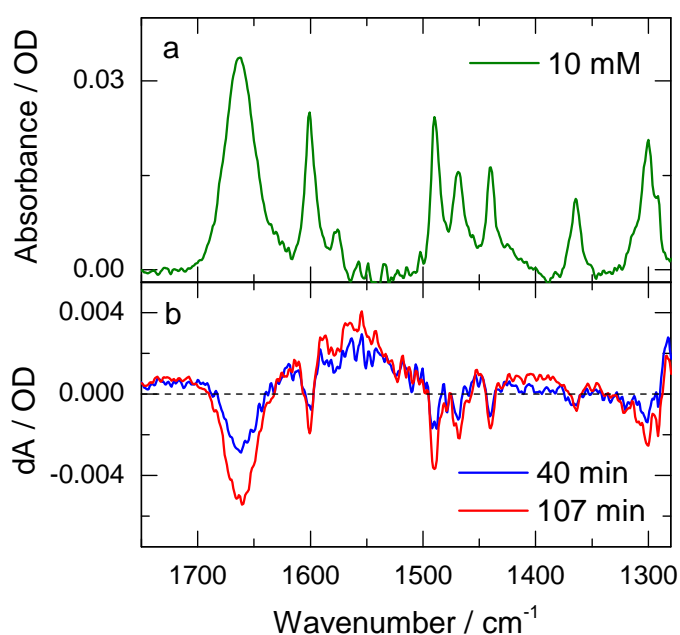


Figure 4.12: (a) The absorption spectrum of 2-M in the MIR range. It has strong absorption bands at 1663 cm^{-1} , 1600 cm^{-1} and 1489 cm^{-1} . (b) Photo-degradation of 2-M after different illumination times.

The IR absorption spectrum of 2-M is displayed in [Figure 4.12a](#). The strong absorption band at 1663 cm^{-1} is assigned to the stretching vibration of the carbonyl group [[TNK56](#), [Gam80](#)]. The band at 1600 cm^{-1} originates from the coupling between the carbonyl group and the phenyl ring [[Bar53](#)]. There is a series of bands between 1500 cm^{-1} and 1300 cm^{-1} . An exact attribution of these bands is difficult due to the delocalization of the normal modes.

The photostability of 2-M is also tested. A neat 2-M solution (10 mM, 1.2 ml) is excited at 320 nm with a pulse energy of $30\text{ }\mu\text{J}$ at a repetition rate of 1 kHz. After 107 minutes about 20% of the 2-M molecules undergo a photodegradation (see the negative bands in [Figure 4.12b](#)). However, in the presence of TpT molecules, 2-M exhibits a much higher photostability. Compared to a neat 2-M solution, TpT acts as an efficient quencher for the triplet excited 2-M. Moreover, to minimize the influence of photodegradation, the pulse energy used in the following stationary illumination measurements is limited to $13\text{ }\mu\text{J}$ and the illumination time is kept below 60 minutes.

4.4 Time-resolved Measurements on 2-Methoxyacetophenone

The stationary absorption and emission measurements provide information on the electronic and vibrational transitions of 2-M. In this section, with the help of the time-resolved measurements important dynamic properties of 2-M will be presented. Firstly, a time-resolved fluorescence measurement in the UV-VIS range is performed to obtain the lifetime of the excited singlet state. Then, by using different laser systems, time-resolved absorption measurements in the MIR range allow to explore the dynamic evolution of 2-M after excitation in the time window from ps to μs . The data analysis procedures allow the identification of the non-radiative deactivation process of the S_1 state as intersystem crossing and the characterization of the triplet state.

4.4.1 Fluorescence Measurement in the Picosecond to Nanosecond Range

With time-resolved fluorescence spectroscopy one can directly measure the lifetime of the excited singlet electronic state after UV excitation. The streak camera system (C5680-24 C, Hamamatsu) is described in detail in [[Fin12](#)]. Briefly, light pulses at a wavelength of 654 nm are generated from a femtosecond laser-amplifier system (Clark CPA 2001, 180 fs, 778 nm, 1 kHz) through a non-collinear optical parametric amplification (NOPA). They are frequency-doubled to an excitation wavelength of 327 nm. The pulse energy at the sample position is $0.15\text{ }\mu\text{J}$. The fluorescence of

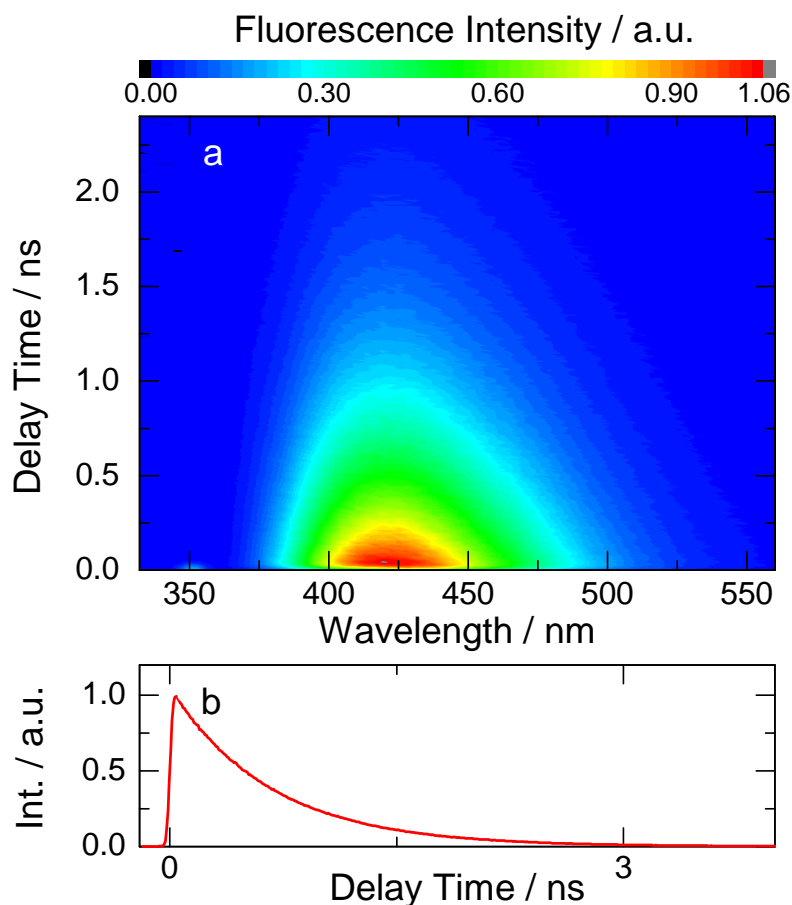


Figure 4.13: (a) Transient emission data from the streak camera experiment on 2-M with the excitation at 327 nm. Fluorescence emission plotted as a function of the probing wavelength and the delay time shown in color coding. 2-M shows a broad emission band between 380 nm and 500 nm. (b) Time dependence of the fluorescence emission recorded between 400 nm and 440 nm, which can be fitted with a decay time constant of 660 ps.

2-M is focused by an achromatic lens to the entrance slit of the spectrograph. In the spectrograph the light is spectrally separated and subsequently imaged on the photocathode of the streak camera. The streak camera system is operated in a single photon counting mode with a continuous streak sweep. A time window of 5 ns is used (time resolution of about 30 ps). The concentration of the 2-M solution is 1.6 mM, the thickness of the sample cuvette is 250 μm , which corresponds to an optical density of 0.2 at the excitation wavelength.

Figure 4.13a shows the time-resolved emission as a function of the probing wavelength (330 nm to 560 nm) and the delay time (0 ns to 2.4 ns). Upon UV absorption 2-M is excited to its singlet excited state. A broad fluorescence band emerges between 380 nm and 480 nm with a maximum at 419 nm. The shape of this band resembles

the shape of the emission spectrum taken from the stationary fluorometer (compare with the green curve in [Figure 4.11](#)). Since this broad emission band decays with the same time constant at all wavelengths, the emission data between 400 nm and 440 nm are averaged in order to reduce the noise ratio. It can be fitted mono-exponentially with a time constant $\tau_{S1} = 660$ ps (see [Figure 4.13b](#)). τ_{S1} is the lifetime of the excited singlet state and agrees well with the estimation based on the Strickler-Berg equation [[SB62](#)] as mentioned earlier in section 4.2 (860 ps).

4.4.2 Absorption Measurement in the Picosecond to Nanosecond Range

Additional information can be obtained from the time-resolved IR absorption measurements. The absorbance changes of a neat 2-M solution (5 mM) recorded as a function of the probing wavenumber (1280 cm^{-1} to 1750 cm^{-1}) and the delay time (1 ps to 1.5 ns) are shown in [Figure 4.14a](#). The pump pulses at 320 nm are generated with a two-step NOPA setup. The pulse energy is 0.6 μJ and pulse duration is 100 fs. A detailed description of the time-resolved absorption experiment can be found in chapter 3. Immediately after excitation negative signals (blue) due to the ground state bleach of 2-M at 1661 cm^{-1} , 1600 cm^{-1} , 1490 cm^{-1} , 1470 cm^{-1} , 1440 cm^{-1} and 1300 cm^{-1} can be observed. At the same time positive bands emerge at 1402 cm^{-1} and 1358 cm^{-1} , which can be assigned to the absorption of the excited singlet state. The transient absorption data can be globally fitted by a multi-exponential function with three time constants. The data analysis is performed for delay times larger than 2 ps. The signals in the vicinity of the zero-point due to coherent artifacts and within the first 2 ps due to the relaxation of the excited vibrational states are neglected. Two time constants ($\tau_1 = 31$ ps and $\tau_2 = 680$ ps) and an offset are obtained from the fit. The decay-associated difference spectra (DADS) are plotted in [Figure 4.14b-d](#). The first component with $\tau_1 = 31$ ps has a relatively small amplitude and can be assigned to rearrangements of 2-M molecules or to the surrounding solvent shell [[Nen10](#)]. The second time constant $\tau_2 = 680$ ps agrees well with the decay time $\tau_{S1} = 660$ ps obtained from the fluorescence emission measurement and can therefore be attributed to the decay of the excited singlet state. The positive amplitudes found in [Figure 4.14c](#) at 1402 cm^{-1} and 1358 cm^{-1} , which describe the decay of the excited state bands, also support this interpretation. Notably, the bleach of the strong ground state bands at 1661 cm^{-1} and 1600 cm^{-1} does not change in the observed time range (1 ps to 1.5 ns). Most likely, the decay of the emitting excited singlet state is not related to a detectable recovery to the original ground state. As a consequence, the state populated within 680 ps is not the original ground state, but a new state X. From the vanishing ground state recovery and the relatively low fluorescence yield $\eta = 2.6\%$ one can estimate that approximately 97.4% of the

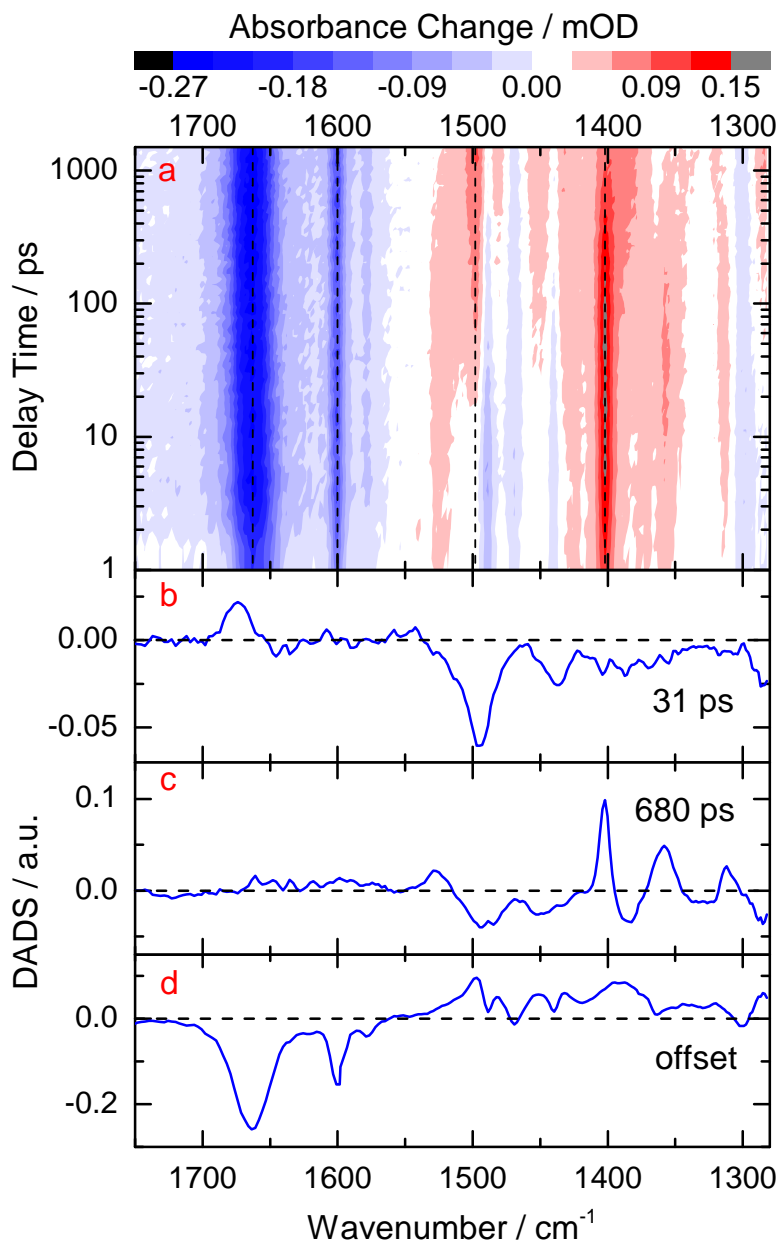


Figure 4.14: Transient IR absorption data for the picosecond experiment with an excitation at 320 nm. (a) Absorbance changes recorded as a function of the probing wavenumber and the delay time shown in color coding. (b)-(d) decay associated difference spectra (DADS) for the time constants 31 ps, 680 ps and the offset, respectively. Reprinted with permission from [Liu15]. Copyright (2015) John Wiley and Sons.

initially excited molecules reach the state X via a non-radiative deactivation process.

The offset spectrum (Figure 4.14d) obtained at the end of the observation window shows negative bands due to the bleach of the original ground state and positive bands due to the marker bands of the new state X.

4.4.3 Absorption Measurement in the Nanosecond to Microsecond Range

The state X has a lifetime beyond the time window of the picosecond measurement. The measurements in the picosecond time range alone do not allow us to assign the state X to a triplet state or another long-living state. Therefore, a time-resolved IR absorption measurement is also performed for 2-M solution at the same concentration, in the same spectral range, but within a longer time window (1 ns to 3 μ s). The excitation wavelength is 320 nm, pulse energy is 6 μ J and pulse duration is 3 ns. Instead of the femtosecond pulses from the NOPA setup, an external nanosecond OPO laser system (NT242, Ekspla) serves as pump source.

Figure 4.15a shows the absorbance changes, where strong absorption transients in the 100 ns to 1 μ s time range are observed. The same spectral features are observed at early delay times in the nanosecond experiment as at the later delay times in the picosecond experiment. The data can be globally fitted by one time constant: $\tau_3 = 400$ ns. The corresponding DADS exactly reproduce the offset spectrum of the picosecond experiment (compare with Figure 4.15b and Figure 4.14d). Therefore, the state X populated from the excited singlet state decays with $\tau_3 = 400$ ns to the ground state. The negative bands at 1661 cm^{-1} , 1600 cm^{-1} , 1470 cm^{-1} and 1300 cm^{-1} are due to the recovery of the ground state bleach of 2-M. The positive bands at 1497 cm^{-1} , 1393 cm^{-1} and 1285 cm^{-1} decay with the same time constant τ_3 . Thus, they are attributed to the characteristic absorption bands of the state X. Considering the comparable lifetime observed for a similar molecule (deuterated acetophenone) at ambient oxygen concentration, one can tentatively assign the state X to a triplet state. At later times only weak absorption changes can be observed, which can be associated to the heating of the solvent by the disposed excitation energy and to the formation of a photoproduct of 2-M with low efficiency.

Additional information is acquired from experiments in which TpT dinucleotides are added to the 2-M solution. This will be discussed in detail in the next chapter. Briefly, by exciting the mixture at 320 nm, the appearance of pronounced TpT triplet bands and the decay of the marker bands of the state X are observed in the time-resolved absorption measurements in the nanosecond time range. In comparison to the absorbance change of the neat 2-M solution, the decay of the mixture is considerably accelerated in the 30 ns - 400 ns range. These observations support the assumption that the state X is a triplet state of 2-M, which populates the TpT triplet state through a triplet-triplet energy transfer (TTET). The high structural similarity

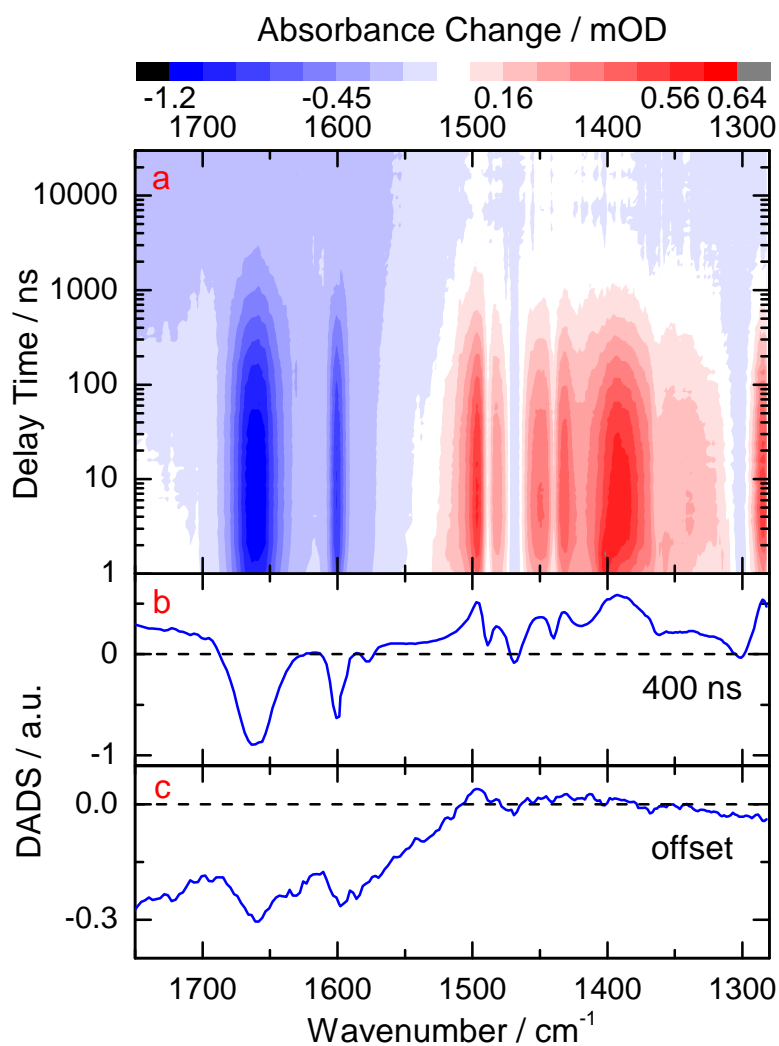


Figure 4.15: Transient absorption data for the nanosecond experiment using excitation pulses at 320 nm. (a) Absorbance changes recorded as a function of the probing wavenumber and the delay time shown in color coding. (b) DADS of the component decaying with a time constant of $\tau_3 = 400$ ns. (c) Offset spectrum showing solvent heating and indications of a minor photoproduct. Reprinted with permission from [Liu15]. Copyright (2015) John Wiley and Sons.

of 2-M and acetophenone together with the evidences from stationary measurements also suggest that a triplet state of 2-M is involved in the formation of the TpT triplet state and the CPD lesions. The time constant $\tau_3 = 400$ ns obtained from the fit procedure is assigned to the lifetime of the triplet state. The non-radiative deactivation process observed in the picosecond measurement is therefore intersystem crossing from the singlet excited state to the triplet state. With the time-resolved

measurement we are able to show that 2-M indeed exhibits a very effective intersystem crossing, which is a prerequisite for a photosensitizer.

4.5 Summary of the Important Properties of 2-Methoxyacetophenone

To summarize, the high extinction coefficient of 2-M in the UV-A range makes it an ideal sensitizer for TpT. CPD formation from the TpT molecules via triplet photosensitization of 2-M is observed. The important photophysical and photochemical properties obtained from the stationary and time-resolved measurements are summarized in Table 4.1.

ϵ_{320}	η	ϕ_{ISC}	τ_{S1}	τ_3
$2560 \text{ M}^{-1}\text{cm}^{-1}$	2.6%	97.4%	660 ps	400 ns

Table 4.1: The important properties of 2-M. ϵ_{320} : extinction coefficient at 320 nm, η : fluorescence emission yield, ϕ_{ISC} : intersystem crossing efficiency, τ_{S1} : lifetime of the singlet excited state, τ_3 : lifetime of the triplet excited state ².

At the excitation wavelength of 320 nm, the extinction coefficient of 2-M ($2560 \text{ M}^{-1}\text{cm}^{-1}$) is more than two orders of magnitude larger than that of TpT ($\sim 10 \text{ M}^{-1}\text{cm}^{-1}$). This makes a selective excitation of 2-M possible. The fluorescence emission has a maximum at 412 nm, which is about 100 nm red-shifted compared to the absorption maximum. The low fluorescence yield $\eta = 2.6\%$ suggests an efficient non-radiative decay process. In the picosecond time-resolved absorption experiment no recovery of the ground state bleach is detected, which excludes the possibility of internal conversion. Therefore, it is concluded that 2-M undergoes very efficient intersystem crossing ($\phi_{ISC} = 97.4\%$) after excitation. In the MIR range 2-M shows a series of marker bands. While the band at 1661 cm^{-1} is due to the carbonyl group, the band at 1600 cm^{-1} is attributed to the coupling between the carbonyl group and the phenyl group. The lifetime of the triplet excited state of 2-M (400 ns) is also determined with a nanosecond time-resolved absorption experiment. Unless specified otherwise, all time-resolved and stationary measurements are performed at ambient oxygen concentration. Here, the experiment of neat 2-M is performed under the same air-saturated condition and the same 2-M concentration (5 mM) as the experiment on the mixtures with TpT (this will be discussed in detail in the next chapter). As long

²This time-resolved measurement is performed at ambient oxygen concentration. Thus, the 400 ns is not the intrinsic lifetime of the triplet state, but an effective lifetime, which also includes the effect of dissolved oxygen.

4 Selection and Characterization of an Appropriate Photosensitizer

as the quenching of the excited triplet state of 2-M by oxygen is constant, oxygen does not influence the result of the data analysis.

5 Formation of CPD Lesions in Thymine Dinucleotide via Triplet Sensitization

In chapter 4, 2-M was selected as an appropriate photosensitizer for the CPD formation. Its photochemical and photophysical properties were intensively investigated. This chapter focuses on the interaction between 2-M and TpT. At the beginning, a diffusion-controlled collisional reaction model describing the sensitized CPD formation is proposed. Afterwards, the quantum yield of CPD formation via the triplet channel, ϕ_{CPD3} , is determined with two independent approaches. While the first uses a set of concentration dependent stationary illumination measurements, the second combines time-resolved and stationary experiments with the same concentration. The influence of dissolved oxygen is excluded with experiments performed at different oxygen concentrations. Since the triplet channels of TpT play a key role in the sensitization process, they are explored with a time-resolved experiment at an excitation wavelength of 250 nm, where TpT has a relatively high intersystem crossing efficiency. This chapter ends with a time-resolved measurement on a mixture containing TpT and 2-M, which provides independent information and supports the validity of the proposed reaction model.

5.1 Reaction Model

From earlier works in our group we know that upon direct UV-C illumination (at 266 nm) of single stranded thymines (dT)₁₈ or the dinucleotide TpT, the CPD lesions are formed predominantly via the singlet excited state [Sch09]. The CPD formation is an ultrafast process, which occurs within 1 ps [Sch07]. The right part of Figure 5.1 presents the reaction scheme for this direct CPD formation process of TpT. Upon excitation of the allowed $^1\pi\pi^*$ transition in the UV-C range, the singlet excited state $^1\text{TpT}^*$ is occupied, which decays afterwards predominantly via an ultrafast internal conversion (IC) back to the ground state. Besides the internal conversion, there is direct CPD formation with a yield $\eta_{CPD1} = 1.5\%$ [Sch09] and intersystem crossing (ISC) with a yield η_{ISC} . Assuming that TpT has the same ISC yield as TMP, one can deduce $\eta_{ISC} \approx 1.3\%$ (at 266 nm) from the literature [Ban12]. From similar experiments performed on (dT)₁₈ [Pil14b], the triplet state (^3TpT) populated by intersystem crossing should decay at first to an intermediate biradical state (^3BR) and subsequently to the ground state. It has also been shown that only a small fraction of the triplet excited TpT can form CPD lesions, i.e. $\phi_{CPD3} < 15\%$.

5 Formation of CPD Lesions in Thymine Dinucleotide via Triplet Sensitization

Here we do not distinguish whether the CPD lesions are formed from ^3TpT or ^3BR . Combining η_{ISC} and ϕ_{CPD3} an upper limit for η_{CPD3} , the contribution of the triplet channel for CPD formation upon direct excitation of $^1\text{TpT}^*$, can be estimated, where $\eta_{CPD3} = \eta_{ISC} \cdot \phi_{CPD3} < 0.2\%$.

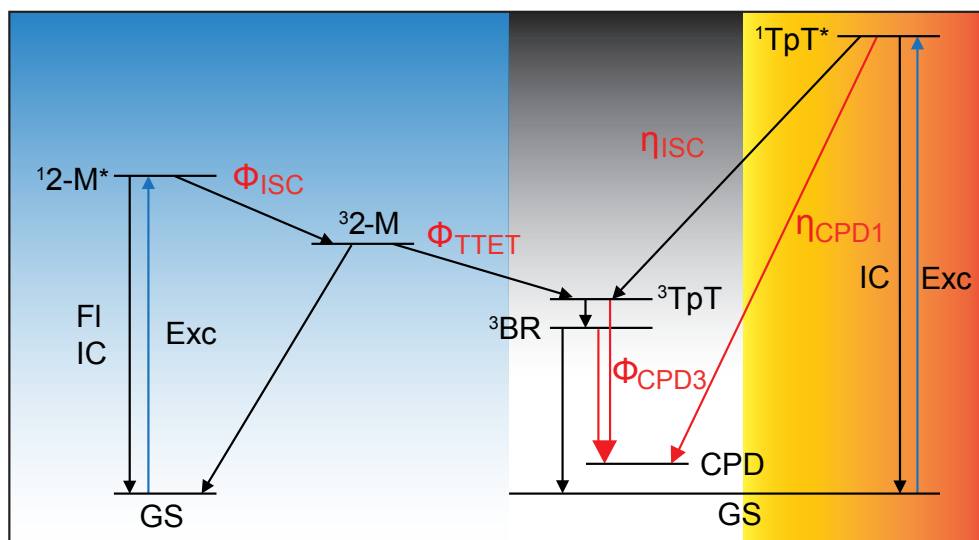


Figure 5.1: Reaction scheme for direct and sensitized CPD formation. Right part: after excitation of the allowed transition, CPD formation may occur in an ultrafast reaction channel directly from $^1\text{TpT}^*$ with an efficiency η_{CPD1} or after intersystem crossing (ISC) with an efficiency $\eta_{CPD3} = \eta_{ISC} \cdot \phi_{CPD3}$. The sensitized reaction channel (left part) requires ISC of the sensitizer and TTET to ^3TpT prior to CPD formation. Its efficiency is given by: $\phi_{CPD-Sens} = \phi_{ISC} \cdot \phi_{TTET} \cdot \phi_{CPD3}$.

In order to acquire an exact value of η_{CPD3} instead of an upper limit, triplet sensitizing experiments are performed on a mixture containing TpT and 2-M with an excitation at 320 nm (see the left part of Figure 5.1). As mentioned before, at this wavelength the extinction coefficient of TpT is so small that a direct excitation of TpT can be excluded. Its triplet state ^3TpT can only be occupied via a triplet-triplet energy transfer (TTET) from the sensitizer 2-M. From the previous chapter we know that the singlet excited state $^12\text{-M}^*$ deactivates predominantly via intersystem crossing. The decay time is circa 680 ps and the yield of intersystem crossing ϕ_{ISC} is 97.4%. In a neat 2-M solution (5 mM) at ambient oxygen concentration, the lifetime of the triplet state $^32\text{-M}$ is $\tau_0 = 1/Z_0 = 400$ ns (Z_0 is defined as the decay rate of $^32\text{-M}$ in the absence of TpT). In the presence of TpT, the triplet state $^32\text{-M}$ may be quenched by TTET upon collision with TpT (transfer rate Z_1). The transfer efficiency for TTET, ϕ_{TTET} , can be expressed by the decay rates Z_0 and Z_1 :

$$\phi_{TTET}(C) = \frac{Z_1(C)}{Z_1(C) + Z_0} \quad (5.1)$$

Here the concentration of the sensitizer 2-M is always set as a constant (5 mM). $Z_1 = Z_1(C)$ only depends on the concentration $C = C(TpT)$ of the triplet quencher TpT:

$$Z_1(C) = \kappa \cdot C = \kappa \cdot C(TpT) \quad (5.2)$$

The bimolecular collision constant κ is related to the diffusion of the involved molecules [Wel59]. After the population of the triplet state 3TpT by TTET, the reaction pathway of 3TpT is the same as for the direct excitation experiment. A small amount of the triplet excited TpT can form the CPD lesions with an efficiency ϕ_{CPD3} . The total CPD formation yield $\phi_{CPD-Sens}$ for the sensitizing experiment is given by:

$$\phi_{CPD-Sens} = \phi_{CPD-Sens}(C) = \phi_{ISC} \cdot \phi_{TTET}(C) \cdot \phi_{CPD3} \quad (5.3)$$

There are two methods to determine the quantum yield ϕ_{CPD3} , which is the most interesting quantity we want to quantify in this thesis:

- One can measure the CPD formation yield $\phi_{CPD-Sens}(C)$ for various TpT concentrations C and use equations 5.1 - 5.3 to determine the collision constant κ and the product $\phi_{ISC} \cdot \phi_{CPD3}$. Since the value of the yield ϕ_{ISC} is known from an earlier measurement, the quantity ϕ_{CPD3} can be easily obtained.
- A second approach uses a time-resolved experiment to determine $\phi_{TTET}(C)$ by measuring the TTET rate Z_1 for a certain TpT concentration. A stationary measurement of $\phi_{CPD-Sens}$ at the same concentration then allows the determination of ϕ_{CPD3} .

5.2 Quantum Yield Determined by Stationary Illumination

In this section, the first method mentioned before, i.e. the concentration dependent illumination experiments, will be used to determine ϕ_{CPD3} . The technical details about the sample circulation setup and the stationary illumination measurements can be found in chapter 3. While different concentrations of TpT ranging from 2.29 mM to 18.32 mM are used, the concentration of 2-M is always 5 mM. Figure 5.2 shows the results for a typical quantum yield measurement, where the absorbance changes of the IR spectra are recorded after different illumination times for a TpT concentration $C(TpT) = 9.16$ mM. Again, as already seen in Figure 4.4b, bleach of the original TpT absorption bands at the 1663 cm^{-1} and 1631 cm^{-1} is observed with rising illumination time. At the same time, there is increased absorption in the range from 1300 cm^{-1} to 1500 cm^{-1} at positions of the marker bands characteristic for the CPD lesions [Sch07]. An analysis of the absorption changes recorded as

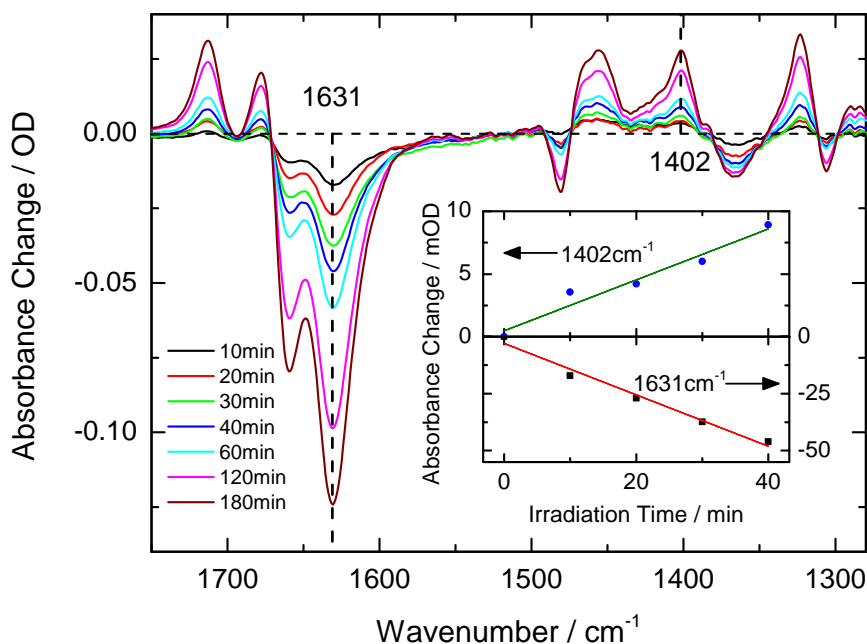


Figure 5.2: Absorbance changes in the MIR of a solution containing TpT (9.16 mm) and 2-M (5 mm) induced by illumination of the sensitizer 2-M at 320 nm after different irradiation times (absorbed irradiation 0.78 J/min). The rise of the CPD lesions is well recognized at the CPD marker bands between 1500 cm^{-1} and 1300 cm^{-1} . The rise of the 1402 cm^{-1} marker band and the bleach of the original TpT band at 1631 cm^{-1} are displayed in the inset.

a function of the absorbed illumination dose allows us to determine the quantum yield for CPD formation. The quantum yield is defined as the number of converted molecules per unit time divided by the number of absorbed photons per unit time [WH00]. Therefore, it can be expressed as:

$$\phi_{CPD-Sens} = \frac{V}{I} \cdot \frac{dC(CPD)}{dt} = \frac{V}{I} \cdot \frac{1}{\Delta\epsilon \cdot d} \cdot \frac{d\Delta A}{dt} \quad (5.4)$$

Here, $V = 1.2 \text{ ml}$ is the volume of the sample. I is the number of absorbed photons of the illumination light per unit time, which is connected with the power of absorbed photons P (P is measured in the unit of mW). At 320 nm, $I = P \times 2.67 \cdot 10^{-9} \text{ mol s}^{-1}$. $dC(CPD)/dt$ is the change of the CPD concentration per time. The change of absorbance per time $d\Delta A/dt$ can be expressed with the Beer-Lambert law as the product of $dC(CPD)/dt$, the change in extinction coefficient $\Delta\epsilon = 343.7 \text{ M}^{-1}\text{cm}^{-1}$ upon CPD formation at 1402 cm^{-1} and the light path $d = 108 \text{ }\mu\text{m}$ of the IR sample cell. The inset of Figure 5.2 displays the absorbance changes ΔA at 1631 cm^{-1} and 1402 cm^{-1} at different illumination times. At low illumination doses the absorbance

Concentration of TpT (mM)	2.29	4.58	9.16	18.32
Concentration of 2-M (mM)	5	5	5	5
Quantum Yield $\phi_{CPD-Sens}$ (%)	2.32	2.99	3.46	3.52

Table 5.1: Quantum Yield $\phi_{CPD-Sens}$ measured at different concentrations of TpT.

change ΔA can be fitted as a linear function of the illumination time [DS63]. In order to fulfill this requirement of low illumination doses, only ΔA at early illumination times are used for the linear fit (here up to 40 minutes, where less than 25% of the TpT molecules are converted to the CPD lesions). The slope of the fitted curve $d\Delta A/dt$ is utilized for the calculation of the quantum yield $\phi_{CPD-Sens}$. For the experiment with a concentration of $C(TpT) = 9.16$ mM, a value of $\phi_{CPD-Sens} = 3.3 \pm 0.2\%$ is obtained by using equation 5.4. Similarly, one can measure the quantum yield for other concentrations $C(TpT) = 2.29$ mM, 4.58 mM and 18.32 mM. The experimental results from a set of independent measurements at each concentration are plotted as symbols in Figure 5.3 and listed in Table 5.1.

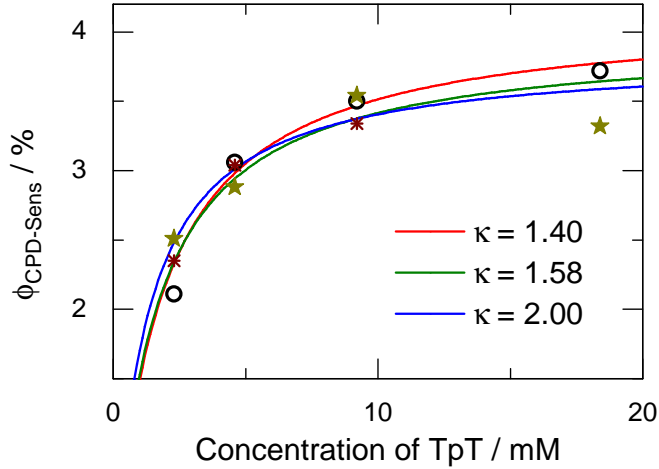


Figure 5.3: Quantum yield $\phi_{CPD-Sens}$ determined for different TpT concentrations (symbols) and a modeling of the quantum yield for different values of κ (solid curves).

As can be seen from equation 5.2, the quantum yield depends on the concentration of TpT. Combining the equations 5.1 - 5.4 leads to an equation which allows to deduce the unknown model parameters from just one plot of the experimental data:

$$\frac{1}{d\Delta A/dt} = a + a \cdot \frac{Z_0}{\kappa} \cdot \frac{1}{C(TpT)} \quad (5.5)$$

where

$$a = \frac{V}{I} \cdot \frac{1}{\Delta\varepsilon \cdot d} \cdot \frac{1}{\phi_{ISC} \cdot \phi_{CPD3}} \quad (5.6)$$

A linear fit of the inverse absorbance change per time as a function of the inverse concentration according to equation 5.5 is plotted in Figure 5.4, which yields the intersection $a = 2.5 \cdot 10^5 \text{ s}$ and the slope $a \cdot \frac{Z_0}{\kappa} = 3.9 \cdot 10^2 \text{ mM s}$. Using the known parameter $1/Z_0 = 400 \text{ ns}$ from section 4.3.3, the bimolecular collision constant $\kappa = 1.6 \cdot 10^9 \text{ M}^{-1}\text{s}^{-1}$ is obtained. It is worth noting that κ is extremely sensitive to the experimental data. In Figure 5.4 each point represents the averaged value from different independent measurements demonstrated as symbols in Figure 5.3. The statistical variations of the individual measurements indicate that κ should be between $1.4 \cdot 10^9 \text{ M}^{-1}\text{s}^{-1}$ and $2.0 \cdot 10^9 \text{ M}^{-1}\text{s}^{-1}$. The curves corresponding to different values of κ are also plotted in Figure 5.3. These values of κ are in good agreement with published data for similar molecules [GWR96], in which $\kappa = 1.8 \cdot 10^9 \text{ M}^{-1}\text{s}^{-1}$ is reported for the interaction between acetophenone and TMP.

At last, we are able to estimate the quantum yield of CPD formation via the triplet channel, ϕ_{CPD3} . By using equation 5.6, the known value of $\phi_{ISC} = 97.4\%$ and the fit parameter a , ϕ_{CPD3} is determined to be $4.1 \pm 0.2\%$.

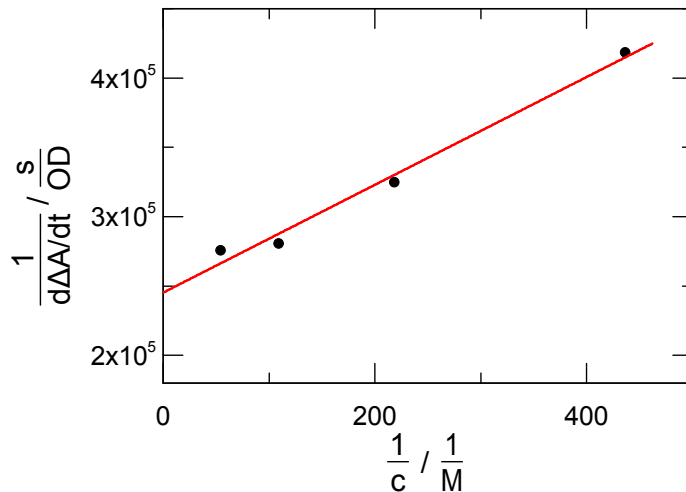


Figure 5.4: A linear fit of the inverse absorption change per time as a function of the inverse concentration of TpT. With the parameters deduced from the fit one can determine the quantum yield of CPD formation via the triplet channel, ϕ_{CPD3} .

5.3 Oxygen Dependent Measurement

Dissolved oxygen molecules in a solution are very efficient triplet quenchers [KB31, Foo68]. The resulting reactive oxygen species (ROS) are responsible for a set of DNA oxidative lesions, such as 8-Oxo-2'-deoxyguanosine [Dev91]. Among all DNA bases, guanine is most vulnerable to oxidative stress and thymine is relatively robust. Thus, we assume that ROS do not influence the observed reaction yield. On the other hand, triplet quenching by oxygen may influence the results of our experiments. To support our assumptions we have to confirm that the quenching due to dissolved oxygen cannot compete with the triplet-triplet energy transfer process between the sensitizer 2-M and TpT. With experiments performed at different oxygen concentrations, we prove that dissolved oxygen at ambient concentrations does not influence the quantum yield of CPD formation.

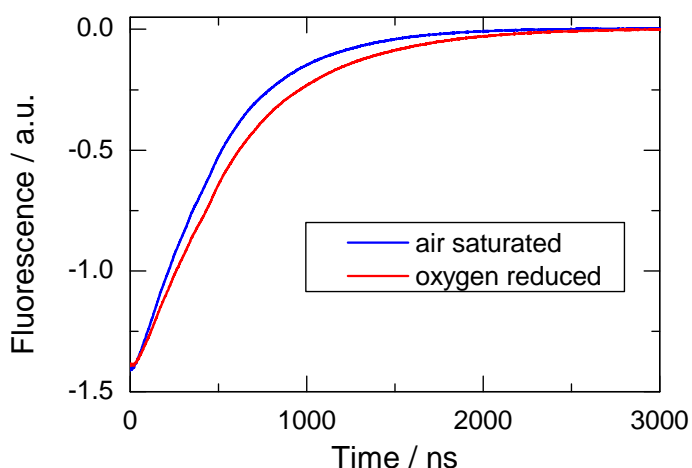


Figure 5.5: The luminescence lifetime of a 0.1 mM Tris(2,2'-bipyridyl)dichlororuthenium(II) hexahydrate solution is measured for different sample circulation setups. The blue curve represents the measurement at ambient oxygen and the red curve represents the measurement at reduced oxygen concentration generated by a degasser.

At first, the oxygen concentrations of the sample circulation setups used in the presented experiments are determined by measuring the luminescence lifetime of a 0.1 mM Tris(2,2'-bipyridyl) dichlororuthenium(II) hexahydrate solution. One sample circulation setup is used for all stationary illumination experiments at ambient oxygen concentration. The sample circulation setup for the oxygen reduced experiment is additionally connected with an online degasser (Knauer) and the sample reservoir is equipped with a nitrogen balloon to avoid contamination by oxygen from the ambient air. The excitation wavelength is 453 nm. The luminescence emission around 630 nm is recorded with a photodiode which is connected with an oscilloscope to measure

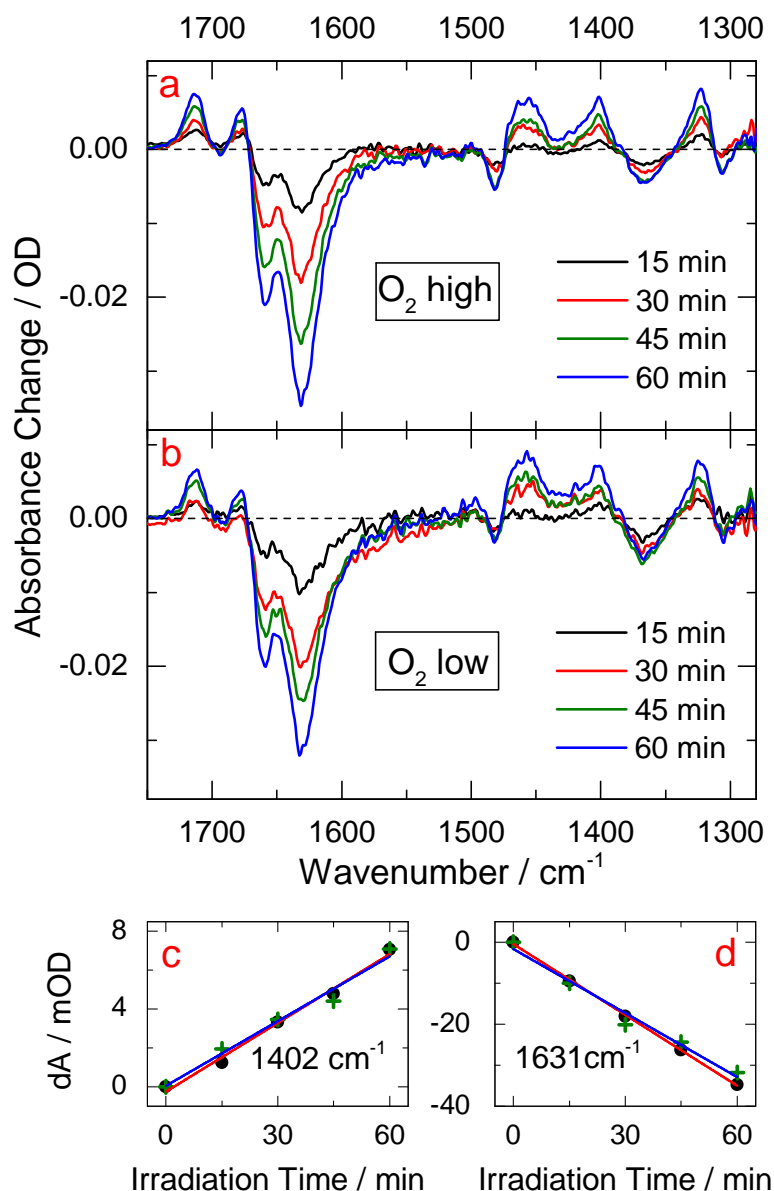


Figure 5.6: Absorbance changes after different irradiation times (absorbed irradiation 0.78 J/min). (a) At ambient oxygen concentration. (b) Same experiment as in (a), with a factor of three lower oxygen concentration. (c) Rise of the CPD marker band at 1402 cm⁻¹ and (d) bleach of the original TpT band at 1631 cm⁻¹. At high (black circles, red line) and low oxygen concentrations (green crosses, blue line) one observes the same slope, i.e. the reaction yield is independent of the oxygen concentration. The graphs show that the variation of the oxygen concentration does not influence the reaction yield.

the time-dependence of the emission. The curves as shown in [Figure 5.5](#) can be fitted mono-exponentially with a time constant τ . For the ambient oxygen and reduced oxygen situations, one finds $\tau = 458$ ns and 569 ns, respectively. The oxygen concentration can be deduced by the following equation:

$$C(O_2) = \frac{1}{\kappa_Q} \cdot \left(\frac{1}{\tau} - \frac{1}{\tau_0} \right) \quad (5.7)$$

which yields $C(O_2) = 0.215$ mM and 0.073 mM, respectively. Here the quenching rate $\kappa_Q = 3.3 \cdot 10^9 \text{ M}^{-1}\text{s}^{-1}$ [[DDH73](#), [LS76](#)] and the intrinsic lifetime of Tris(2,2'-bipyridyl)dichlororuthenium(II) hexahydrate in the absence of oxygen $\tau_0 = 650$ ns [[Nak82](#)] are taken from literature. The decrease in oxygen concentration by a factor of three is achieved by using a simple setup, which requires only 1.8 ml of solution. A further reduction is limited by the use of a peristaltic pump and Teflon tubes, which allow the penetration of oxygen. For a stronger oxygen reduction by a factor of five, a larger volume (>5 ml) of the solution is needed. However, if oxygen does play a significant role by the quenching, the reduction of oxygen concentration by a factor of three should allow us to observe a different quantum yield of CPD formation.

To demonstrate the influence of oxygen, solutions containing 9.16 mM TpT and 5 mM 2-M are illuminated at 320 nm. The quantum yields of CPD formation are compared for ambient and a reduced oxygen condition. The absorbance changes in the MIR range at early illumination times are plotted in [Figure 5.6a](#) and [b](#). Rise of the CPD marker band at 1402 cm^{-1} ([Figure 5.6c](#)) and bleach of the original TpT band at 1631 cm^{-1} ([Figure 5.6d](#)) at different times are demonstrated with different symbols. As already mentioned in the last section, the slope obtained from a linear fit of the corresponding measuring points is proportional to the quantum yield. In [Figure 5.6c](#) and [d](#), these lines overlap with each other. Thus, within experimental error, changes in oxygen concentration do not influence the experiments. These oxygen concentration dependent measurements exclude the role of quenching by oxygen under the experimental conditions. This result is not unexpected considering the concentration of dissolved oxygen in an aqueous solution (circa 0.1 mM) and the concentration of TpT (circa 10 mM). At these concentrations quenching by oxygen cannot compete with quenching by TpT.

5.4 Time-resolved Measurement on TpT

The triplet channel of TpT plays a very important role in the whole reaction scheme, as can be seen in [Figure 5.1](#). In order to clarify its reaction dynamics, a time-resolved measurement on a neat TpT solution (5 mM) is performed. We use an excitation at 250 nm, since according to [[Ban12](#)], the intersystem crossing efficiency of TMP

decreases from 250 nm to 280 nm with rising excitation wavelengths. The same trend is also observed for single-stranded (dT)₁₈, where the intersystem crossing efficiency at 250 nm is higher than at 266 nm [Pil16].

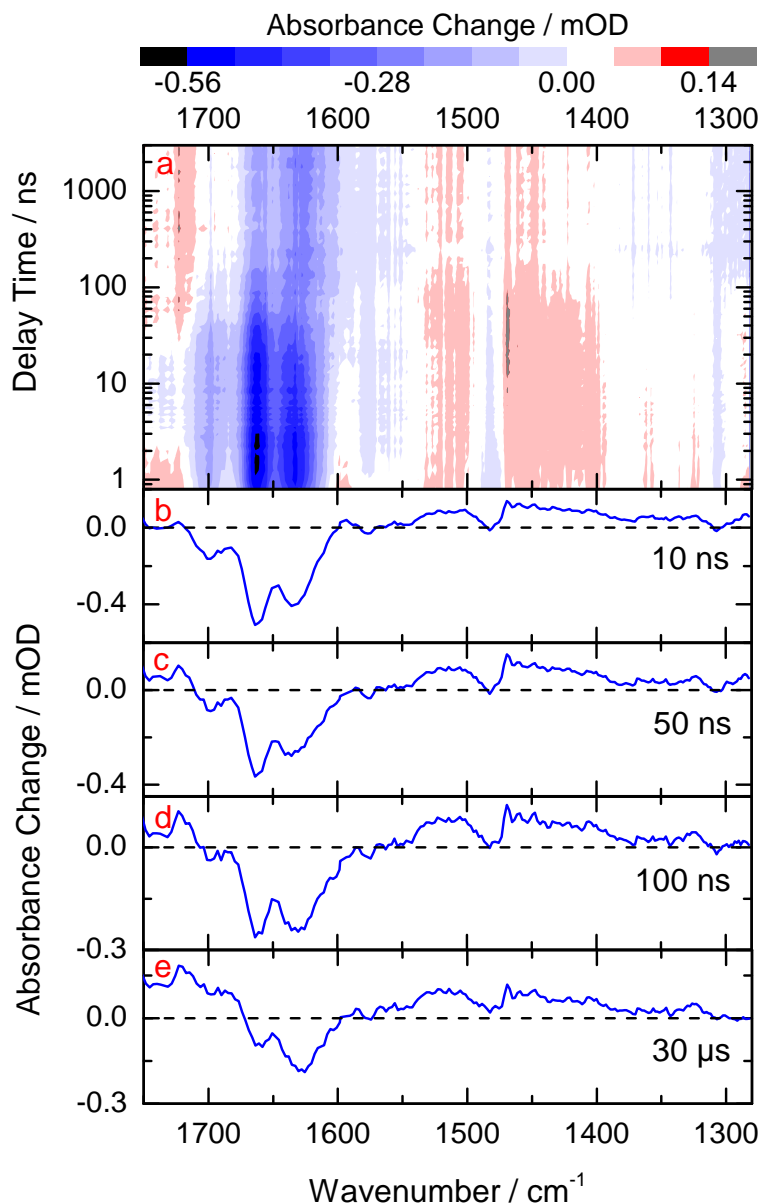


Figure 5.7: Transient absorption data for a TpT solution excited with nanosecond pulses at 250 nm. (a) Absorbance changes recorded as a function of the probing wavenumber and the delay time in color coding. Transient absorbance difference spectra recorded at delay times of 10 ns (b), 50 ns (c), 100 ns (d) and at the end of the observation range at 30 μs (e). Reprinted with permission from [Liu16]. Copyright (2016) American Chemical Society.

5.4.1 Experimental Results

The excitation pulse duration is about 3 ns and the pulse energy is 4 μJ . Considering the ultrashort lifetime of the singlet excited state ^1TpT (< 1 ps), the intersystem crossing process of TpT cannot be resolved in this experiment. Therefore, the triplet state ^3TpT seems to be instantly occupied after the excitation by nanosecond pulses. The absorbance changes recorded as a function of the probing wavenumber (1280 cm^{-1} to 1750 cm^{-1}) and the delay time (0.8 ns to 3 μs) are displayed in Figure 5.7a. At late delay times (3 μs to 30 μs , data not shown) we do not observe further absorbance changes. Transient spectra at different delay times are plotted in Figure 5.7b - e. Due to the very efficient and fast internal conversion (IC) and the following heat exchange between the TpT molecules and the solvent molecules, the solution is heated within 10 ps and reaches its thermal equilibrium [PPK01]. This contribution of solvent heating is corrected for the entire experimental data. At early delay times significant negative signals due to the ground state bleach can be observed between 1700 cm^{-1} and 1600 cm^{-1} . At the same time, some positive bands appear between 1550 cm^{-1} and 1300 cm^{-1} . The most pronounced absorbance changes occur within the first 100 ns. At a late delay time (30 μs), the remaining positive features are probably due to the formation of some CPD lesions, which are present from the beginning and do not change in the entire observation time window. Therefore, the CPD lesions are formed predominantly via the singlet excited state. However, the possibility of CPD formation via the triplet channel cannot be excluded. Although it exists, its amplitudes are too small to be detected in this experiment.

5.4.2 Modeling and Interpretation of the Data

From recent investigations on the comparable molecule $(\text{dT})_{18}$ [Pil14b] one learns that the decay of the triplet excitation also happens in the time range up to 100 ns and involves two triplet transient species: the triplet state $^3(\text{dT})_{18}$ and the biradical state ^3BR . Under the same experimental conditions (same excitation wavelength, pulse energy and concentration of thymine bases), the transient data for $(\text{dT})_{18}$ could be globally fitted with two time constants ($\tau_1 = 12$ ns and $\tau_2 = 59$ ns) [Pil14b]. Using the sequential reaction model proposed in Figure 5.1, τ_1 is attributed to the decay from $^3(\text{dT})_{18}$ to ^3BR and τ_2 from ^3BR to the ground state. The SADS for $(\text{dT})_{18}$ (red curves) are demonstrated in Figure 5.8. The triplet state $^3(\text{dT})_{18}$ shows the characteristic band at 1600 cm^{-1} and the negative bands due to the bleach of the carbonyl band between 1700 cm^{-1} and 1630 cm^{-1} . On the other hand, the biradical state ^3BR shows distinct features between 1700 cm^{-1} and 1600 cm^{-1} . While the bleach of the 1630 cm^{-1} band decreases significantly, a positive band around 1620 cm^{-1} emerges. At the same time, the 1600 cm^{-1} triplet band vanishes.

A similar data processing procedure is performed here for the measurement of TpT. At first, the DADS are obtained and shown in Figure 5.9. The global fit yields two

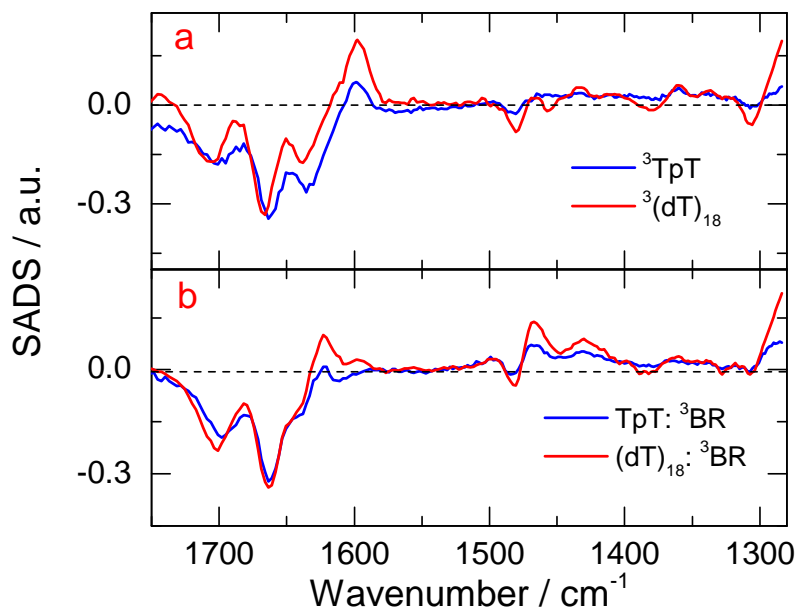


Figure 5.8: The species associated absorption difference spectra (SADS) calculated from the absorption difference data for TpT (blue curves) and for (dT)₁₈ (red curves). (a) SADS corresponding to the triplet state and (b) to the biradical state.

somehow larger time constants ($\tau_1 = 22.5$ ns and $\tau_2 = 62$ ns). The discrepancy of τ_1 can be explained by the different numbers of neighboring thymine bases for TpT and (dT)₁₈. While each excited triplet thymine base in the long single-stranded oligonucleotide (dT)₁₈ can react with its two neighboring bases to form a biradical state, an excited thymine base in the dinucleotide TpT has only one neighboring base. Thus, the decay time from the triplet state to the biradical state increases from 12 ns for (dT)₁₈ to 22.5 ns for TpT. In contrast, the decay from the biradical state to the ground state is not strongly influenced by the number of neighboring bases. Again, one can calculate the corresponding SADS (see Figure 5.8, blue curves). They exhibit the similar features for the respective states as described before for (dT)₁₈. The nice agreement of the two species, as can be seen in Figure 5.8, supports the validity of the reaction model (Figure 5.1) and the data analysis procedure. The results for ³TpT will be used in the next section for the sensitizing experiment.

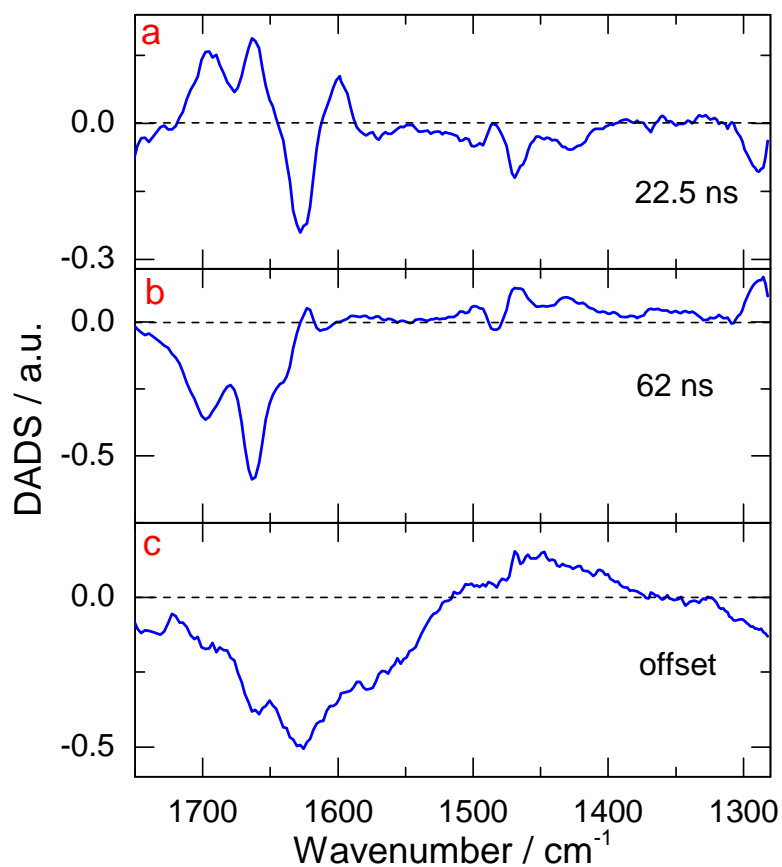


Figure 5.9: The decay associated difference spectra (DADS) for a TpT solution (5 mM) excited at 250 nm. The transient absorption data are globally fitted using a sum of two exponential functions and an offset convoluted with the instrumental response function. (a) represents the decay from ^3TpT to ^3BR , (b) the decay from ^3BR to the ground state and (c) the spectral changes due to solution heating and product formation.

5.5 Time-resolved Measurement on 2-M and TpT Mixtures

In this section, combined time-resolved and stationary quantum yield measurements performed with the same concentrations, are used to estimate ϕ_{CPD_3} independently.

5.5.1 Low Concentration of TpT (9.16 mM)

At first, a solution containing TpT (9.16 mM) and 2-M(5 mM) is illuminated with nanosecond pulses at 320 nm. With these pulses 2-M is excited exclusively.

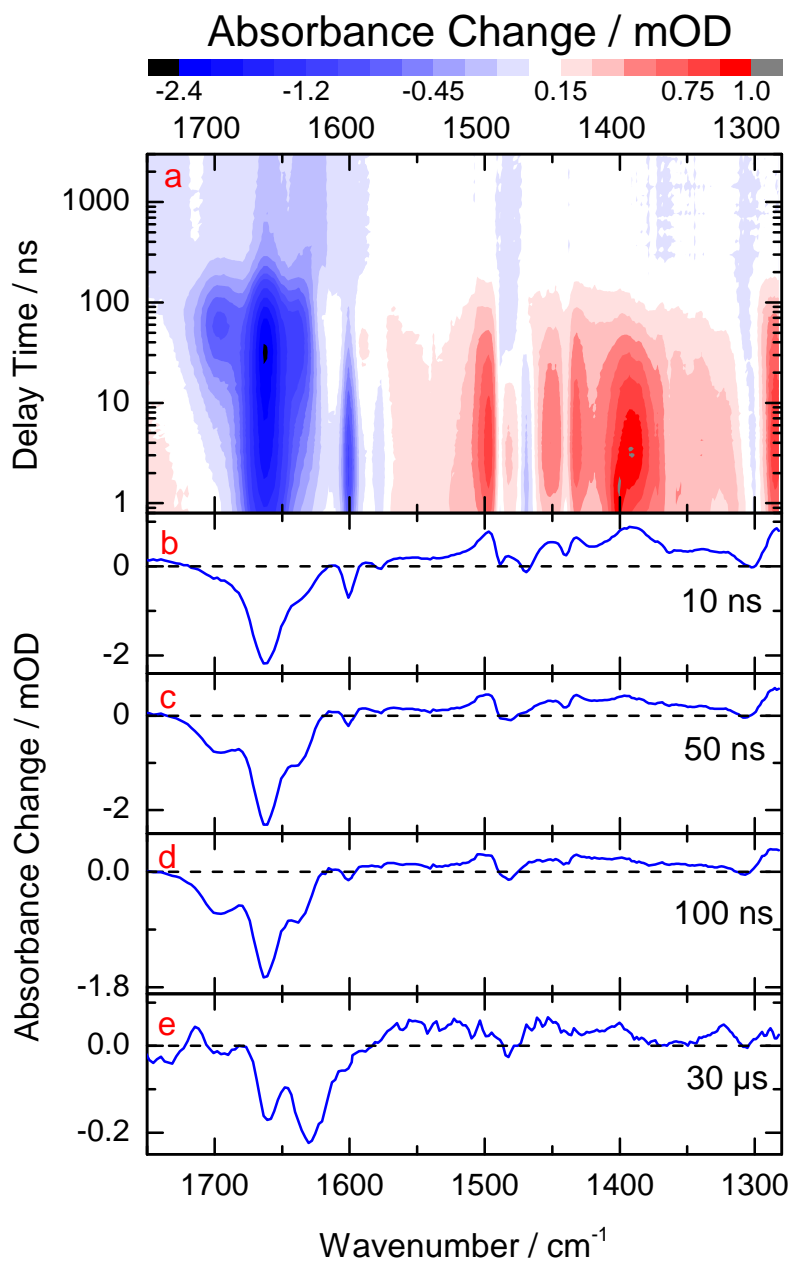


Figure 5.10: Transient absorption data for the sensitizing reaction (solution containing 2-M (5 mM) and TpT (9.16 mM), excited with nanosecond pulses at 320 nm). (a) Absorbance changes recorded as a function of the probing wavenumber and the delay time in color coding. Absorption difference spectra recorded at delay times of 10 ns (b), 50 ns (c), 100 ns (d) and at the end of the observation range at 30 μs (e).

The excitation pulse duration is about 3 ns and the pulse energy is 6 μJ. The ab-

sorbance changes recorded as a function of the probing wavenumber (1280 cm^{-1} to 1750 cm^{-1}) and the delay time (0.8 ns to 3 μs) are shown in Figure 5.10a. No significant dynamics are observed at late delay times (3 μs to 30 μs , data not shown). The contribution of solvent heating is corrected for the entire experimental data. Transient spectra recorded at 10 ns, 50 ns, 100 ns and a late delay time (30 μs) are displayed in Figure 5.10b - e. Immediately after excitation (10 ns), negative bands at 1663 cm^{-1} and 1600 cm^{-1} due to the ground state bleach of 2-M and positive bands at 1497 cm^{-1} , 1393 cm^{-1} and 1285 cm^{-1} due to the induced absorption of $^3\text{2-M}$ are observed. The spectra at early delay times resemble the spectra of the nanosecond experiment on a neat 2-M solution (see Figure 4.15). At 320 nm only the sensitizer 2-M is excited. These spectral features point to the presence of the triplet state $^3\text{2-M}$. The triplet bands of 2-M decay on the 50 ns time scale. At 50 ns and 100 ns the transient spectra display characteristic features known for the TpT triplet state ^3TpT . Apparently, the triplet-triplet energy transfer from $^3\text{2-M}$ to ^3TpT occurs in this time range. At a late delay time (50 μs) the spectrum contains negative bands due to the bleach of TpT and some positive bands probably due to the formation of CPD lesions and other photoproducts.

Further data processing is hampered by the fact that the estimated time of TTET (circa 50 ns) falls into the same range as the decay of the ^3BR state of TpT (circa 60 ns). A global fit using close-lying time constants often leads to spectra with mirroring features, which do not represent the true transitions. In order to achieve a better separation of the TTET and the subsequent decay of ^3BR , the TTET process has to be accelerated. From equation 5.2 we know that the TTET rate Z_1 depends on the concentration of TpT. Thus, a higher concentration of TpT is needed.

5.5.2 High Concentration of TpT (18.32 mM)

A similar experiment on a solution containing a higher concentration of TpT (18.32 mM) and 2-M (5 mM) is performed. The experimental conditions are the same as in section 5.5.1.

Experimental Results

The absorbance changes recorded as a function of the probing wavenumber (1280 cm^{-1} to 1750 cm^{-1}) and the delay time (0.8 ns to 3 μs) are shown in Figure 5.11a. No significant changes are observed at late delay times (3 μs to 50 μs , data not shown). The contribution of solvent heating is corrected for the entire experimental data. Transient spectra recorded at 10 ns, 50 ns, 100 ns and a late delay time (50 μs) are displayed in Figure 5.11b - e. The spectra are similar as already observed in the previous experiment using low concentration of TpT. Immediately after excitation (10 ns), negative bands at 1663 cm^{-1} and 1600 cm^{-1} due to the ground state bleach of 2-M combined with positive bands at 1497 cm^{-1} , 1393 cm^{-1} and 1285 cm^{-1} due

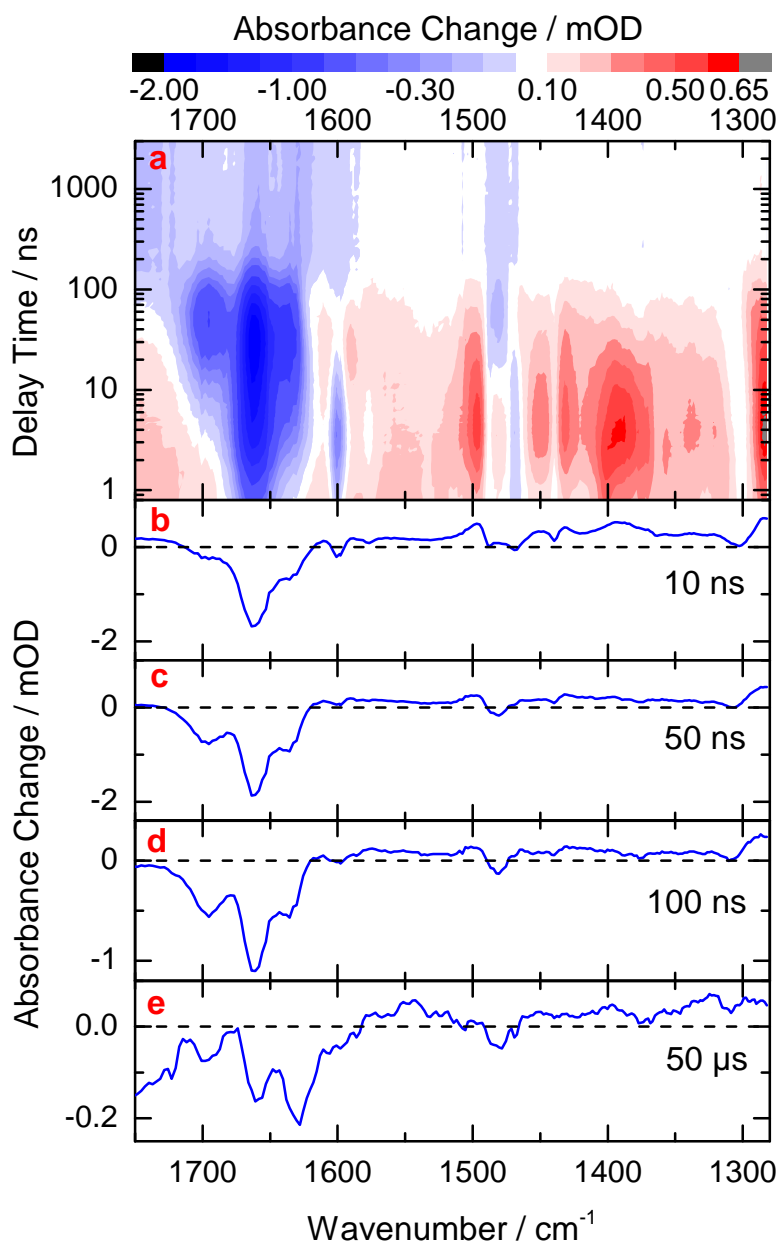


Figure 5.11: Transient absorption data for the sensitizing reaction (solution containing 2-M (5 mM) and TpT (18.32 mM)) excited with nanosecond pulses at 320 nm. (a) Absorbance changes recorded as a function of the probing wavenumber and the delay time in color coding. Absorption difference spectra recorded at delay times of 10 ns (b), 50 ns (c), 100 ns (d) and at the end of the observation range at 50 μs (e). Reprinted with permission from [Liu16]. Copyright (2016) American Chemical Society.

to the induced absorption of $^3\text{2-M}$ are observed. The spectra at early delay times suggest the presence of the triplet state $^3\text{2-M}$. The triplet bands of 2-M decay on the 30 ns time scale. At 50 ns and 100 ns the transient spectra display characteristic features known for the triplet state ^3TpT . Apparently, the triplet-triplet energy transfer from $^3\text{2-M}$ to ^3TpT occurs in this time range. At a late delay time (50 μs) the spectrum contains negative bands due to the bleach of TpT and some positive bands probably due to the formation of CPD lesions and other photoproducts.

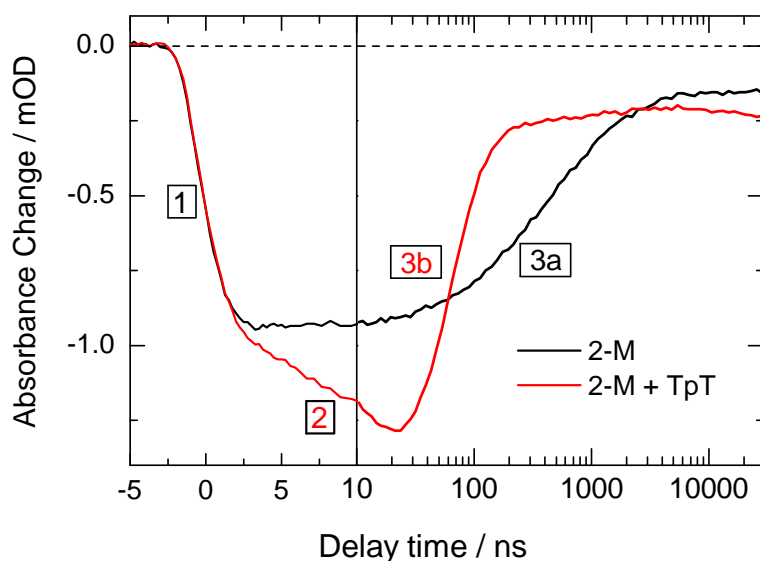


Figure 5.12: Time dependent absorbance changes for a neat 2-M solution (black) and a mixture solution containing 2-M and TpT (red) recorded at 1663 cm^{-1} . While the rise of the absorption bleach upon excitation and formation of $^3\text{2-M}$ is similar in both samples (phase 1), the pure 2-M solution shows a late absorption recovery with a time constant of 400 ns (phase 3a). For the mixture there is a secondary absorption bleach up to 30 ns (phase 2) due to TTET to TpT before the absorption recovers with a time constant of 60 ns (phase 3b).

In [Figure 5.12](#) the reaction dynamics of the neat 2-M experiment (black curve) and the sensitizing experiment (red curve) are compared at 1663 cm^{-1} , where both TpT and 2-M have strong ground state absorption. These two experiments are performed under the same experimental conditions (the excitation wavelength is 320 nm, pulse energy is 6 μJ and the concentration of 2-M is 5 mM). For the neat 2-M solution, a fast bleach indicates the excitation of 2-M (phase 1). Thereafter, a slow decay occurs, which can be fitted with a time constant of circa 400 ns (phase 3a). The time constant and the transient spectrum point to the presence of $^3\text{2-M}$ during the whole time range. The mixture solution containing 2-M and TpT shows at early delay times the same bleach (phase 1), because only the sensitizer 2-M is excited. Interestingly,

the bleach increases further on the 10 ns time scale and reaches its maximum at circa 25 ns. It is again a strong evidence for the existence of the triplet-triplet energy transfer from $^3\text{2-M}$ to ^3TpT . ^3TpT decays subsequently much faster with a time constant of circa 60 ns to the ground state (phase 3b). This time constant agrees well with the typical decay time known for ^3TpT , as described in the last section.

Modeling and Interpretation of the Data In order to obtain more dynamic information for the sensitizing experiment, the experimental data are fitted by a sum of exponential functions. Using the known bimolecular rate constant $\kappa = 1.6 \cdot 10^9 \text{ M}^{-1}\text{s}^{-1}$ from the stationary illumination measurements, the concentration of TpT (18.32 mM) and equation 5.2, the triplet-triplet energy transfer time (τ_{TTET}) is calculated to be 34 ns. The lifetime of $^3\text{2-M}$ (τ_{3-2M}) can be further estimated by:

$$\frac{1}{\tau_{3-2M}} = \frac{1}{\tau_3} + \frac{1}{\tau_{TTET}} \quad (5.8)$$

This yields $\tau_{3-2M} = 31$ ns. Here, the effective lifetime of 2-M $\tau_3 = 400$ ns is used from the time-resolved experiment on a neat 2-M solution as described in section 4.3.3. τ_{3-2M} lies in the same time range as the time constants for the decay of the triplet state ^3TpT ($\tau_1 = 22.5$ ns) and the subsequent biradical state ^3BR ($\tau_2 = 62$ ns). This makes the global fit mathematically unstable, because a simple fit according to the proposed reaction model requires three unrestricted time constants between 10 ns and 100 ns. Therefore, the time constants τ_1 and τ_2 are predetermined by using the values from the last section. $\tau_{3-2M} = 33 \pm 10$ ns is deduced from the global fit for the experimental data of the sensitizing experiment as the only free time constant. The related DADS of all time constants are shown in [Figure 5.13](#). Comparing [Figure 5.9](#) and [Figure 5.13](#), the two spectra at 62 ns show very similar features. Thus, τ_2 describes the decay of ^3BR . In contrast, the two spectra at 22.5 ns display completely different features. The 22.5 ns spectrum shown in [Figure 5.9a](#) looks similar to the 33 ns spectrum shown in [Figure 5.13a](#). Considering the similar time scale, a clear separation of the TTET from $^3\text{2-M}$ to ^3TpT and the subsequent decay from ^3TpT to ^3BR is difficult. It is possible that the longer TTET process also contains some features of the shorter ^3TpT to ^3BR decay. The question whether the CPD lesions are formed from ^3TpT or ^3BR or from both states cannot be answered unambiguously from the data evaluation procedures. The difficulty comes from the presence of three time constants between 10 ns and 100 ns, the precision of the experimental data and the low efficiency of CPD formation.

The bimolecular rate constant κ can also be estimated independently from the time-resolved experiment. By using the relation $1/\tau_{TTET} = \kappa \cdot C(\text{TpT})$ and equation 5.8, $\kappa = 1.5 \cdot 10^9 \text{ M}^{-1}\text{s}^{-1}$ is obtained. It is in the same range as $\kappa = 1.6 \cdot 10^9 \text{ M}^{-1}\text{s}^{-1}$ obtained from the stationary quantum yield measurements. The SADS acquired by using the same approach as in the last section are plotted in [Figure 5.14](#) (blue curves) and compared with the SADS obtained from the neat TpT measurement (red

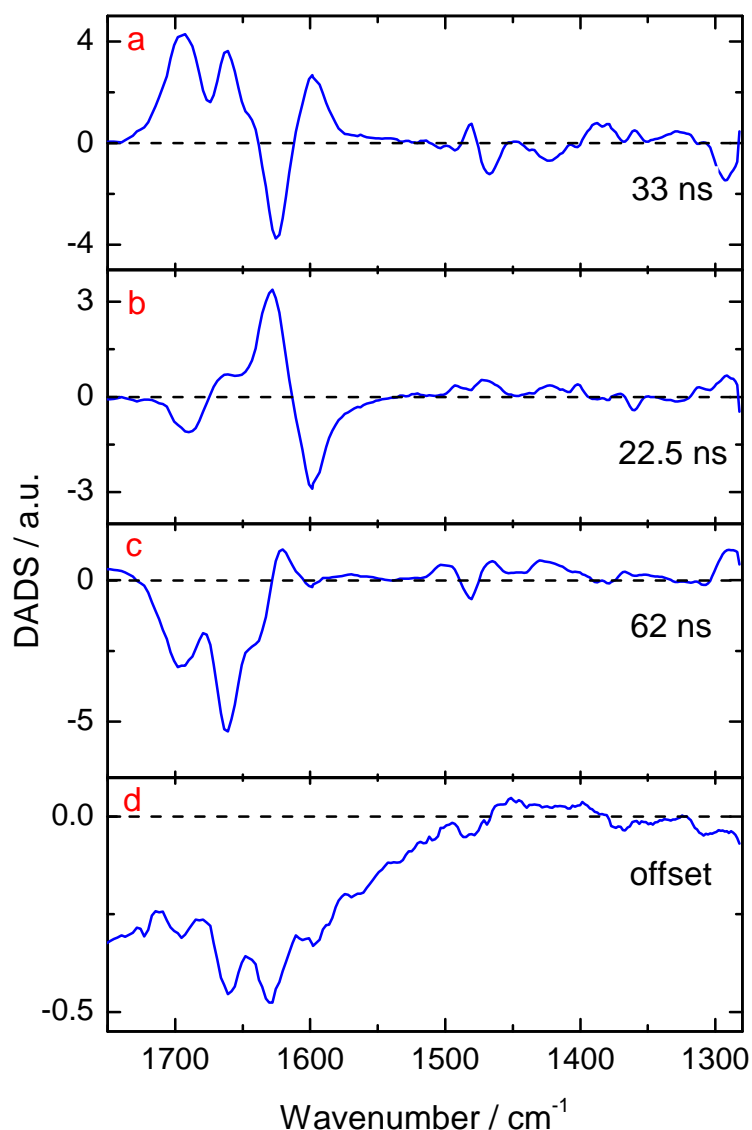


Figure 5.13: Decay associated difference spectra (DADS) for the sensitizing experiment. The transient absorption data are globally fitted using a sum of three exponential functions and an offset convoluted with the instrumental response function. Here, the second time constant $\tau_1 = 22.5$ ns (b) and the third time constant $\tau_2 = 62$ ns (c) are predetermined as described in the text. The offset (d) represents the end spectra related to solution heating and product formation. The remaining time constant τ_{3-2M} (a) is the only time constant fitted in the modeling procedure.

curves). In [Figure 5.14a](#) the SADS for ³2-M is given, which does not exist for the neat TpT measurement. While the negative bands at 1661 cm^{-1} and 1600 cm^{-1} are

due to the ground state bleach of 2-M, a series of positive bands between 1500 cm^{-1} and 1300 cm^{-1} are assigned to the marker bands of $^3\text{2-M}$. Figure 5.14b compares the SADS of ^3TpT from the two independent measurements. The bleaches between 1700 cm^{-1} and 1630 cm^{-1} and the marker band at 1600 cm^{-1} appear in both curves, which are characteristic for ^3TpT . Likewise, the SADS of ^3BR show similar features as well. The positive band at 1600 cm^{-1} for ^3TpT shifts to 1620 cm^{-1} . The nice agreement of almost all spectral features strongly supports the reaction model and the data analysis procedure.

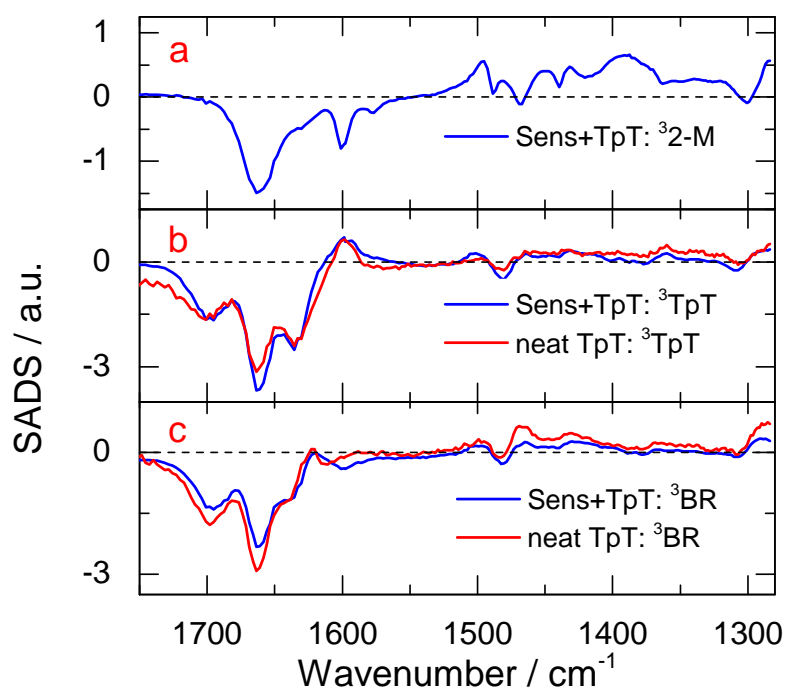


Figure 5.14: Species associated absorption difference spectra (SADS) calculated for the neat TpT (excited at 250 nm, red curves) and for the sensitizing experiment (solution containing the sensitizer 2-M (5 mM) and TpT (18.32 mM), excited at 320 nm, blue curves). (a) SADS corresponding to the triplet state $^3\text{2-M}$ and (b) to the triplet state ^3TpT and (c) to the biradical state ^3BR . Reprinted with permission from [Liu16]. Copyright (2016) American Chemical Society.

Finally, one can calculate the quantum yield of CPD formation via the triplet channel ϕ_{CPD3} . From Table 5.1 the CPD formation quantum yield $\phi_{CPD-Sens}$ at $C(\text{TpT}) = 18.32\text{ mM}$ is 3.52%. Using the bimolecular rate constant κ obtained from this time-resolved experiment, the TTET efficiency ϕ_{TTET} is determined to be 91.7%. Equation 5.3 readily leads to the result: $\phi_{CPD3} = 3.9\%$.

5.6 Discussion

The quantum yield of CPD formation via the triplet channel, ϕ_{CPD3} , is determined to be circa 4% with two independent approaches, as can be seen in section 5.2 and section 5.5. The similar values obtained from different methods also support the validity of the proposed reaction model. CPD formation of TpT after excitation of 2-M occurs through a triplet-triplet energy transfer photosensitization process. For the excited 2-M molecules, the quenching due to dissolved oxygen cannot compete with the quenching by TpT.

CPD Formation Efficiency upon UV-C Irradiation

Using the determined value of ϕ_{CPD3} , one can estimate the quantum yield η_{CPD3} for CPD formation via the triplet channel upon direct excitation with UV-C light as mentioned in section 5.1. For an excitation at 266 nm the triplet yield of TMP is deduced from literature [Ban12] to be $\eta_{ISC} = 1.3\%$. In the thesis of B. Pilles [Pil16] it is shown that the triplet yields of the monomer TMP and the oligonucleotide (dT)₁₈ are the same upon excitation at 250 nm. It seems that the stacking of the thymine bases does not influence the triplet yield. Thus, we can use the value of $\eta_{ISC} = 1.3\%$ also for TpT. Using the relation $\eta_{CPD3} = \eta_{ISC} \cdot \phi_{CPD3}$, one obtains $\eta_{CPD3} \approx 0.05\%$. In comparison, the quantum yield of CPD formation via the singlet channel upon direct excitation at 266 nm, η_{CPD1} , is circa 1.5% for TpT [Sch09]. Therefore, the CPD formation at 266 nm via the singlet channel occurs 30 times more efficiently than via the triplet channel. This finding supports the assumption that upon UV-C excitation the CPD lesions are formed predominantly via the singlet channel [Sch09]. The relative importance of the singlet channel becomes even larger with increasing illumination wavelengths in the UV-C range¹. The situation is entirely different in the UV-A range, where the solar irradiation reaches the earth's surface with much higher efficiency than in the UV-B and UV-C range. The direct absorption of DNA bases in the UV-A range can almost be neglected. However, in the presence of sensitizer molecules, the occupation of the triplet channel from TTET plays a dominant role.

The Different Molecular Mechanisms of CPD Formation

The molecular processes of CPD formation are also different for the singlet channel and the triplet channel. The CPD formation via the singlet channel is faster than 1 ps [Sch07]. The corresponding molecular process occurs on a time scale where the relative arrangement of the adjacent bases is essentially frozen. Quantum chemical modeling and molecular dynamics show that only those molecules which are already appropriately prearranged at the instant of the photon absorption are able to form

¹At 280 nm the triplet yield is smaller than at 250 nm, while the quantum yield of CPD formation does not change [Ban12].

CPD lesions [JW07, Law08]. The relative low quantum yield η_{CPD1} (1.5%) is limited by the probability of a suitable reactive arrangement of adjacent bases. The energetic constraints are relaxed due to the large energy excess of the singlet state to the CPD lesions. On the other hand, with a typical lifetime in the 10 ns range for the triplet state, adjacent bases can test the entire conformation space of arrangements, especially for the biradical state 3BR where one bond of the CPD lesions is already preformed [Pil14b]. The still relatively low yield ϕ_{CPD3} (4%) is probably due to the energetic constraints. The energy of the triplet state is well below that of the singlet state. Therefore, less energy is available for CPD formation and the reaction rate is strongly reduced.

6 Formation and Deamination of CPD Lesions in Cytosine Containing Dinucleotides

In chapter 5, the formation of CPD lesions via the triplet channel was intensively investigated for the dinucleotide TpT. We know that CPD lesions occur most frequently between two thymine bases. However, as already discussed in section 2.3.1, cytosine containing CPD lesions are much more mutagenic, because the cytosine base can easily deaminate to a uracil base if the C5=C6 double bond is saturated [BCL95]. In this chapter, we extend the use of the sensitizer 2-M to cytosine containing dinucleotides, i.e. TpC, CpT and CpC. The deamination processes of corresponding photoproducts are observed and quantified at a certain wavenumber in the mid-IR range.

6.1 Spectroscopic Characterization of the Dinucleotides

The dinucleotide TpT has already been characterized with UV and IR spectroscopic methods before. In this section, TpC and CpT will be measured with the same methods under the same conditions. The UV absorption spectra of all dinucleotides are displayed in Figure 6.1. TpT has a maximum at 266 nm and shows a non-vanishing wing at wavelengths above 300 nm¹. The spectrum is in good agreement with the corresponding literature value [Voe63]. As already discussed in section 2.2.2, the strong absorption bands between 250 nm and 280 nm for all three dinucleotides are assigned to $^1\pi\pi^*$ transitions. TpC and CpT show similar absorption features, which can be seen as a superposition of TpT and CpC. Notably, all three dinucleotides have very weak absorption in the UV-A range. The selective excitation of 2-M at 320 nm can always be fulfilled.

Figure 6.2 shows the IR absorption spectra of TpT, TpC and CpT. For TpT, the strong absorption bands at 1663 cm^{-1} and 1632 cm^{-1} mainly arise from the stretching vibrations of the C2=O2, C4=O4 and C5=C6 double bonds of thymine. In addition, the in-plane ring vibration also contributes to the 1632 cm^{-1} band. The band at 1480 cm^{-1} is attributed to the vibration of the C4-C5 and the C2-N1 bond of thymine. TpC and CpT display very similar absorption features. The absorption

¹This weak wing cannot be clearly seen in Figure 6.1 using a linear scale for the absorbance. Its existence can be confirmed using a logarithmic scale as shown in Figure 4.10.

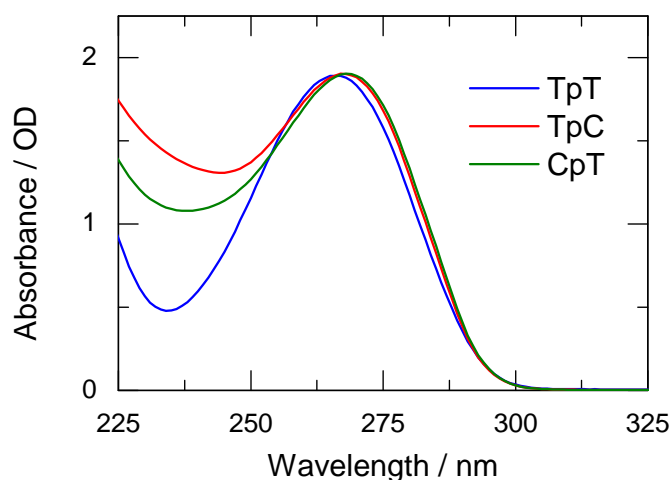


Figure 6.1: The absorption spectra of the dinucleotides in the UV range, recorded from 225 nm to 325 nm, measured at same concentrations (0.2 mM), TpT (blue), TpC (red) and CpT (green).

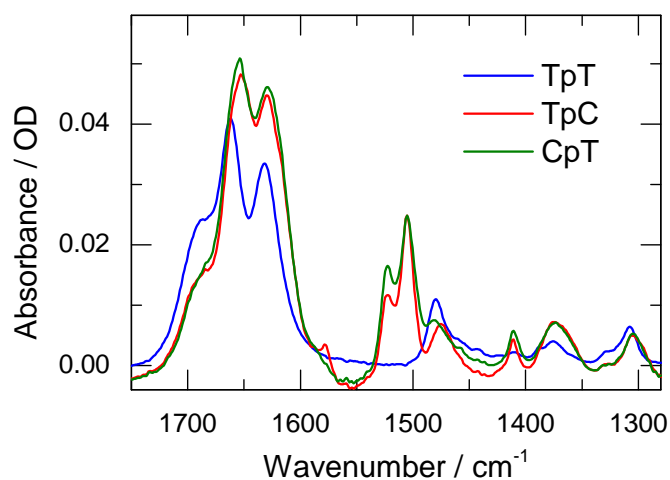


Figure 6.2: The absorption spectra of the dinucleotides in the MIR range, measured at same concentrations (2.5 mM), TpT (blue), TpC (red) and CpT (green).

band at 1653 cm^{-1} is assigned to the stretching vibration of the $\text{C}2=\text{O}2$ double bond of cytosine. The band at 1522 cm^{-1} due to the in-plane vibration and at 1505 cm^{-1} due to the C-N vibration are characteristic for cytosine. The spectral assignments of the IR absorption bands refer to [BSG03, LGT87].

6.2 Formation of Cytosine Containing CPD Lesions

After the spectral characterization of the dinucleotides, we want to examine their interaction with the sensitizer molecules. While thymine is the main target of sensitization due to its lowest triplet energy among the four DNA bases, cytosine possesses the highest triplet energy [GES67]². As a consequence, the frequently used photosensitizer, acetophenone, cannot sensitize cytidine monophosphate (CMP) [GWR96]. Considering the relatively high triplet energy and strong absorption in the UV-A range, we use the sensitizer 2-M and test whether it can also sensitize cytosine containing dinucleotides.

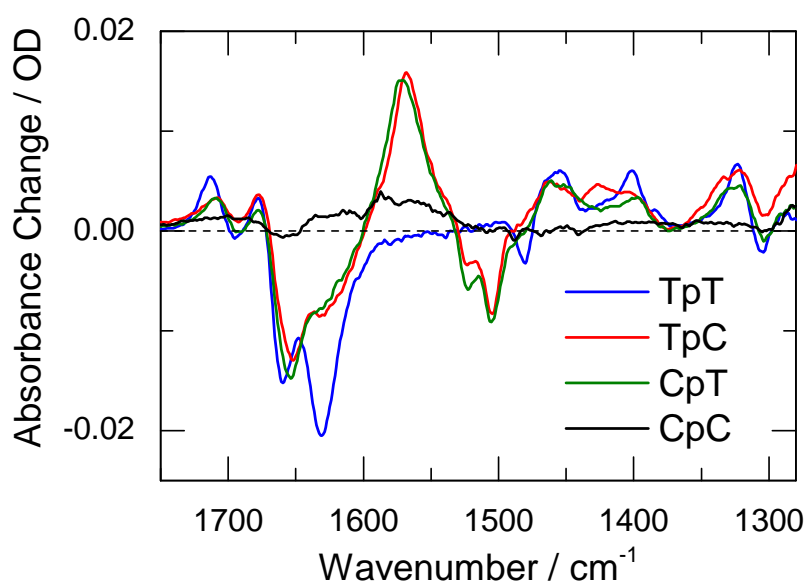


Figure 6.3: The IR difference absorption spectra of TpT (blue), TpC (red), CpT (green) and CpC (black) solutions recorded after the same illumination time. Each solution contains 5 mM 2-M and 2.5 mM dinucleotides. For TpT, TpC and CpT, CPD marker bands in the fingerprint region and the bleach due to the original thymine or cytosine bases are observed. For CpC, only minor changes are detected which are due to the photo-bleach of the sensitizer 2-M.

Solutions containing 2-M (5 mM) and different dinucleotides (2.5 mM) are illuminated under the same experimental conditions at 320 nm. Their absorbance changes in the IR range after 40 minutes of illumination are displayed in Figure 6.3. For TpT, as already seen many times before, positive CPD marker bands in the fingerprint region and negative bands due to the bleach of the thymine base are observed. For TpC and CpT, similar spectral features indicate the formation of CPD lesions. While the

²The triplet energies for TMP and CMP in aqueous solution at room temperature are 310 kJ/mol and 321 kJ/mol, respectively [WR96].

positive bands in the 1500 cm^{-1} to 1300 cm^{-1} range have slight differences compared to the marker bands of TpT, the negative bands at 1522 cm^{-1} and 1505 cm^{-1} are attributed to the distinct bleach of the cytosine base. The bleaches between 1700 cm^{-1} and 1600 cm^{-1} result from both the cytosine and the thymine base. It is worth noting that a huge absorption band emerges around 1567 cm^{-1} for TpC and CpT. Since no (6-4) photoproduct and other photoproducts are reported after UV-A irradiation [Dou03], we tentatively assign this new band to another marker band of the CPD lesions, which is unique for cytosine containing CPD. For CpC, there are only minor changes which resemble the spectrum shown in Figure 4.12b. This points to a photo-degradation of 2-M in the mixture solution. At the same time, CpC remains intact during the illumination.

The different experimental results for the four dinucleotides suggest that 2-M can only sensitize the thymine base. Its triplet energy is not sufficient for an efficient TTET to the cytosine base. For the dinucleotides TpC and CpT, independent of the position of the thymine base, 2-M can transfer its triplet energy to thymine as it does in the case of TpT. Afterwards, the thymine in the triplet excited state can further interact with the adjacent cytosine to form a CPD lesion. This process may involve a biradical state as an intermediate, where one bond of the CPD lesion is already preformed.

6.3 Deamination of Cytosine Containing CPD Lesions

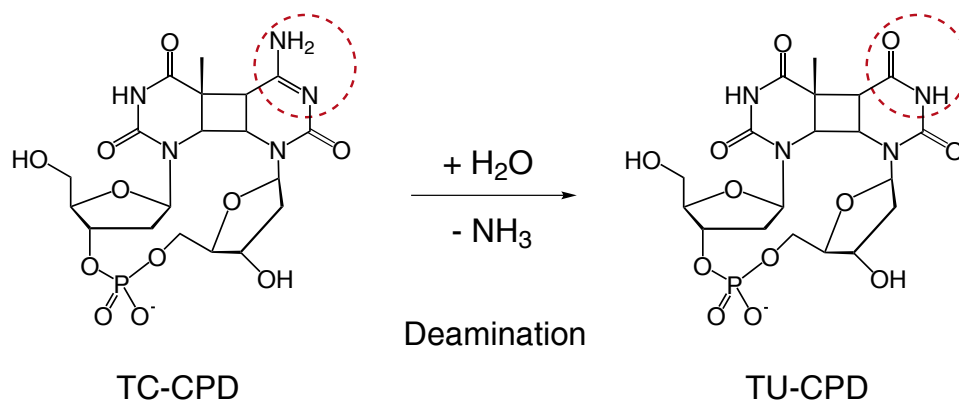


Figure 6.4: A schematic description of the deamination process from TC-CPD to TU-CPD. The relevant groups of the cytosine base and the uracil base are marked with red circles.

In this section, the large band at 1567 cm^{-1} , which is unique for the cytosine containing CPDs, is tentatively assigned to another marker band for the cytosine containing CPD lesions. From section 2.3.1 we know that the cytosine containing CPD can easily

undergo a deamination process and thus become a uracil containing CPD. Figure 6.4 shows a schematic description of the deamination process from TC-CPD to TU-CPD. In order to verify whether the deamination occurs or not, solutions containing 5 mM 2-M and 2.5 mM TpC or TpU are irradiated at 320 nm under the same experimental conditions. Their IR absorption difference spectra immediately after the illumination are shown in Figure 6.5. The blue curve represents the TU-CPD and the red curve represents the TC-CPD.

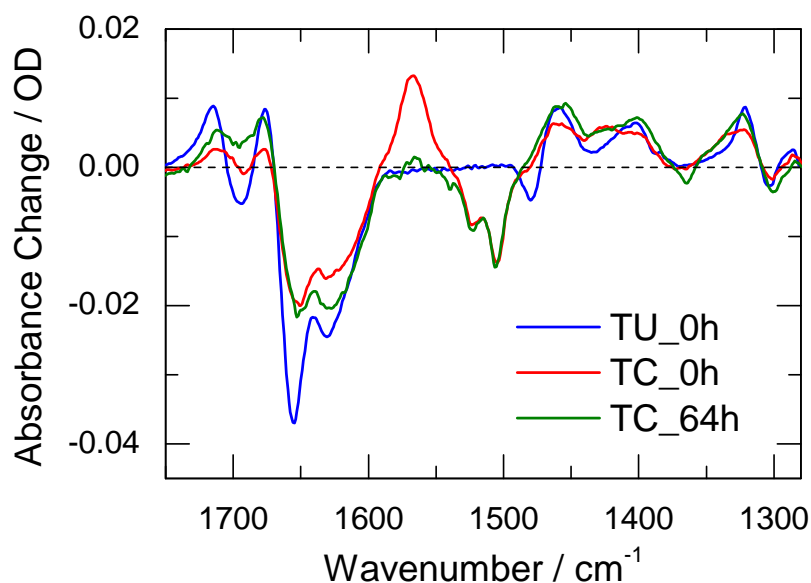


Figure 6.5: The IR difference absorption spectra of TU-CPD immediately after illumination (blue), TC-CPD immediately after illumination (red) and TC-CPD 64 hours after the illumination (green).

The negative bands between 1700 cm^{-1} and 1500 cm^{-1} are due to the bleach of the corresponding nucleobases. The induced absorptions in the fingerprint region look similar with only subtle differences, which are assigned to the CPD lesions. The marker bands at 1460 cm^{-1} and 1320 cm^{-1} for TC-CPD are weaker than for TU-CPD. While the band at 1402 cm^{-1} becomes a broad plateau for TC-CPD, another band around 1430 cm^{-1} emerges for TC-CPD only. Most strikingly, there is a large band at 1567 cm^{-1} exclusively for TC-CPD. Since TC-CPD is an unstable product which can undergo deamination, an absorbance change of the IR spectrum for TC-CPD is expected to occur at later times. To study the related spectral changes the IR absorption difference spectra of TU-CPD (data not shown) and TC-CPD (see Figure 6.5, green curve) are also recorded 64 hours after illumination. The photoproduct TU-CPD is thermally stable. No absorbance change is observed after 64 hours. In contrast, the spectrum of TC-CPD shows significant absorbance changes, especially the 1567 cm^{-1} band almost vanishes. Beside that, the bands at 1460 cm^{-1}

and 1320 cm^{-1} and the shoulder around 1402 cm^{-1} in the fingerprint region increase. After 64 hours, the spectrum of TC-CPD looks more similar to the spectrum of TU-CPD. It should be noted that the negative bleach of the blue curve and the green curve do not agree. This is due to the fact that TpC is converted to TU-CPD (green curve) while TpU is converted to TU-CPD (blue curve). The different spectra show the bleach of the original cytosine and uracil bands, respectively. With the results from IR measurements we are able to confirm the existence of the deamination process.

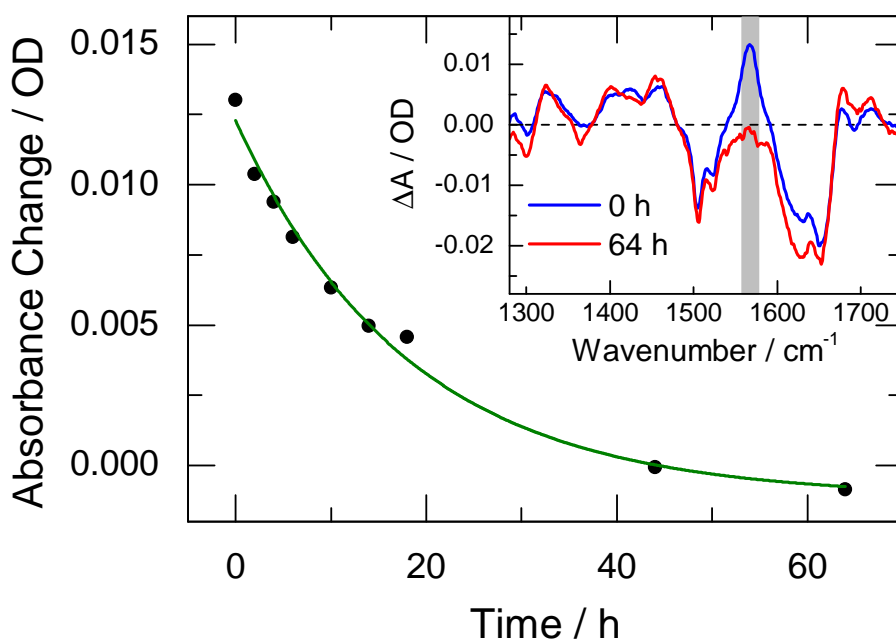


Figure 6.6: Time dependent absorbance changes of TC-CPD recorded at 1567 cm^{-1} . The data can be fitted mono-exponentially with a time constant of 17.9 hours.

It is interesting to quantify the rate of the deamination process from TC-CPD to TU-CPD. From Figure 6.5 we learn that the 1567 cm^{-1} band undergoes significant reduction after 64 hours. Therefore this band is selected and observed at different times. A mixture containing 5 mM 2-M and 2.5 mM TpC is illuminated at 320 nm for 4.5 hours. The pulse energy is $4.2\text{ }\mu\text{J}$. Thereafter the IR spectrum of the photo-product is recorded every 2 hours. The IR absorbance difference spectra of TC-CPD immediately after illumination and 64 hours later are shown in the inset of Figure 6.6, in which the 1567 cm^{-1} band is marked with a gray shadow. Figure 6.6 (black points) displays the decrease of the 1567 cm^{-1} band as a function of time. The data can be fitted mono-exponentially with a time constant of 17.9 hours, which corresponds to a half-life of 12.4 hours. This value agrees well with the literature value for the

deamination of cis-syn TC-CPD at room temperature and pH=7 [LR93], in which a half-life of 7.7 hours is reported.

Outlook

Considering the important role of deamination in UV induced DNA mutations, the deamination processes of cytosine containing CPDs have been widely investigated at different temperatures and different pH values for plasmid DNA [BCL95], TpC [LR93] and CpT [DC92]. While the former uses a complicated bioassay system, the other studies are based on a HPLC (High Performance Liquid Chromatography) separation. Here, we provide an easy method to study the deamination process by means of IR spectroscopy. The band at 1567 cm^{-1} is identified as a marker band of cytosine containing CPDs.

In our measurements we cannot distinguish the deamination of different stereoisomers of TC-CPD. Both the cis-syn and the trans-syn isomer of TC-CPD emerge from the photosensitizing illumination and undergo deamination with different time constants. Investigations using acetophenone as a sensitizer revealed that three TC-CPD stereoisomers (one cis-syn and two trans-syn) can be formed with a ratio of 4:3:1 [LY78, KSK91]. During illumination of TpC a small amount of TC-CPD is already converted to TU-CPD by deamination. This means that immediately after illumination the sample contains at least six photoproducts influencing the absorption dynamics.

7 Summary and Outlook

Cyclobutane Pyrimidine Dimer (CPD) is the most frequent UV-induced DNA damage. The mechanism of its formation upon UV-B illumination was well investigated in recent years. In contrast, the reaction mechanism in the UV-A range is an issue of discussion. This thesis focuses on the CPD formation in the model system pyrimidine dinucleotides via UV-A photosensitization. The UV-A range is particularly important considering its dominance in the solar UV-spectrum. The sensitizer molecules are able to absorb photons in the UV-A range and then transfer their triplet energy to the DNA bases. The frequent used sensitizers, such as acetophenone, show very weak absorption in the UV-A range, which makes time-resolved measurements in the MIR range difficult. In the first part of this thesis, an appropriate sensitizer 2'-methoxyacetophenone (2-M) was selected. Its absorption and emission properties were characterized by means of stationary and time-resolved spectroscopy. In the second part of this thesis, the interaction between 2-M and the thymine dinucleotide TpT was studied. The most interesting value, the quantum yield ϕ_{CPD3} of the CPD formation via the triplet channel of TpT, was identified with different methods to be 4%. The cytosine containing CPD lesions were also investigated in the sensitizing experiments. These lesions are highly mutagenic, because the cytosine base can easily deaminate to a uracil base if the C5=C6 double bond is saturated. The time-dependence of the deamination of cytosine containing CPD lesions was measured.

The selection and characterization of a suitable sensitizer

In the first step, different acetophenone substitutions were tested. Mixture solutions containing the thymine dinucleotide TpT and these different substitutions were illuminated at 320 nm. Among them, 2'-methoxyacetophenone (2-M) presented itself as the best candidate. Its triplet energy is high enough to allow an efficient triplet-triplet energy transfer (TTET) to TpT. CPD formation of TpT via triplet photosensitization of 2-M was observed. More importantly, it has much stronger absorption in the UV-A range than acetophenone. Its extinction coefficient at 320 nm is $2560 \text{ M}^{-1} \text{ cm}^{-1}$, which is two orders of magnitude larger than that of TpT and acetophenone. This makes a selective excitation on the sensitizer possible even in a solution containing TpT with high concentration. The low emission yield (2.6%) from the steady-state fluorescence measurement suggests an efficient non-radiative decay process.

In the second step, time-resolved absorption measurement was performed on deuterated acetophenone (APd8), which serves as the model molecule for 2-M. The ab-

sorption of APd8 is very weak in the UV-A range. Thus, its S_1 state can hardly be optically excited. The excitation wavelength was set at 300 nm and the concentration of APd8 was relative high (30 mM). Notably, the excitation at 300 nm leads to the population of the S_2 state of APd8. The S_2 state shows much more complicated photophysics and photochemistry than the S_1 state. Upon excitation with nanosecond pulses, the transient spectra of APd8 require two time constants for the fit. The 46 ns process is tentatively assigned to the transition from the triplet state to the radical state. The 248 ns component represents the decay from the radical state to the ground state. It is worth noting that the time constant 46 ns falls into the same range of the triplet-triplet energy transfer between the sensitizer and the TpT molecules. This makes a clear separation of these two processes in APd8-TpT solution difficult.

In the third step, a series of time-resolved measurements were conducted on 2-M. For the experiments on 2-M, the excitation wavelength is always 320 nm. In the fluorescence experiment on 2-M in the picosecond to nanosecond range, the emission spectra can be fitted mono-exponentially with a time constant of $\tau_{S_1} = 660$ ps, which describes the decay of the excited singlet state. This value is in good agreement with the estimation based on Strickler-Berg equation (860 ps). In the absorption experiment on 2-M in the picosecond to nanosecond range, no recovery of the original bleach to the ground state was observed. Thus, the non-radiative decay deduced from the steady-state fluorescence measurement was identified as an intersystem crossing. In the absorption experiment on 2-M in the nanosecond to microsecond range, the transient spectra can be fitted with a single time constant of 400 ns. This is attributed to the effective triplet lifetime of 2-M at ambient oxygen concentration. Unlike APd8, there is only one decay process in the nanosecond to microsecond range for 2-M. All the properties make 2-M an ideal sensitizer for the investigation of CPD formation via the triplet channel.

Using 2-M to investigate CPD lesions formed via sensitization

At first, 2-M was used to investigate CPD formation via the triplet channel of TpT. A diffusion controlled reaction model was presented for the sensitizing experiments. It is assumed that the sensitizer 2-M undergoes efficient intersystem crossing and then transfers its triplet energy to TpT. Thereafter, the quantum yield of CPD formation via the triplet channel of TpT, ϕ_{CPD_3} was quantified with two approaches. The first method was based on a series of stationary illumination experiments, where the concentration dependent quantum yields of CPD formation were measured. Using a wide range of the concentration of TpT from 2.29 mM to 18.32 mM, ϕ_{CPD_3} was determined to be circa 4.1%. The second method combined time-resolved and stationary quantum yield measurements at a same concentration (either 9.16 mM or 18.32 mM) of TpT. The TTET process from 2-M to TpT was clearly observed from the transient spectra. The species associated absorption difference spectra (SADS) deduced from independent time-resolved measurements agrees well with each other. Finally, ϕ_{CPD_3}

was determined to be circa 3.9%. Using the value $\phi_{CPD3} \approx 4\%$, we can estimate that CPD lesions after absorption of a photon at 266 nm into the $^1\pi\pi^*$ state of TpT occur 30 times more often via the singlet channel than via the triplet channel. However, the indirect sensitizing reaction with the abundant light in the UV-A range may be of major importance in surroundings with suitable sensitizing molecules. The molecular processes of CPD formation are also different for the singlet channel and the triplet channel. For the singlet channel, the relative low quantum yield is limited by the probability for a suitable reactive arrangement of the adjacent bases. In contrast, the small energy difference between the triplet state and the product CPD should be responsible for the low quantum yield ϕ_{CPD3} .

The CPD lesions occur most frequently between two thymine bases. However, cytosine containing CPD lesions are much more mutagenic, because the cytosine base can easily deaminate to a uracil base if the C5=C6 double bond is saturated. Indeed, 2-M is able to sensitize the dinucleotides TpC and CpT to form CPD lesions, but not CpC. This suggests that the triplet state of thymine is the main target of the sensitizer, because among the DNA bases, thymine and cytosine has the lowest and highest triplet energy, respectively. The thermal instable TC-CPD undergoes deamination to TU-CPD. This process was observed via IR spectroscopy to occur with a half-life of 12.4 hours.

Outlook

Acetophenone was widely used as a photosensitizer for DNA bases. Despite being the simplest model for aromatic ketones, its photophysics and photochemistry are not fully understood due to the presence of three close lying excited states (S_1 , T_1 and T_2). The newly introduced sensitizer 2-M has a much simple photophysics and high extinction coefficient in the UV-A range. We are convinced that this sensitizer molecule will play an important role in future experiments with UV-A excitation.

List of Figures

2.1	The nomenclature of DNA	5
2.2	DNA backbones and Watson-Crick base pairs	6
2.3	DNA absorption and solar UV irradiation spectra	7
2.4	Jablonski diagram for different transitions and states	9
2.5	Conical intersection	10
2.6	The different excited states of thymine	11
2.7	Structure of CPD	14
2.8	CPD mutation	15
2.9	6-4 photoproduct formation	16
2.10	Dewar photoproduct formation	16
2.11	(6-4) mutation	17
2.12	Structure of 8-oxo-dG	18
2.13	Structure and extinction coefficient of acetophenone	20
2.14	$S_1/T_1/T_2$ intersection	21
2.15	Triplet energy of acetophenone, CMP, TMP and thymine in DNA strands	22
3.1	The principle of the UV-pump MIR-probe spectroscopy	24
3.2	MIR probe pulses generation	25
3.3	NOPA pump pulses generation	26
3.4	A scheme of Ekspla	27
3.5	A scheme of the sample circulation setup	31
4.1	The molecular structures of AP and 2-M	34
4.2	UV absorption spectra of acetophenone and different acetophenone substitutions	35
4.3	UV absorption spectra of mixtures	36
4.4	IR absorption difference spectra of 4-M mixture and 2-M mixture	37
4.5	IR absorption difference spectra of TpT illuminated at 266 nm and 320 nm	38
4.6	IR absorption spectra of acetophenone and deuterated acetophenone	40
4.7	Time-resolved nanosecond absorption measurement on acetophenone excited at 300 nm	41
4.8	DADS for the ns absorption measurement on acetophenone excited at 300 nm	42

4.9	Reaction scheme for acetophenone upon excitation to the S_2 state and the corresponding SADS	43
4.10	Extinction coefficients	45
4.11	Absorption and emission spectra of 2-M	45
4.12	IR absorption spectra of 2-M	46
4.13	Time-resolved picosecond emission measurement on 2-M excited at 327 nm	48
4.14	Time-resolved picosecond absorption measurement on 2-M excited at 320 nm	50
4.15	Time-resolved nanosecond absorption measurement on 2-M excited at 320 nm	52
5.1	Reaction scheme	56
5.2	Quantum yield measurement	58
5.3	Quantum yield at different concentrations of TpT	59
5.4	Linear fit of the inverse absorbance change per time as a function of the inverse concentration	60
5.5	Oxygen concentration measurement	61
5.6	Oxygen concentration dependent quantum yield measurement	62
5.7	Time-resolved nanosecond absorption measurement on TpT excited at 250 nm	64
5.8	SADS comparison between TpT and $(dT)_{18}$	66
5.9	DADS for the ns absorption measurement on TpT excited at 250 nm	67
5.10	Time-resolved nanosecond absorption measurement on the mixture of TpT and 2-M (9.16 mM) excited at 320 nm	68
5.11	Time-resolved nanosecond absorption measurement on the mixture of TpT and 2-M (18.32 mM) excited at 320 nm	70
5.12	Absorbance changes at 1663 cm^{-1}	71
5.13	DADS for the sensitizing experiment	73
5.14	SADS comparison between the neat TpT experiment and sensitizing experiment	74
6.1	UV absorption spectra of different dinucleotides	78
6.2	IR absorption spectra of different dinucleotides	78
6.3	IR difference spectra of different dinucleotides after illumination	79
6.4	A schematic description of the deamination process from TC-CPD to TU-CPD	80
6.5	IR spectral comparison between TC-CPD and TU-CPD	81
6.6	Absorbance changes at 1567 cm^{-1}	82

List of Tables

2.1	The excited states energies of acetophenone	21
4.1	The important properties of 2-M	53
5.1	$\phi_{CPD-Sens}$ at different concentrations	59

Bibliography

- [Ban12] A. BANYASZ et al. *Electronic Excited States Responsible for Dimer Formation upon UV Absorption Directly by Thymine Strands: Joint Experimental and Theoretical Study*. *Journal of the American Chemical Society* 134(36) (2012), pp. 14834–14845.
- [Bar53] G. M. BARROW. *Conjugation and the Intensity of the Infrared Carbonyl Band*. *The Journal of Chemical Physics* 21(11) (1953), pp. 2008–2011.
- [BB60] R. BEUKERS and W. BERENDS. *Isolation and identification of the irradiation product of thymine*. *Biochimica et Biophysica Acta* 41(3) (1960), pp. 550–551.
- [BCL95] Y. BARAK, O. COHEN-FIX, and Z. LIVNEH. *Deamination of Cytosine-containing Pyrimidine Photodimers in UV-irradiated DNA: SIGNIFICANCE FOR UV LIGHT MUTAGENESIS*. *Journal of Biological Chemistry* 270(41) (1995), pp. 24174–24179.
- [BIL54] G. BÜCHI, C. G. INMAN, and E. S. LIPINSKY. *Light-catalyzed Organic Reactions. I. The Reaction of Carbonyl Compounds with 2-Methyl-2-butene in the Presence of Ultraviolet Light*. *Journal of the American Chemical Society* 76(17) (1954), pp. 4327–4331.
- [Bos06] F. BOSCA, V. LHIAUBET-VALLET, M. C. CUQUERELLA, J. V. CASTELL, and M. A. MIRANDA. *The Triplet Energy of Thymine in DNA*. *Journal of the American Chemical Society* 128(19) (2006), pp. 6318–6319.
- [BS75] M. BERGER and C. STEEL. *Photochemical and photophysical processes in acetophenone*. *Journal of the American Chemical Society* 97(17) (1975), pp. 4817–4821.
- [BSG03] M. BANYAY, M. SARKAR, and A. GRÄSLUND. *A library of IR bands of nucleic acids in solution*. *Biophysical Chemistry* 104(2) (2003), pp. 477–488.
- [Buc14] D. B. BUCHER, B. M. PILLES, T. CARELL, and W. ZINTH. *Charge separation and charge delocalization identified in long-living states of photoexcited DNA*. *Proceedings of the National Academy of Sciences* 111(12) (2014), pp. 4369–4374.
- [Cad85] J. CADET et al. *Characterization of thymidine ultraviolet photoproducts. Cyclobutane dimers and 5,6-dihydrothymidines*. *Canadian Journal of Chemistry* 63(11) (1985), pp. 2861–2868.

- [CK70] W. A. CASE and D. R. KEARNS. *Investigation of S→T and S→S Transitions by Phosphorescence Excitation Spectroscopy VII. 1Indanone and Other Aromatic Ketones*. The Journal of Chemical Physics 52(5) (1970), pp. 2175–2191.
- [COO03] M. S. COOKE, M. D. EVANS, M. DIZDAROGLU, and J. LUNEC. *Oxidative DNA damage: mechanisms, mutation, and disease*. The FASEB Journal 17(10) (2003), pp. 1195–1214.
- [Cre04] C. E. CRESPO-HERNÁNDEZ, B. COHEN, P. M. HARE, and B. KOHLER. *Ultrafast Excited-State Dynamics in Nucleic Acids*. Chemical Reviews 104(4) (2004), pp. 1977–2020.
- [Cuq12] M. C. CUQUERELLA, V. LHIAUBET-VALLET, J. CADET, and M. A. MIRANDA. *Benzophenone Photosensitized DNA Damage*. Accounts of Chemical Research 45(9) (2012), pp. 1558–1570.
- [DC01] T. DOUKI and J. CADET. *Individual Determination of the Yield of the Main UV-Induced Dimeric Pyrimidine Photoproducts in DNA Suggests a High Mutagenicity of CC Photolesions*. Biochemistry 40(8) (2001), pp. 2495–2501.
- [DC92] T. DOUKI and J. CADET. *Far-UV photochemistry and photosensitization of 2'-deoxycytidylyl-(3'-5')-thymidine: Isolation and characterization of the main photoproducts*. Journal of Photochemistry and Photobiology B: Biology 15(3) (1992), pp. 199–213.
- [DDH73] J. N. DEMAS, D. DIEMENTE, and E. W. HARRIS. *Oxygen quenching of charge-transfer excited states of ruthenium(II) complexes. Evidence for singlet oxygen production*. Journal of the American Chemical Society 95(20) (1973), pp. 6864–6865.
- [Dev91] T. P. A. DEVASAGAYAM, S. STEENKEN, M. S. W. OBENDORF, W. A. SCHULZ, and H. SIES. *Formation of 8-hydroxy(deoxy)guanosine and generation of strand breaks at guanine residues in DNA by singlet oxygen*. Biochemistry 30(25) (1991), pp. 6283–6289.
- [Dew69] J. DEWAR. *5. On the Oxidation of Phenyl Alcohol, and a Mechanical Arrangement adapted to illustrate Structure in the Nonsaturated Hydrocarbons*. Proceedings of the Royal Society of Edinburgh 6 (1869), pp. 82–86.
- [DM13] E. DUMONT and A. MONARI. *Benzophenone and DNA: Evidence for a Double Insertion Mode and Its Spectral Signature*. The Journal of Physical Chemistry Letters 4(23) (2013), pp. 4119–4124.
- [Dom14] P. N. DOMINGUEZ et al. *Primary reactions in photosynthetic reaction centers of Rhodobacter sphaeroides – Time constants of the initial electron transfer*. Chemical Physics Letters 601 (2014), pp. 103–109.

- [Dou00] T. DOUKI, M. COURT, S. SAUVAIGO, F. ODIN, and J. CADET. *Formation of the Main UV-induced Thymine Dimeric Lesions within Isolated and Cellular DNA as Measured by High Performance Liquid Chromatography Tandem Mass Spectrometry*. *Journal of Biological Chemistry* 275(16) (2000), pp. 11678–11685.
- [Dou03] T. DOUKI, A. REYNAUD-ANGELIN, J. CADET, and E. SAGE. *Bipyrimidine Photoproducts Rather than Oxidative Lesions Are the Main Type of DNA Damage Involved in the Genotoxic Effect of Solar UVA Radiation*. *Biochemistry* 42(30) (2003), pp. 9221–9226.
- [DS63] R. A. DEERING and R. B. SETLOW. *Effects of ultraviolet light on thymidine dinucleotide and polynucleotide*. *Biochimica et Biophysica Acta - Specialized Section on Nucleic Acids and Related Subjects* 68 (1963), pp. 526–534.
- [Dum15] E. DUMONT et al. *Resolving the Benzophenone DNA-Photosensitization Mechanism at QM/MM Level*. *The Journal of Physical Chemistry Letters* 6(4) (2015), pp. 576–580.
- [Dza04] L. DZANTIEV et al. *A Defined Human System That Supports Bidirectional Mismatch-Provoked Excision*. *Molecular Cell* 15(1) (2004), pp. 31–41.
- [Fan08] W.-H. FANG. *Ab Initio Determination of Dark Structures in Radiationless Transitions for Aromatic Carbonyl Compounds*. *Accounts of Chemical Research* 41(3) (2008), pp. 452–457.
- [FG53] R. E. FRANKLIN and R. G. GOSLING. *Molecular Configuration in Sodium Thymonucleate*. *Nature* 171(4356) (1953), pp. 740–741.
- [Fin12] B. P. FINGERHUT et al. *Dynamics of ultraviolet-induced DNA lesions: Dewar formation guided by pre-tension induced by the backbone*. *New Journal of Physics* 14(6) (2012), p. 065006.
- [FKS90] L. A. FREDERICO, T. A. KUNKEL, and B. R. SHAW. *A sensitive genetic assay for the detection of cytosine deamination: determination of rate constants and the activation energy*. *Biochemistry* 29(10) (1990), pp. 2532–2537.
- [Foo68] C. S. FOOTE. *Photosensitized oxygenations and the role of singlet oxygen*. *Accounts of Chemical Research* 1(4) (1968), pp. 104–110.
- [Foo91] C. S. FOOTE. *DEFINITION OF TYPE I and TYPE II PHOTOLENSITIZED OXIDATION*. *Photochemistry and Photobiology* 54(5) (1991), pp. 659–659.
- [FP02] W.-H. FANG and D. L. PHILLIPS. *The Crucial Role of the S1/T2/T1 Intersection in the Relaxation Dynamics of Aromatic Carbonyl Compounds upon $n \rightarrow \pi^*$ Excitation*. *ChemPhysChem* 3(10) (2002), pp. 889–892.

- [Gam80] A. GAMBI, S. GIORGIANNI, A. PASSERINI, R. VISINONI, and S. GHERSETTI. *Infrared studies of acetophenone and its deuterated derivatives*. Spectrochimica Acta Part A: Molecular Spectroscopy 36(10) (1980), pp. 871–878.
- [GC57] M. GREEN and S. S. COHEN. *STUDIES ON THE BIOSYNTHESIS OF BACTERIAL AND VIRAL PYRIMIDINES: III. DERIVATIVES OF DIHYDROCYTOSINE*. Journal of Biological Chemistry 228(2) (1957), pp. 601–609.
- [GES67] M. GUÉRON, J. EISINGER, and R. G. SHULMAN. *Excited States of Nucleotides and Singlet Energy Transfer in Polynucleotides*. The Journal of Chemical Physics 47(10) (1967), pp. 4077–4091.
- [GJ68] C. L. GREENSTOCK and H. E. JOHNS. *Photosensitized dimerization of pyrimidines*. Biochemical and Biophysical Research Communications 30(1) (1968), pp. 21–27.
- [Gon15] J. GONTCHAROV. *Infrared Spectroscopy of the Photosensitized Formation of Pyrimidine Lesions*. Thesis. 2015.
- [GWR96] I. G. GUT, P. D. WOOD, and R. W. REDMOND. *Interaction of Triplet Photosensitizers with Nucleotides and DNA in Aqueous Solution at Room Temperature*. Journal of the American Chemical Society 118(10) (1996), pp. 2366–2373.
- [Hag05] S. HAGHDOOST, S. CZENE, I. NÄSLUND, S. SKOG, and M. HARMS-RINGDAHL. *Extracellular 8-oxo-dG as a sensitive parameter for oxidative stress in vivo and in vitro*. Free Radical Research 39(2) (2005), pp. 153–162.
- [Hai12a] K. HAISER. *Femtosekunden-Infrarotspektroskopie von UV-induzierten Photoschäden in Nukleinsäuren*. Thesis. 2012.
- [Hai12b] K. HAISER et al. *Mechanism of UV-Induced Formation of Dewar Lesions in DNA*. Angewandte Chemie International Edition 51(2) (2012), pp. 408–411.
- [Har08] P. M. HARE, C. T. MIDDLETON, K. I. MERTEL, J. M. HERBERT, and B. KOHLER. *Time-resolved infrared spectroscopy of the lowest triplet state of thymine and thymidine*. Chemical Physics 347(1–3) (2008), pp. 383–392.
- [HCK07] P. M. HARE, C. E. CRESPO-HERNÁNDEZ, and B. KOHLER. *Internal conversion to the electronic ground state occurs via two distinct pathways for pyrimidine bases in aqueous solution*. Proceedings of the National Academy of Sciences 104(2) (2007), pp. 435–440.
- [Hoe09] J. H. J. HOEIJMAKERS. *DNA Damage, Aging, and Cancer*. New England Journal of Medicine 361(15) (2009), pp. 1475–1485.

- [HSF13] M. HUIX-ROTLANT, D. SIRI, and N. FERRÉ. *Theoretical study of the photochemical generation of triplet acetophenone*. Physical Chemistry Chemical Physics 15(44) (2013), pp. 19293–19300.
- [Hui15] M. HUIX-ROTLANT, E. DUMONT, N. FERRÉ, and A. MONARI. *Photo-physics of Acetophenone Interacting with DNA: Why the Road to Photosensitization is Open*. Photochemistry and Photobiology 91(2) (2015), pp. 323–330.
- [IBT78] T. ITOH, H. BABA, and T. TAKEMURA. *Phosphorescence Emissions and Nonradiative Properties of Vapors of Aromatic Carbonyl Compounds at Low Pressure*. Bulletin of the Chemical Society of Japan 51(10) (1978), pp. 2841–2846.
- [Jia09] Y. JIANG et al. *UVA Generates Pyrimidine Dimers in DNA Directly*. Biophysical Journal 96(3) (2009), pp. 1151–1158.
- [Jor87] M. S. JORNS, E. T. BALDWIN, G. B. SANCAR, and A. SANCAR. *Action mechanism of Escherichia coli DNA photolyase. II. Role of the chromophores in catalysis*. Journal of Biological Chemistry 262(1) (1987), pp. 486–491.
- [JPP99] R. E. JOHNSON, S. PRAKASH, and L. PRAKASH. *Efficient Bypass of a Thymine-Thymine Dimer by Yeast DNA Polymerase, Pol η* . Science 283(5404) (1999), pp. 1001–1004.
- [JT93] N. JIANG and J. S. TAYLOR. *In vivo evidence that UV-induced C→T mutations at dipyrimidine sites could result from the replicative bypass of cis-syn cyclobutane dimers or their deamination products*. Biochemistry 32(2) (1993), pp. 472–481.
- [JW07] A. T. JOHNSON and O. WIEST. *Structure and Dynamics of Poly(T) Single-Strand DNA: Implications toward CPD Formation*. The Journal of Physical Chemistry B 111(51) (2007), pp. 14398–14404.
- [Kas50] M. KASHA. *Characterization of electronic transitions in complex molecules*. Discussions of the Faraday Society 9 (1950), pp. 14–19.
- [KB31] H. KAUTSKY and H. de BRUIJN. *Die Aufklärung der Photoluminescenztilgung fluoreszierender Systeme durch Sauerstoff: Die Bildung aktiver, diffusionsfähiger Sauerstoffmoleküle durch Sensibilisierung*. Naturwissenschaften 19(52) (1931), pp. 1043–1043.
- [KC66] D. R. KEARNS and W. A. CASE. *Investigation of Singlet→Triplet Transitions by the Phosphorescence Excitation Method. III. Aromatic Ketones and Aldehydes*. Journal of the American Chemical Society 88(22) (1966), pp. 5087–5097.

- [KMP08] W.-M. KWOK, C. MA, and D. L. PHILLIPS. *A Doorway State Leads to Photostability or Triplet Photodamage in Thymine DNA*. Journal of the American Chemical Society 130(15) (2008), pp. 5131–5139.
- [KN65] K. KIMURA and S. NAGAKURA. *Vacuum ultraviolet spectra of styrene, benzaldehyde, acetophenone, and benzonitrile*. Theoretica chimica acta 3(2) (1965), pp. 164–173.
- [KSK91] T. M. G. KONING, J. J. G. van SOEST, and R. KAPTEIN. *NMR studies of bipyrimidine cyclobutane photodimers*. European Journal of Biochemistry 195(1) (1991), pp. 29–40.
- [Kub09] J. K. KUBON. *Untersuchung von Photoschäden der DNA und RNA mit Femtosekunden IR-Spektroskopie*. Thesis. 2009.
- [Küb13] C. KÜBEL. *Anreg-Abtast-Experiment zur Entfaltung des schaltbaren Peptids AzoTrpZip2 - Integration eines abstimmbaren ns-Lasersystem*. Thesis. 2013.
- [Lam67] A. A. LAMOLA, M. GUÉRON, T. YAMANE, J. EISINGER, and R. G. SHULMAN. *Triplet State of DNA*. The Journal of Chemical Physics 47(7) (1967), pp. 2210–2217.
- [LAM89] R. S. LAHUE, K. G. AU, and P. MODRICH. *DNA mismatch correction in a defined system*. Science 245(4914) (1989), pp. 160–164.
- [Law08] Y. K. LAW, J. AZADI, C. E. CRESPO-HERNÁNDEZ, E. OLMON, and B. KOHLER. *Predicting Thymine Dimerization Yields from Molecular Dynamics Simulations*. Biophysical Journal 94(9) (2008), pp. 3590–3600.
- [LBC00] J.-H. LEE, S.-H. BAE, and B.-S. CHOI. *The Dewar photoproduct of thymidylyl(3'→5')- thymidine (Dewar product) exhibits mutagenic behavior in accordance with the 'A rule'*. Proceedings of the National Academy of Sciences 97(9) (2000), pp. 4591–4596.
- [LBL73] H. LUTZ, E. BREHERET, and L. LINDQVIST. *Effects of solvent and substituents on the absorption spectra of triplet acetophenone and the acetophenone ketyl radical studied by nanosecond laser photolysis*. The Journal of Physical Chemistry 77(14) (1973), pp. 1758–1762.
- [LBL91] J. E. LECLERC, A. BORDEN, and C. W. LAWRENCE. *The thymine-thymine pyrimidine-pyrimidone (6-4) ultraviolet light photoproduct is highly mutagenic and specifically induces 3' thymine→cytosine transitions in Escherichia coli*. Proceedings of the National Academy of Sciences 88(21) (1991), pp. 9685–9689.

- [Leo81] D. G. LEOPOLD, R. J. HEMLEY, V. VAIDA, and J. L. ROEBBER. *Direct absorption spectra of higher excited states of jetcooled monosubstituted benzenes: Phenylacetylene, styrene, benzaldehyde, and acetophenone*. The Journal of Chemical Physics 75(10) (1981), pp. 4758–4769.
- [LGT87] R. LETELLIER, M. GHOMI, and E. TAILLANDIER. *Normal coordinate analysis of 2'-deoxythymidine and 2'-deoxyadenosine*. European Biophysics Journal 14(7) (1987), pp. 423–430.
- [LH65] A. A. LAMOLA and G. S. HAMMOND. *Mechanisms of Photochemical Reactions in Solution. XVIII. Intersystem Crossing Efficiencies*. The Journal of Chemical Physics 43(6) (1965), pp. 2129–2135.
- [LHC99] J.-H. LEE, G.-S. HWANG, and B.-S. CHOI. *Solution structure of a DNA decamer duplex containing the stable 3' T·G base pair of the pyrimidine(6–4)pyrimidone photoproduct [(6–4) adduct]: Implications for the highly specific 3' T→C transition of the (6–4) adduct*. Proceedings of the National Academy of Sciences 96(12) (1999), pp. 6632–6636.
- [Lin74] T. LINDAHL. *An N-Glycosidase from Escherichia coli That Releases Free Uracil from DNA Containing Deaminated Cytosine Residues*. Proceedings of the National Academy of Sciences 71(9) (1974), pp. 3649–3653.
- [Liu15] L. LIU, B. M. PILLES, A. M. REINER, J. GONTCHAROV, and W. ZINTH. *2'-Methoxyacetophenone: An Efficient Photosensitizer for Cyclobutane Pyrimidine Dimer Formation*. ChemPhysChem 16(16) (2015), pp. 3483–3487.
- [Liu16] L. LIU, B. M. PILLES, J. GONTCHAROV, D. B. BUCHER, and W. ZINTH. *Quantum Yield of Cyclobutane Pyrimidine Dimer Formation Via the Triplet Channel Determined by Photosensitization*. The Journal of Physical Chemistry B 120(2) (2016), pp. 292–298.
- [LR93] D. G. E. LEMAIRE and B. P. RUZSICKA. *Kinetic analysis of the deamination reactions of cyclobutane dimers of thymidyl-3',5'-2'-deoxycytidine and 2'-deoxycytidyl-3',5'-thymidine*. Biochemistry 32(10) (1993), pp. 2525–2533.
- [LS76] C.-T. LIN and N. SUTIN. *Quenching of the luminescence of the tris(2,2'-bipyridine) complexes of ruthenium(II) and osmium(II). Kinetic considerations and photogalvanic effects*. The Journal of Physical Chemistry 80(2) (1976), pp. 97–105.
- [LY67] A. A. LAMOLA and T. YAMANE. *Sensitized photodimerization of thymine in DNA*. Proceedings of the National Academy of Sciences of the United States of America 58(2) (1967), pp. 443–446.

- [LY78] F.-T. LIU and N. C. YANG. *Photochemistry of cytosine derivatives. 1. Photochemistry of thymidyl-(3'→5')-deoxycytidine*. *Biochemistry* 17(23) (1978), pp. 4865–4876.
- [Mas99] C. MASUTANI et al. *The XPV (xeroderma pigmentosum variant) gene encodes human DNA polymerase η* . *Nature* 399(6737) (1999), pp. 700–704.
- [McM41] H. L. MCMURRY. *The Long WaveLength Spectra of Aldehydes and Ketones Part I. Saturated Aldehydes and Ketones*. *The Journal of Chemical Physics* 9(3) (1941), pp. 231–240.
- [Mou06] S. MOURET et al. *Cyclobutane pyrimidine dimers are predominant DNA lesions in whole human skin exposed to UVA radiation*. *Proceedings of the National Academy of Sciences* 103(37) (2006), pp. 13765–13770.
- [Mou10] S. MOURET et al. *UVA-induced cyclobutane pyrimidine dimers in DNA: a direct photochemical mechanism?* *Organic & Biomolecular Chemistry* 8(7) (2010), pp. 1706–1711.
- [Nak82] K. NAKAMARU. *Synthesis, Luminescence Quantum Yields, and Lifetimes of Trischelated Ruthenium(II) Mixed-ligand Complexes Including 3,3'-Dimethyl-2,2'-bipyridyl*. *Bulletin of the Chemical Society of Japan* 55(9) (1982), pp. 2697–2705.
- [Nen10] A. NENOV, T. CORDES, T. T. HERZOG, W. ZINTH, and R. d. VIVIEREDLE. *Molecular Driving Forces for Z/E Isomerization Mediated by Heteroatoms: The Example Hemithioindigo*. *The Journal of Physical Chemistry A* 114(50) (2010), pp. 13016–13030.
- [OSI88] N. OHMORI, T. SUZUKI, and M. ITO. *Why does intersystem crossing occur in isolated molecules of benzaldehyde, acetophenone, and benzophenone?* *The Journal of Physical Chemistry* 92(5) (1988), pp. 1086–1093.
- [PFZ06] S. T. PARK, J. S. FEENSTRA, and A. H. ZEWEIL. *Ultrafast electron diffraction: Excited state structures and chemistries of aromatic carbonyls*. *The Journal of Chemical Physics* 124(17) (2006), p. 174707.
- [Pil14a] B. M. PILLES et al. *Identification of charge separated states in thymine single strands*. *Chemical Communications* 50(98) (2014), pp. 15623–15626.
- [Pil14b] B. M. PILLES et al. *Mechanism of the Decay of Thymine Triplets in DNA Single Strands*. *The Journal of Physical Chemistry Letters* 5(9) (2014), pp. 1616–1622.
- [Pil16] B. PILLES. *Monitoring the Excited State Dynamics of Thymine by Time-resolved IR Spectroscopy*. Thesis. 2016.

- [PPK01] J.-M. L. PECOURT, J. PEON, and B. KOHLER. *DNA Excited-State Dynamics: Ultrafast Internal Conversion and Vibrational Cooling in a Series of Nucleosides*. *Journal of the American Chemical Society* 123(42) (2001), pp. 10370–10378.
- [RDC01] J.-L. RAVANAT, T. DOUKI, and J. CADET. *Direct and indirect effects of UV radiation on DNA and its components*. *Journal of Photochemistry and Photobiology B: Biology* 63(1–3) (2001), pp. 88–102.
- [Rie00] E. RIEDLE et al. *Generation of 10 to 50 fs pulses tunable through all of the visible and the NIR*. *Applied Physics B* 71(3) (2000), pp. 457–465.
- [San87a] G. B. SANCAR et al. *Action mechanism of Escherichia coli DNA photolyase. I. Formation of the enzyme-substrate complex*. *Journal of Biological Chemistry* 262(1) (1987), pp. 478–485.
- [San87b] G. B. SANCAR et al. *Action mechanism of Escherichia coli DNA photolyase. III. Photolysis of the enzyme-substrate complex and the absolute action spectrum*. *Journal of Biological Chemistry* 262(1) (1987), pp. 492–498.
- [Sat04] H. SATZGER. *Untersuchung initialer Schritte der Peptidfaltung mit Ultrakurzzeitspektroskopie*. Thesis. 2004.
- [Say63] M. A. ELSAYED. *Spin-Orbit Coupling and the Radiationless Processes in Nitrogen Heterocyclics*. *The Journal of Chemical Physics* 38(12) (1963), pp. 2834–2838.
- [SB62] S. J. STRICKLER and R. A. BERG. *Relationship between Absorption Intensity and Fluorescence Lifetime of Molecules*. *The Journal of Chemical Physics* 37(4) (1962), pp. 814–822.
- [Sch07] W. J. SCHREIER et al. *Thymine Dimerization in DNA Is an Ultrafast Photoreaction*. *Science* 315(5812) (2007), pp. 625–629.
- [Sch08] W. J. SCHREIER. *UV-Strahlung und DNA-Schäden - Untersuchung UV-induzierter Prozesse in Nukleinsäuren mit Femtosekunden Infrarotspektroskopie*. Thesis. 2008.
- [Sch09] W. J. SCHREIER et al. *Thymine Dimerization in DNA Model Systems: Cyclobutane Photolesion Is Predominantly Formed via the Singlet Channel*. *Journal of the American Chemical Society* 131(14) (2009), pp. 5038–5039.
- [Ser14] D.-C. SERGENTU, R. MAURICE, R. W. A. HAVENITH, R. BROER, and D. ROCA-SANJUAN. *Computational determination of the dominant triplet population mechanism in photoexcited benzophenone*. *Physical Chemistry Chemical Physics* 16(46) (2014), pp. 25393–25403.

- [SH02] R. P. SINHA and D.-P. HADER. *UV-induced DNA damage and repair: a review*. Photochemical & Photobiological Sciences 1(4) (2002), pp. 225–236.
- [Spö01] S. SPÖRLEIN. *Femtosekunden-Spektroskopie schnellster Strukturänderungen in Peptid-Chromophor-Komplexen*. Thesis. 2001.
- [SR78] A. SANCAR and C. S. RUPERT. *Cloning of the phr gene and amplification of photolyase in Escherichia coli*. Gene 4(4) (1978), pp. 295–308.
- [SR83] A. SANCAR and W. D. RUPP. *A novel repair enzyme: UVRABC excision nuclease of Escherichia coli cuts a DNA strand on both sides of the damaged region*. Cell 33(1) (1983), pp. 249–260.
- [Tay02] J.-S. TAYLOR. *New structural and mechanistic insight into the A-rule and the instructional and non-instructional behavior of DNA photoproducts and other lesions*. Mutation Research/Fundamental and Molecular Mechanisms of Mutagenesis 510(1–2) (2002), pp. 55–70.
- [Tay94] J. S. TAYLOR. *Unraveling the Molecular Pathway from Sunlight to Skin Cancer*. Accounts of Chemical Research 27(3) (1994), pp. 76–82.
- [TK93] D. C. THOMAS and T. A. KUNKEL. *Replication of UV-irradiated DNA in human cell extracts: evidence for mutagenic bypass of pyrimidine dimers*. Proceedings of the National Academy of Sciences 90(16) (1993), pp. 7744–7748.
- [TNK56] J. TANAKA, S. NAGAKURA, and M. KOBAYASHI. *Ultraviolet and Infrared Absorption Spectra of Substituted Acetophenones and Benzoic Acids*. The Journal of Chemical Physics 24(2) (1956), pp. 311–315.
- [Voe63] D. VOET, W. B. GRATZER, R. A. COX, and P. DOTY. *Absorption spectra of nucleotides, polynucleotides, and nucleic acids in the far ultraviolet*. Biopolymers 1(3) (1963), pp. 193–208.
- [VW68] A. J. VARGHESE and S. Y. WANG. *Thymine-Thymine Adduct as a Photoproduct of Thymine*. Science 160(3824) (1968), pp. 186–187.
- [WB86] J. A. WARREN and E. R. BERNSTEIN. *The S₂₀ laser photoexcitation spectrum and excited state dynamics of jetcooled acetophenone*. The Journal of Chemical Physics 85(5) (1986), pp. 2365–2367.
- [WC53] J. D. WATSON and F. H. C. CRICK. *Molecular Structure of Nucleic Acids: A Structure for Deoxyribose Nucleic Acid*. Nature 171(4356) (1953), pp. 737–738.
- [Wel59] A. WELLER. *Outer and inner mechanism of reactions of excited molecules*. Discussions of the Faraday Society 27 (1959), pp. 28–33.

- [WH00] K. L. WILLETT and R. A. HITES. *Chemical Actinometry: Using o-Nitrobenzaldehyde to Measure Lamp Intensity in Photochemical Experiments*. Journal of Chemical Education 77(7) (2000), pp. 900–902.
- [WR96] P. D. WOOD and R. W. REDMOND. *Triplet State Interactions between Nucleic Acid Bases in Solution at Room Temperature: Intermolecular Energy and Electron Transfer*. Journal of the American Chemical Society 118(18) (1996), pp. 4256–4263.
- [WSW53] M. H. F. WILKINS, A. R. STOKES, and H. R. WILSON. *Molecular Structure of Nucleic Acids: Molecular Structure of Deoxypentose Nucleic Acids*. Nature 171(4356) (1953), pp. 738–740.
- [WV67] S. Y. WANG and A. J. VARGHESE. *Cytosine-thymine addition product from DNA irradiated with ultraviolet light*. Biochemical and Biophysical Research Communications 29(4) (1967), pp. 543–549.
- [Yab10] S. YABUMOTO, S. SHIGETO, Y.-P. LEE, and H.-o. HAMAGUCHI. *Ordering, Interaction, and Reactivity of the Low-Lying $n\pi^*$ and $\pi\pi^*$ Excited Triplet States of Acetophenone Derivatives*. Angewandte Chemie International Edition 49(48) (2010), pp. 9201–9205.
- [Yas14] M. YASUI et al. *Tracing the fates of site-specifically introduced DNA adducts in the human genome*. DNA Repair 15 (2014), pp. 11–20.
- [YOK02] R. YOSHIDA, Y. OGAWA, and H. KASAI. *Urinary 8-Oxo-7,8-dihydro-2'-deoxyguanosine Values Measured by an ELISA Correlated Well with Measurements by High-Performance Liquid Chromatography with Electrochemical Detection*. Cancer Epidemiology Biomarkers & Prevention 11(10) (2002), pp. 1076–1081.
- [Yoo00] J.-H. YOON, C.-S. LEE, T. R. O'CONNOR, A. YASUI, and G. P. PFEIFER. *The DNA damage spectrum produced by simulated sunlight*. Journal of Molecular Biology 299(3) (2000), pp. 681–693.
- [YPF06] P. YAKOVCHUK, E. PROTOZANOVA, and M. D. FRANK-KAMENETSKII. *Base-stacking and base-pairing contributions into thermal stability of the DNA double helix*. Nucleic Acids Research 34(2) (2006), pp. 564–574.

List of Abbreviations

2-M	2'-methoxyacetophenone
AgGaS ₂	silver thiogallate
APd8	deuterated acetophenone
BaF ₂	barium fluoride
BBO	beta barium borate
CaF ₂	calcium fluoride
CpC	deoxycytidylyl-(3'→5')-deoxycytidine
CPD	cyclobutane pyrimidine dimer
CpT	deoxycytidylyl-(3'→5')-thymidine
DADS	decay associated difference spectra
DFM	difference frequency mixing
DNA	deoxyribonucleic acid
(dT) ₁₈	18er thymine oligonucleotide
HPLC	high performance liquid chromatography
IC	internal conversion
ISC	intersystem crossing
MIR	mid infrared
MCT	mercury cadmium telluride
NOPA	non-collinear optical parametric amplifier
NIR	near infrared
OPA	optical parametric amplifier
OPO	optical parametric oscillator
PPO	2,5-diphenyloxazole
RNA	ribonucleic acid
SADS	species associated difference spectra
SFG	sum frequency generation
SHG	second harmonic generation
THG	third harmonic generation
TMP	thymidine monophosphate
TpC	thymidylyl-(3'→5')-deoxycytidine
TpT	thymidylyl-(3'→5')-thymidine
TpU	thymidylyl-(3'→5')-uridine
TTET	triplet-triplet energy transfer
WL	white-light

Publications

Publication in Journals:

- Bert M. Pilles, Dominik B. Bucher, Lizhe Liu, Pascale Clivio, Peter Gilch, Wolfgang Zinth and Wolfgang J. Schreier. Mechanism of the Decay of Thymine Triplets in DNA Single Strands. *The Journal of Physical Chemistry Letters* 2014, 5 (9), 1616-1622.
- Bert M. Pilles, Dominik B. Bucher, Lizhe Liu, Peter Gilch, Wolfgang Zinth and Wolfgang J. Schreier. Identification of Charge Separated States in Thymine Single Strands. *Chemical Communications* 2014, 50 (98), 15623-15626.
- Lizhe Liu, Bert M. Pilles, Anne M. Reiner, Julia Gontcharov, and Wolfgang Zinth. 2'-Methoxyacetophenone: An Efficient Photosensitizer for Cyclobutane Pyrimidine Dimer Formation. *ChemPhysChem* 2015, 16 (16), 3483-3487.
- Lizhe Liu, Bert M. Pilles, Julia Gontcharov, Dominik B. Bucher, and Wolfgang Zinth. Quantum Yield of Cyclobutane Pyrimidine Dimer Formation Via the Triplet Channel Determined by Photosensitization. *The Journal of Physical Chemistry B* 2016, 120 (2), 292-298.

Talks and Poster Presentations:

- Talk at the Annual Meeting of Munich-Centre for Advanced Photonics (MAP) 2014 in Rudolfshütte, Austria.
- Poster at the XVII. International Conference on Time-Resolved Vibrational Spectroscopy 2015 in Madison, USA.

Acknowledgment

At this place I want to thank all the people who have helped me during my PhD thesis. Especially I would like to thank:

Prof. Dr. Wolfgang Zinth for giving me the opportunity to complete my PhD thesis at the chair of biomolecular optics. I would like to express my sincere gratitude for your supervision and numerous inspired discussions.

Prof. Dr. Regina de Vivie-Riedle for being the second supervisor of my PhD thesis.

Bert Pilles for the amazing technical support in time-resolved IR measurements and many helpful suggestions.

My former Master student **Julia Gontcharov** for the nice teamwork on the sensitizer project.

Dr. Dominik Bucher for the first-class introduction to the time-resolved and stationary measurements and allround support in chemistry.

Dr. Wolfgang Schreier for the patient introduction to the laboratory.

Qi Hu for being my good friend. It is such a good feeling that I can practice my mother tongue everyday.

Ms. Alexandra Michaelis and **Ms. Marianne Widmann-Diermeier** for helping in organizational issues.

Dr. Karl-Heinz Mantel and **Florian Trommer** for their excellent IT-support. Special thanks to Karl-Heinz Mantel for accompanying me by jogging in the Englischer Garten.

The workshop: Rudolf Schwarz, Alfons Stork, Christian Hausmann and Harald Hoppe for the very competent technical works.

My office colleagues: Bert Pilles, Ilvana Turkanovic, Dominik Bucher, Michael Rampp, Andreas Deeg, Julia Gontcharov, Alexander Schlüter and Carmen Kübel for the pleasant atmosphere. Special thanks to Bert Pilles and Ilvana Turkanovic for the tolerance when discussing about some social issues.

My colleagues: Teja Herzog, Karin Haiser, Florian Lederer, Julian Schauseil, Pablo Dominguez, Franziska Graupner, Florian Trommer, Benjamin März, Elena Samoylova, Anne Reiner, Stefan Hofmann, Corinna Kufner, Bastian Baudisch, Roland Wilcken and other group members for the wonderful working atmosphere and of course the delicate cakes and ice creams. Special thanks to Anne Reiner, Bastian Baudisch and Roland Wilcken for helping me with the fluorescence and oxygen dependent measurements.

The proofreaders: Ilvana Turkanovic, Julia Gontcharov, Corinna Kufner, Anne Reiner and Elena Samoylova.

Acknowledgment

My father Min Liu, my mother Beihua Wang and my girlfriend Ye Li for their support.